UTILIZING MODELING TOOLS TO DESIGN A REACTOR AND A CATALYST FOR DRY REFORMING OF METHANE

A Thesis

by

MURTAZA ALI KHAN

Submitted to the Graduate and Professional School of
Texas A&M University
in partial fulfillment of the requirements for the degree of

MASTER OF SCIENCE

Chair of Committee,	Dr. Nimir Elbashir
Committee Members,	Dr. Konstantinos Kakosimos
	Dr. Reza Tafreshi
Head of Department,	Dr. Patrick Linke

August 2021

Major Subject: Chemical Engineering

ABSTRACT

Dry reforming of methane (DRM) is a catalytic reaction in which two greenhouse gases (CO_2 and CH_4) are converted to synthesis gas (a mixture of CO and H_2), an important precursor to produce various chemical products. DRM is highly attractive due to its ability to convert greenhouse gases; however more research is required to address its process challenges: (a) high energy requirement, (b) low synthesis gas quality, and (c) catalyst deactivation due to carbon formation. Nickel (Ni) catalyst is widely used for methane reforming and thus suitable for DRM as well. However, it is prone to carbon formation due to reactions like methane decomposition and Boudouard reaction causing deactivation. A novel bimetallic nickel-copper (Ni-Cu) catalyst was previously developed in our research group at an atomistic scale using density functional theory (DFT) approach to address the Ni catalyst's carbon formation challenge. The Ni-Cu catalyst provides significant carbon resistance and superior stability compared to the conventional Ni catalyst. The catalyst's performance was proven and validated experimentally in our laboratory's state-of-the-art bench-top reactor.

The scope of this thesis is to explore the scalability of the novel Ni-Cu catalyst using a mathematical modeling approach. The approach comprises of utilizing an existing one-dimensional (1-D) pseudo-homogeneous reactor bed model supported by lumped kinetics of a network of complex reactions that take place during DRM. This model was updated by including accountability of carbon formation and advancing further to account for detailed transport properties. The kinetics of Ni to Ni-Cu catalyst were scaled using a

novel approach utilizing DFT and results in providing predictions for the bulk-scale kinetics performance in terms of carbon formation rates.

The experimental validation of the model was first tested using a conventional monoatomic Ni catalyst then later extended to predict the performance of the Ni-Cu catalyst. The 1-D model yielded results that match within an error margin of 5% with experimental data especially on CH_4 conversions. The developed 1-D model serves as a tool to predict the performance of the Ni-Cu catalyst at various reactor scales and to conduct future optimization and process intensification studies for DRM process by maximizing feed conversions.

DEDICATION

I, first and foremost, am thankful to Allah the Almighty, whose presence has helped me to persevere throughout all my efforts in life.

To my dearest Mom and Dad, I dedicate this work to you as a testament to your efforts in helping me attain quality education and providing me with unwavering support and prayers.

And last, but not least, my siblings, Mujtaba, Ariba and Nabia, who have always remained as a pillar in my life, I dedicate this work to you for your compassionate warmth and support.

I hope to become an aspiring researcher in the future and as I dedicate this thesis to you all, this is just a humble beginning in this career.

A big thank you to you all from the bottom of my heart!

ACKNOWLEDGEMENTS

I would like to firstly acknowledge and extend my sincerest gratitude to my supervisor, *Prof. Nimir Elbashir*, for his generous support in both technical and personal perspectives, and sheer guidance that he provided in this work. It has been a huge honor to learn from him and be able to work on this thesis under his guidance.

I would like to extend this gratitude to all members of our research team, especially *Dr. Mohamed Sufiyan Challiwala*. His constant support, encouragement, and availability to answer my queries throughout this work have been monumental and would not have seen the light of day without his support. I would also like to acknowledge the support of former team member *Dr. Minhaj Ghouri* for his helpful discussions and guidance in this campaign of research.

I would also like to extend my gratitude to my committee members, *Prof. Konstantinos Kakosimos* and *Prof. Reza Tafreshi* for their valuable insights and advice. A special mention to the efforts of the Texas A&M University at Qatar's Computational Research Team, including *Prof. Othmane Bouhali* and his team whose efforts assisted me in the work of this thesis. I would also like to extend my gratitude to the staff at the Office of Graduate Studies at TAMUQ especially *Mrs. Hania Ayyash* whose consistent efforts facilitated my master's journey at ease.

I would like to thank all my friends and colleagues here in TAMUQ for making my experience one to cherish forever, and finally, my family, for their eternal love.

CONTRIBUTORS AND FUNDING SOURCES

Contributors

This work was supervised by a thesis committee consisting of Professors Nimir Elbashir and Konstantinos Kakosimos from the Department of Chemical Engineering and Professor Reza Tafreshi from the Department of Mechanical Engineering.

The one-dimensional model was developed with the help of Dr. Mohamed Sufiyan Challiwala. The experimental campaign for determining the catalytic conversions for dry reforming of methane, used later to validate the model, were done in Professor Elbashir's lab at Texas A&M University at Qatar by Dr. Anjaneyulu Chatla and Mr. Anuj Varghese Prakash. Training to conduct ab-initio calculations and learn the appropriate software was done under supervision of Dr. Minhaj Ghouri.

All other work conducted for the thesis was completed by the student independently.

Funding Sources

Graduate study was supported by a fellowship from Texas A&M University at Qatar. This work was also made possible in part by the Qatar National Research Fund (QNRF), a member of Qatar Foundation, under NPRP Exceptional Proposal (EP) award with Grant Number NPRP X-100-2-024. Its contents are solely the responsibility of the authors.

NOMENCLATURE

1-D	One dimensional
a	Heat exchange area per unit volume of reactor tube
A_t	Cross sectional area of reactor tube
C	Carbon
C_{P_j}	Heat capacity of species ‘j’
CAPEX	Capital expenditure
CH_4	Methane
CO	Carbon monoxide
CO_2	Carbon dioxide
D	Diameter of reactor tube
D_p	Diameter of catalyst particle
DFT	Density functional theory
DRM	Dry reforming of methane
EF	Empirical factor
EOS	Equation of state
eV	Electrovolt
F_j	Molar flow rate of species ‘j’
F_{tot}	Total molar flow rate inside reactor tube
F_{tot0}	Initial total molar flow rate at reactor tube inlet
FT	Fischer-Tropsch

G	Superficial mass velocity
GHG	Greenhouse gas
GHSV	Gas hourly space velocity
H_2	Hydrogen (gas)
He	Helium
H_2O	Steam
ID	Internal diameter
I_i	Initial molar flow rate of species ‘i’ at reactor tube inlet
k	Rate constant
k_i	Kinetic parameter
K_i	Kinetic parameter
LHHW	Langmuir-Hinshelwood-Hougen-Watson
$M_{m,i}$	Molecular mass of species ‘i’
MF_{tot}	Total mass flow rate inside reactor tube
MF_{tot0}	Initial total mass flow rate at reactor tube inlet
O_2	Oxygen (gas)
OPEX	Operational expenditure
p_j	Partial pressure of species ‘j’
P	Pressure
P_{tot0}	Initial pressure of reactor inlet stream
POX	Partial oxidation of methane
Q_j	Volumetric flow rate of species ‘j’ inside reactor tube

$Q_{j,0}$	Initial volumetric flow rate of species ‘j’ at reactor tube inlet
Q_{tot0}	Initial total volumetric flow rate at reactor tube inlet
r_{ij}	Rate of reaction
R	Universal gas constant
RDS	Rate determining step
RWGS	Reverse water-gas shift reaction
SRM	Steam reforming of methane
STP	Standard temperature and pressure
Syngas	Synthetic gas
T	Temperature
T_0	Initial temperature of reactor inlet stream
TEM	Transmission electron microscopy
TOS	Time on stream
u	Superficial velocity
U	Heat transfer coefficient for reactor tube
V	Volume of reactor tube
W	Weight of catalyst inside reactor tube
WGSR	Water-gas shift reaction
WHSV	Weight hourly space velocity
$x_{init,i}$	Mass fraction of species ‘i’ at reactor tube inlet
x_j	Mass fraction of species ‘j’ inside reactor tube
$y_{init,i}$	Mole fraction of species ‘i’ at reactor tube inlet

y_j	Mole fraction of species ‘j’ inside reactor tube
°C	Degree Celsius
$\Delta H°$	Heat of reaction
$\Delta H_{Rxij}(T)$	Heat of reaction ‘x’ at temperature, T
$\emptyset$	Porosity of reactor bed
μ	Viscosity of gas mixture inside reactor tube
μ_i	Viscosity of pure species ‘i’
ρ	Instantaneous gas density inside reactor tube
ρ_b	Bulk density of catalyst
ρ_i	Density of species ‘i’
ρ_0	Gas density of reactor tube inlet

TABLE OF CONTENTS

Page

LIST OF FIGURES

Page

LIST OF TABLES

Page

1. INTRODUCTION

An impasse in the 2019 United Nations Climate Change Conference, popularly known as COP25, signaled to the modern world the impact of how big of discord there has been in the scientific argument and the action taken by worldwide bodies with regards to climate change. However, all scientific studies agree that rising emissions in greenhouse gases (GHGs) will be the cause of harsher weather conditions around the globe in the form of storms, extreme heat waves, changes in weather patterns, etc. [1]. Some of the countries directly responsible for such emissions, such as China, the United States, and India, were hesitant to opt for a call for more decisive action to reduce their climate change targets by reducing their GHG emissions [1]. Therefore, it is vital to address the rising concern over climate change, which the significant increase in GHG emissions has brought about. In 2020, a year hit by the COVID-19 pandemic, global carbon dioxide (CO_2) emissions (from both fossil and land-use changes) slumped with up to 39 gigatons of CO_2 emitted into the atmosphere, a 7% decrease from the previous year [2]. Usage of fossil fuels has been known to exacerbate the emissions of CO_2 in the atmosphere. Although there have been consistent efforts from various government bodies such as those in Europe to contain the global impact caused by GHG emissions from fossil fuel sources, these fuels still hold a majority in the global energy mix [3]. Therefore, carbon capture and utilization of CO_2 via usage as fuel or chemical feedstock [4] presents an excellent prospect for environmental sustainability. Moreover, utilization of CO_2 can provide a financial incentive for industries and the political landscape to embrace a carbon-neutral world.

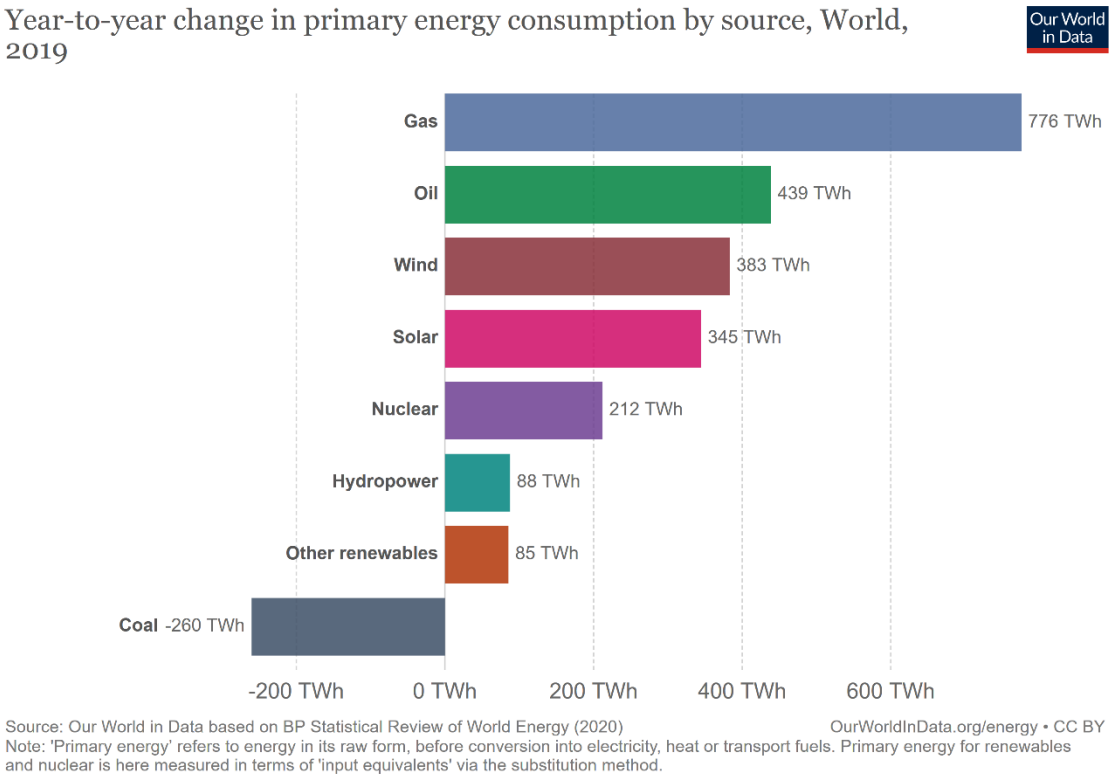

Figure 1: Annual change for sources in energy consumption show natural gas rising to be the most significant source of energy consumption in the future [3]

According to the calculations conducted by NASA [5], the global surface temperature has shown an increasing trajectory since the 1950s, with the average increase in surface temperature reaching around 0.99 °C in 2019. One of the reasons for this temperature rise is our consumption of fossil fuels, which releases many GHGs into the atmosphere. In line with our energy consumption, as seen in Figure 1, natural gas is emerging as one of the biggest sources for energy consumption worldwide, as demand for traditional fuels such as coal is declining. Natural gas primarily consists of methane (CH_4) and lighter C_2-C_4 fractions, and is projected to emerge as a critical clean energy resource [6].

Countries that are abundant in natural gas, such as Russia, Qatar, and the United States, are monetizing natural gas to run the local and global economy while reducing their carbon footprint to become environmentally more sustainable [7-9]. One of the approaches to monetize natural gas is to convert it into a more valuable compound such as synthesis gas or 'syngas' via methane reforming [10, 11]. In methane reforming, CH_4 reacts with an oxidant (such as steam, oxygen, carbon dioxide or their combination), and is converted to syngas, a mixture of carbon monoxide (CO) and hydrogen (H_2) [8]. Depending on the type of reforming technology and the feed involved, syngas typically consists of about 30-60% of CO, 25-30% of H_2, 5-15% of CO_2 and about 0-5% of CH_4 with minor amount of trace components [12].

Traditional forms of oxidants involved in methane reforming include either steam (H_2O), such as in steam reforming of methane (SRM), or oxygen (O_2), such as in partial oxidation of methane (POX) [13]. SRM is a relatively mature reforming technology used to convert CH_4 and obtain H_2 industrially, with an annual output of H_2 obtained from SRM reaching up to 10 million metric tons. In SRM, CH_4 reacts with H_2O ranging from temperatures between 700-1000 °C and 3-25 bar of pressures to yield syngas with a ratio (H_2:CO) of 3:1 [14]. Despite the substantial H_2 output obtained in SRM, the harsh reaction conditions and significantly high production and energy costs affect the SRM's prowess in the industry [14]. Moreover, SRM, when coupled with the water-gas shift reaction (WGSR), can coproduce CO_2, which adds an additional penalty in terms of CO_2 footprint [15] as shown below [16]:

$$CO + H_2O \rightarrow CO_2 + H_2 \qquad \Delta H° = -41.2\ kJ.mol^{-1} \qquad (1)$$

Meanwhile, POX is less energy-intensive compared to other reforming technologies and is exothermic [13]. In POX, CH_4 reacts with O_2 non-stoichiometrically inside a reactor, operating at temperatures between 1200-1500 °C (without catalyst), yielding syngas with a ratio of 2:1 [16]. POX usually requires a very pure oxygen supply since it is a homogeneous reaction. Maintaining such an oxygen supply requires the need of air separation units, which make the POX process expensive [15]. Therefore, methane reforming technologies have garnered much research interest, which could allow the utilization of CH_4 and address the concern of rising CO_2 production.

This interest in research leads us towards DRM, a catalytic process that utilizes both CO_2 and CH_4 to convert GHGs to syngas, which is converted to fuels and value-added products [17-20]. In the DRM process, one molecule of CH_4 and CO_2 react to produce syngas in the presence of a catalyst. The DRM, along with the SRM and POX reactions, are described below [17]:

DRM:

$$CH_4 + CO_2 \rightarrow 2CO + 2H_2 \qquad \Delta H° = +247\ kJ.mol^{-1} \qquad (2)$$

SRM:

$$CH_4 + H_2O \rightarrow CO + 3H_2 \qquad \Delta H° = +206\ kJ.mol^{-1} \qquad (3)$$

POX**:**

$$CH_4 + ½O_2 \rightarrow CO + 2H_2 \qquad \Delta H° = -36\ kJ.mol^{-1} \qquad (4)$$

The use of syngas is to obtain ultra-clean fuels and valuable products like hydrocarbons such as diesel, gasoline, naphtha, methanol via Fischer-Tropsch synthesis (FTS) and other essential reactions [21-23].

While DRM provides an exciting prospect for natural gas monetization and CO_2 conversion, it still has its challenges. Technologies such as SRM and POX are exothermic, but on the contrary, the DRM reaction is heavily endothermic. A temperature of at least 850 °C or above is required to maintain high syngas production while mitigating the impact of competing reactions, that lead to carbon formation [24].

The formation of carbon is a second and significant challenge as carbon deposition results in a drop in catalyst efficiency due to fast deactivation [25] and therefore hinders the industrial application of DRM. Another limitation of DRM is that the syngas produced need to be upgraded for downstream applications for processes like methanol and FT technologies that generally operate at a syngas ratio of 2:1. DRM produces syngas with a ratio of around 1:1 and needs either removal of carbon monoxide or additional hydrogen to maintain the ratio of 2:1, which demands additional CAPEX and OPEX [26].

Therefore, to ensure a smooth and more prolonged operation for DRM, it is crucial to research and produce more efficient, stable, and economic catalysts. While combined reforming and process optimization [17, 26] has been proposed to address these drawbacks, the development of novel catalysts [20, 25] that hinder the formation of carbon is essential for the commercialization of DRM technology.

2. LITERATURE SURVEY

DRM presents a good opportunity to reform CH_4 and utilize CO_2 to produce syngas. To commercialize this technology, a great deal of research has been conducted both in terms of finding better DRM catalysts as well as understanding the different kinetic models to understand the DRM's behavior in terms of scalability. In the sections to follow, a thorough literature review is presented to explain these approaches consisting of catalysis studies in which commercial DRM catalysts are upgraded via forming bimetallic catalysts that acts as precursor for studying its scalability. Moreover, discussion on developing a reactor bed model has also been presented along with a great emphasis on selecting an appropriate model to lump DRM and SRM kinetics.

2.1. Catalysts for dry reforming of methane (DRM)

This section describes how interest in DRM has peaked research into developing and searching novel catalysts on an atomistic level, where these catalysts can help maintain the activity while reducing the formation of carbon in the DRM reaction. The discussion starts with using nickel (Ni) as a catalyst, the mechanistic pathways in which Ni catalyzes DRM, and how carbon forms on the Ni catalyst. This discussion is followed by a review of how Ni catalyst, when upgraded with a transition metal to create a bimetallic catalyst, can help address the DRM challenges.

2.1.1. Ni catalyst for DRM

Pakhare and Spivey [25] investigated the effect of various noble metal catalysts on the mechanism and kinetics of the DRM reaction. Various noble metals have been

researched, including platinum (Pt), rhodium (Rh), and ruthenium (Ru), among others. They observed that Rh and Ru demonstrate elongated catalytic stability and superior activity, and carbon resistance. However, these noble metals are known to be very expensive and in less abundance in nature, which tends to restrict their economic use [27, 28]. On the contrary, Ni catalysts on various supports such as Al_2O_3 or La_2O_3 are cheaper, readily available, and demonstrate catalytic activity comparable to noble metals [29, 30]. Several properties play a significant role in the synthesis and design of DRM catalysts that dictate their performance. These properties, as shown in Figure 2 below, include but are not limited to size and dispersion, redox property, a good interaction between metal and support, surface area, porosity, and basicity among others [28]. A compromise is reached between desired aspects such as deposition of carbon or catalytic activity, achieved by controlling and adjusting the previously mentioned properties on DRM catalysts.

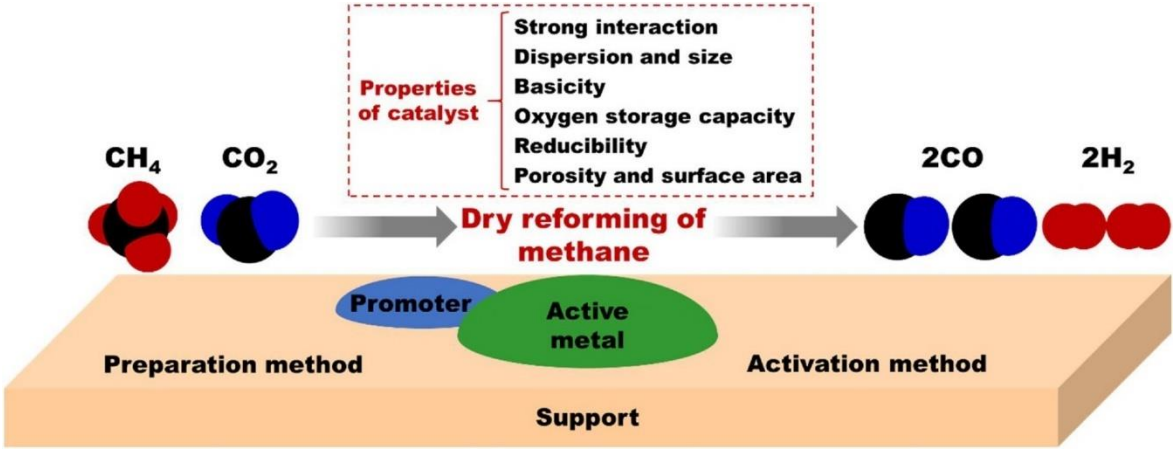

Figure 2: Summary of various properties affecting catalyst preparation for DRM reaction [20]

A tremendous amount of research has been done to illustrate insights on the mechanistic pathways using Ni as a DRM catalyst. These insights have been gathered with

experimental campaigns and have also been illustrated through significant efforts of studying the surface chemistry via means of ab-initio methods, namely DFT studies. Usage of DFT has become prevalent in the past decades, especially in heterogeneous catalysis. DFT acts as a precursor to find inputs towards a microkinetic model, which can accurately capture the dynamic sequence of events happening on the catalyst surface and make it comparable to experimentally obtained data via computational means [31].

Zhu et al. [32] observed from their comprehensive DFT study of DRM over Ni (111) surface of the pure Ni catalyst and found that direct decomposition of CO_2 to form atomic O is the most dominant pathway. This decomposition is followed by the dissociation of methane generating CH and then eventually C. After generation of C, the subsequent oxidation of CH and C occurs by atomic O and culminates in the decomposition of the CHO intermediate to yield CO. They stress that apart from O, the OH oxidant and its effect on the DRM mechanism cannot be ignored [32]; their proposed mechanism for DRM can be seen in Figure 3. Kroll, Swaan and Mirodatos [33] studied the deactivation of Ni/SiO_2 catalysts and found that nickel carbide forms an active phase in the reaction. Wang et al. [34] further took these findings to study the mechanism of carbon deposition on different Ni surfaces and found that nickel carbide plays a central role in the fast deposition of carbon which deactivates the catalyst as the deposition of carbon is very sensitive to the metal structure of the Ni surface. This surface structure also dictates the minimization of carbon formation in the DRM reaction, with the 111-surface having the most negligible diffusion of carbon.

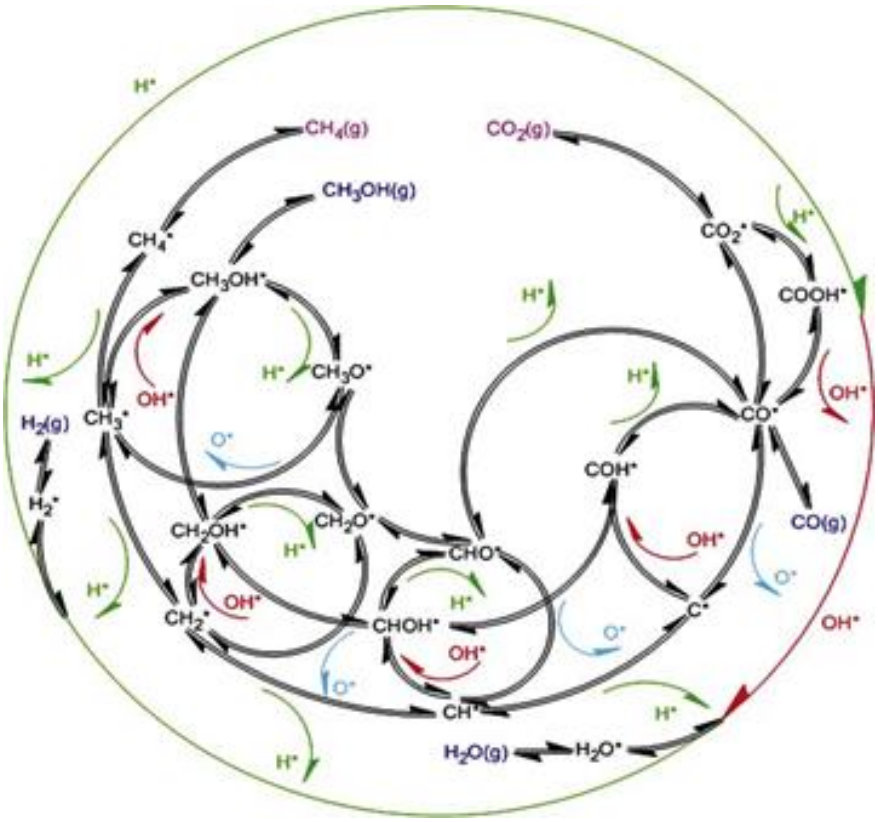

Figure 3: Schematic of the mechanism proposed for Ni (111) catalyst for DRM [32]

Another factor that could help solve the problem of carbon formation is the particle size of the catalyst. A smaller particle size helps prevent carbon deposition, which a strong interaction of Ni could achieve with the metal support [35]. Experiments conducted by Bhavani et al. [36] found that a catalyst size of approximately 5 nm helped achieve significant carbon minimization on the Ni catalyst. Ni as a catalyst can allow industrial feasibility for DRM by minimizing the formation of carbon as seen in the preceding discussion; however, Ni can be further upgraded to create a more efficient catalyst.

2.1.2. Bimetallic catalysts for DRM

A facet that has gained much traction recently in DRM catalysis is doping the Ni catalyst surface with another metal. Such doping helps create bimetallic catalysts that change the surface structure and create a synergistic effect due to two active metals that improve catalytic activity and influence the formation of carbon [37]. Ni, therefore, could be doped with either a noble metal or a transition metal to bring about that synergistic effect. As mentioned in the previous section, several noble metal catalysts such as Ru, Ir, and Pd have been studied for DRM, but their higher associated costs and reduced availability [37] make their industrial viability questionable. Therefore, most of the focus has shifted chiefly towards using non-noble metals, namely transition metals such as copper (Cu), in conjunction with Ni. Some of the properties affecting the second metal to create a bimetallic catalyst alongside Ni are given in Figure 4.

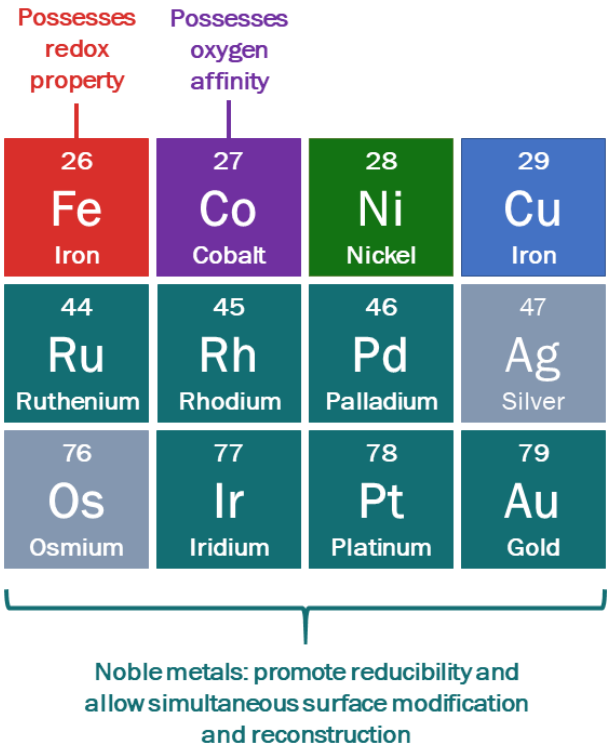

Figure 4: Summary of various characteristics affecting various Ni-based bimetallic catalysts (adapted from [38])

Cu has been studied as part of Ni-Cu bimetallic catalysts. In DRM, Cu is known as an active promoter and could assist with diminishing the formation of coke. Experiments conducted by Lee et al. [39] demonstrated that the addition of 1 wt% of Cu in a Ni/Al_2O_3 catalyst helped minimize the Cu-rich alloy effect and decrease the carbon deposition. Ghouri [40] in our group, independently confirmed the findings of Lee et al. [39] and found that catalytic stability increased by adding Cu into the Ni-Ni network, minimizing the adsorption of carbon on the Ni-Cu interface. Wang et al. [41] studied ethanol steam reforming over Ni and Ni-Cu supported catalysts and found that Ni-Cu catalysts had a stable catalytic activity for a 40 h on stream at 650 °C without undergoing

severe deactivation of catalyst due to carbon formation, suggesting that the addition of Cu to the catalyst could change the electronic feature and affinity of carbon towards the Ni particle. While a Ni:Cu loading of 3:1 was known to establish significant catalytic activity and carbon minimization, increasing the Cu content decreased that effect and reduced the catalyst activity [39, 41]. A Ni-Cu surface has lower surface energy due to the surface enrichment effect caused by Cu, which could explain that at higher Cu content, the number of Ni active sites might decrease on the catalyst surface and affect the CH_4 activation on the catalyst [42].

Such findings were also verified via DFT calculations as well. Liu et al. [43] carried out a comprehensive DFT study on the NiCu (111) surface, investigating the decomposition of CH_4. In another study, Liu et al. [44] studied the deposition of carbon on elementary metallic (Ni, Co, Cu, and Fe) and bimetallic (NiCu, NiCo, and NiFe) surfaces. They were able to show that surface rich with Cu was superior in terms of resisting carbon formation, and NiCu surface has the least amount of deposited carbon in contrast to the Ni (111) surface [43, 44]. Liu et al. [43] also propose that CH dissociation forms the rate-limiting step for the Ni-Cu catalyst with a NiCu (111) surface, and the energy barrier for this reaction was higher than that of pure Ni catalyst on the Ni (111) surface. Zhang et al. [45] emphasized the role of oxygen (O) using DFT calculations to eliminate carbon from the surface and mention that apart from O, the OH species also has a crucial role in removing carbon from pure Ni and Ni-Cu catalysts. They found that average adsorption energies of C+O or C+OH and their activation barriers have a linear relationship, meaning that as the adsorption ability of C+O or C+OH decreases on the

metal surface, the ability to eliminate carbon increases on the same corresponding metal surface [45]. This effect allows the inhibition of carbon by an efficient periodic cycle of carbon forming and being removed on the NiCu (111) surface owing to its greater stability [45].

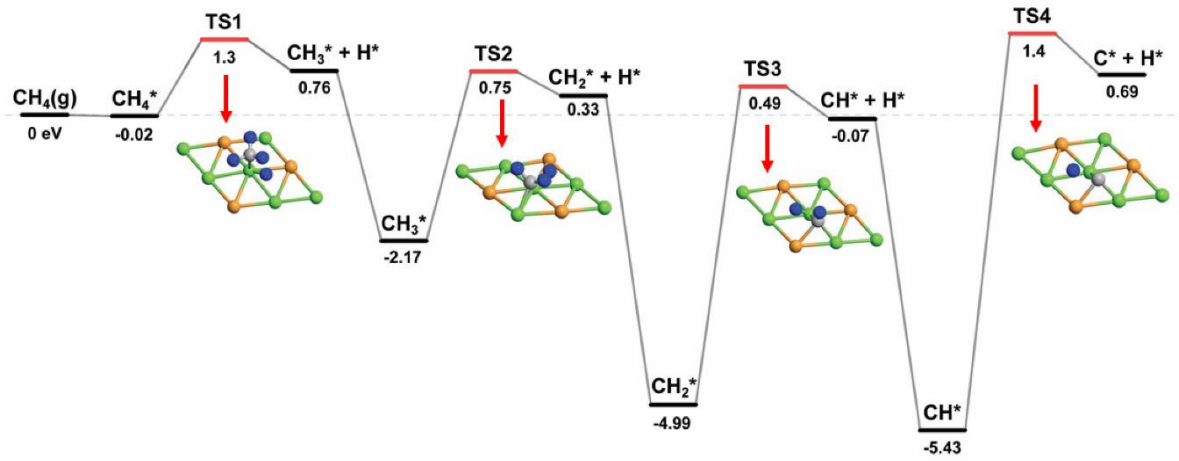

Figure 5: Energy barriers for CH_4 dissociation steps for DRM on Ni-Cu bimetallic catalyst [46]

The precursor to the work of this thesis, Omran et al. [46] in our group developed a comprehensive mechanism for the novel Ni-Cu bimetallic catalyst with a Ni_2Cu (111) surface and investigated the mechanistic insights for the DRM reaction pathways. Omran et al. [46] confirmed the results presented previously in literature [43-45] and found that CH dissociation is indeed the rate-limiting step with the highest energy barrier of 1.41 eV, as shown in Figure 5, when compared to pure Ni or Ni-Fe bimetallic catalysts. Omran et al. [46] also confirmed the major source of carbon to be CH_4 rather than CO_2, as suggested by Wang et al. [41]. Omran et al. [46] also found that in terms of C/CH oxidation, the C+O

pathway was the most favorable with an energy barrier of 0.72 eV, half than that of the same reaction on pure Ni or Ni-Fe bimetallic catalysts. Omran et al. [46] agree that even though C+O is the more favorable oxidation pathway, the role of oxidation by OH species cannot be entirely ignored in the simultaneous carbon formation and removal from the Ni_2Cu (111) surface and have hence proposed a mechanism as shown in Figure 6.

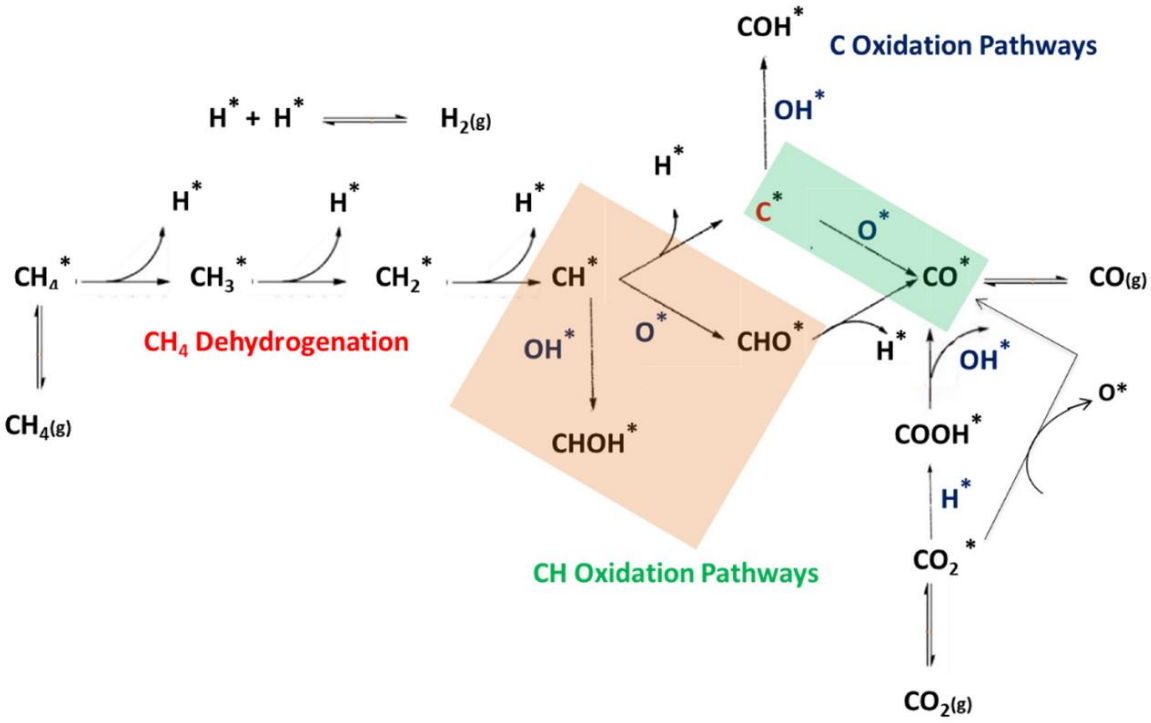

Figure 6: Schematic of the mechanism proposed for Ni-Cu bimetallic catalyst for DRM [46]

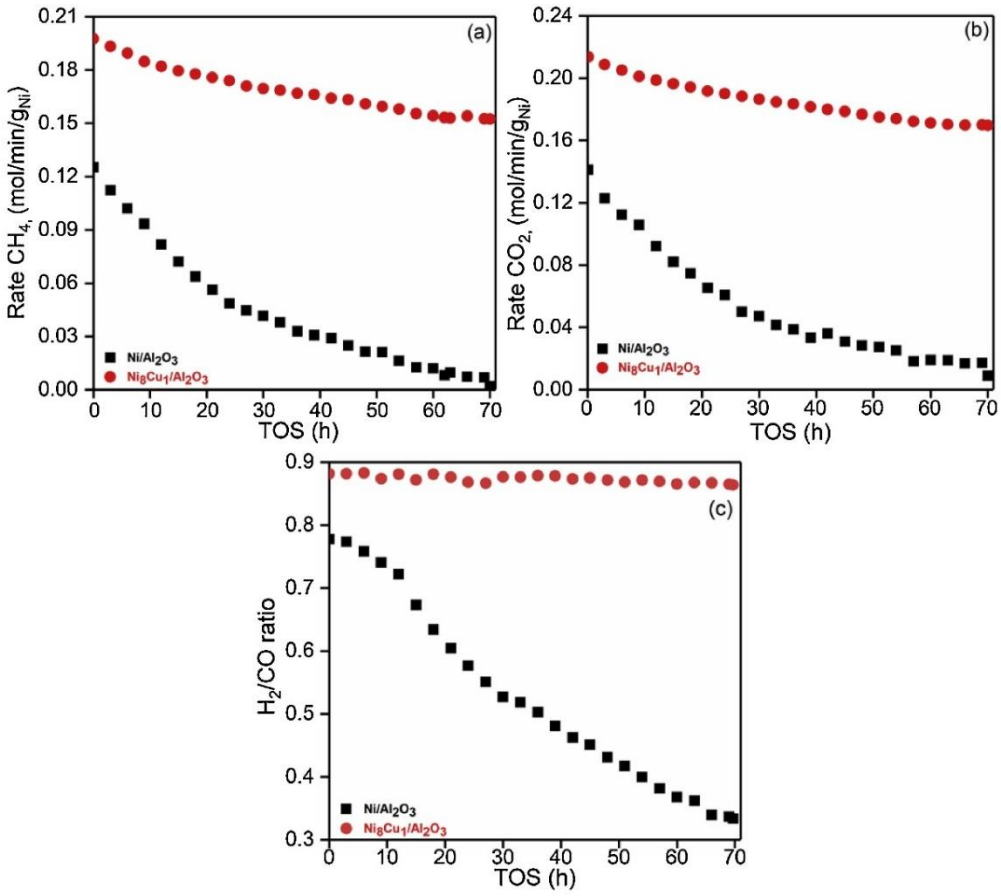

Figure 7: Conversions and syngas ratio variations compared between Ni-Cu bimetallic and pure Ni catalysts for DRM show dominance of Ni-Cu catalyst [47]

In addition to the DFT studies, Professor Elbashir's group (Chatla et al. [47]) had earlier experimentally synthesized the novel Ni-Cu catalyst with an 8:1 loading, creating a Ni_2Cu (111) surface in essence. They also found that for greater time on stream (TOS), the Ni-Cu catalyst remained active for longer period and did not deactivate as quickly as the commercial Ni catalyst, suggesting that coke deposition has been minimized in case of Ni-Cu catalyst [47]. Figure 7 shows that the novel Ni-Cu catalyst maintains a greater activity with higher stability on the H_2:CO ratio in contrast to the pure Ni catalyst. Therefore, to a great extent, it can be established that adding Cu to Ni can greatly influence

the stability of the Ni-Cu bimetallic catalyst and help increase the DRM activity while minimizing carbon formation.

Searching for novel catalysts allowed us to see the effect of using Ni as a potentially viable catalyst for DRM and how the addition of another metal, Cu, in the catalyst's structure, helps achieve a synergistic effect that reduces the carbon formation on the surface. The effect of the previously established Ni-Cu bimetallic catalyst now needs to be seen on a greater scope to assess its performance. The section ahead describes how utilizing an approach involving studying process parameters could help achieve scalability using the Ni-Cu catalyst from an atomistic to a larger scale.

2.2. Assessing scalability via reactor bed modeling

This section describes a brief literature review on the approach from process systems engineering taken to develop a scalability model to assess the DRM catalysts. To develop such a model, firstly a thorough discussion on various kinetic models used in both DRM and SRM are presented. Next, a brief discussion on literature of reactor bed modeling is presented. This section then provides a discussion on the mechanism of carbon deposition in DRM and which reactions contribute significantly towards carbon in most DRM catalysts.

2.2.1. Kinetics of DRM

In Section 2.1.2, an extensive amount of literature was presented to demonstrate how implementing Cu in the Ni-Ni framework to develop a novel Ni-Cu catalyst could help to tackle the issue of carbon formation in DRM, with studies done in our group [46, 47] on an atomistic level. To assess the feasibility of the novel synthesized Ni-Cu catalyst

for DRM, an appropriate reactor model needs to be developed to simulate and predict the feed conversions by changing the various process parameters. Such a model could also be programmed to predict the amount of carbon formed by implementing the appropriate reactions that contribute to carbon formation in DRM. Therefore, an appropriate kinetic model needs to be used to encapsulate the different reactions happening in DRM.

There have been several studies investigating various DRM catalysts [48-50] to model their kinetic behavior and understand the mechanistic pathway on an atomic level. The development of such kinetic models can be categorized into three main types: (1) Power law models, (2) Eley-Rideal (ER) models, and (3) Langmuir Hinshelwood-Hougen Watson (LHHW) models [51].

Power-law models can be used as a rough estimate for determining the basic kinetic parameters and do not necessarily capture the whole schematic of all the various reactions happening in DRM [51]. These models exist to interpret the kinetic behavior for DRM and provide an initial estimation for mapping out a more complex model that might require the use of a larger data set [51]. Generally, the power-law models can be represented as follows:

$$r = k\left[P_{CH_4}\right]^m\left[P_{CO_2}\right]^n \quad (5)$$

There have been various studies conducted on a variety of Ni-based catalysts that fit their data according to the power-law. Bradford and Vannice [52] had studied the DRM reaction over Ni catalyst supported over SiO_2 among other forms of support at different temperatures. They found that the partial pressure dependencies for both CH_4 and CO_2 had followed the power-law patterns with the rate expressions obtained as below [52]:

$$r_{CH_4} = k\left[P_{CH_4}\right]^{0.44}\left[P_{CO_2}\right]^{0.15} \quad (6)$$

$$r_{CO_2} = k\left[P_{CH_4}\right]^{0.27}\left[P_{CO_2}\right]^{0.64} \quad (7)$$

In a similar manner, using photoacoustic spectroscopy, Kim et al. [53] had conducted a thorough analysis the DRM reaction over Ni/Al_2O_3 catalyst and found that the rate of consumption of CO_2 followed a pattern of power-law as given below:

$$r_{CO_2} = k\left[P_{CH_4}\right]^{0.48}\left[P_{CO_2}\right]^{0.45} \quad (7)$$

Given the simplicity of the power-law model, to better understand the insights in DRM, ER and LHHW models are preferred. For DRM, two forms of ER models can exist. In the first ER model (ER 1), CH_4 first adsorbs on the catalytic surface in the first step, and CO_2 reacts with the adsorbed CH_4 in the second step; the second step being the rate-determining step (RDS) in the process [54]. Simultaneously, in the second ER model (ER 2), the vice versa occurs where CO_2 first adsorbs on the surface and CH_4 then reacts with the adsorbed CO_2; the latter once again being the RDS [54]. Both models then yield the following rate expressions [54]:

ER 1: $$r_{ref} = \frac{k_{ref}K_{CH_4}\left(P_{CH_4}P_{CO_2} - \frac{P_{CO}^2 P_{H_2}^2}{K_{ref}}\right)}{1 + K_{CH_4}P_{CH_4}} \quad (8)$$

ER 2: $$r_{ref} = \frac{k_{ref}K_{CO_2}\left(P_{CH_4}P_{CO_2} - \frac{P_{CO}^2 P_{H_2}^2}{K_{ref}}\right)}{1 + K_{CO_2}P_{CO_2}} \quad (9)$$

For Ni-based catalysts, there are not many studies available using ER models; however two known studies are that of Akpan et al. [55] and Becerra et al. [56]. Akpan et al. [55] used a packed bed tubular reactor to run the DRM reaction over a Ni/CeO_2-ZrO_2 catalyst, where they postulated a mechanism in which the dissociation of CH_4 on the catalyst was

considered to be the RDS after studying various models and found their final rate equation to be:

$$-r_A = \frac{2.1\times10^{17} e^{-222800/RT}\left(N_A - \frac{N_C^2 N_D^2}{K_P N_B}\right)}{\left(1+34.3 N_D^{\frac{1}{2}}\right)^5} \quad (10)$$

Becerra et al. [56], on the other hand used Ni/Al_2O_3 to perform their experimental study on the DRM reaction. They postulated that the adsorbed methyl species, which is yielded from the dissociation of CH_4, reacts with the CO_2 in the RDS and had the following main rate expression:

$$r_{ref} = \frac{k_1 K_{CH_4}\left(P_{CH_4} P_{CO_2} - \frac{P_{CO}^2 P_{H_2}^2}{K_1}\right)}{1+K_{CH_4} P_{CH_4}} \quad (11)$$

Both Akpan et al. [55] and Becerra et al. [56] had reported that their postulated kinetic models possesses good agreement with experimental results and based on the expressions, both their models generally resemble the ER 1 model as described previously, with the model of Becerra et al. [56] resembling the ER 1 model with extremely good accuracy.

Most mechanisms for DRM proposed in literature are based using the LHHW principles. The LHHW model mainly assumes that while all other reactions are in a state of having achieved thermodynamic equilibrium, one of the reaction steps in the overall mechanisms is slow and is therefore the RDS [54]. However, unlike the ER models, the LHHW models are generally more complex and can encapsulate a bigger picture in terms of what happens in various reactions at the atomic level. Most LHHW models for DRM involve CH_4 and CO_2 undergoing dissociative adsorption which forms to be the RDS, however there have been various LHHW based models proposed in which the RDS is not

defined in a simplistic manner. Some of these LHHW models for various Ni catalysts are discussed in this section.

Zhang and Verykios [57] conducted an extensive DRM study over Ni catalyst supported on Al_2O_3 and moreover with an addition of CaO promoter to the said catalyst. By assuming that the dissociation of CH_4 to be the RDS, as it is activated by the presence of Ni, they noted that their results fit the LHHW proposed scheme as follows [57]:

$$r_{ref} = \frac{aP_{CH_4}P_{CO_2}^2}{\left(P_{CO_2} + bP_{CO_2}^2 + cP_{CH_4}\right)^2} \tag{12}$$

Osaki et al. [58] compared disulfide catalysts along with Ni/SiO_2 catalyst for DRM and found that CH_4 dissociates to the CH_x species while CO_2 dissociates to CO and O on the catalyst surface. They proposed that the reaction between CH_x species with O on the catalyst surface is the RDS, and therefore found the following rate expression:

$$r_{ref} = \frac{k_{ref}\sqrt{K_{CH_4}K_{CO_2}P_{CH_4}P_{CO_2}}}{\left(1+\sqrt{K_{CH_4}P_{CH_4}}+\sqrt{K_{CO_2}P_{CO_2}}\right)^2} \tag{13}$$

While studying the DRM reaction over Ni/Al_2O_3 as well as Ni/CeO_2-Al_2O_3 catalysts, Wang and Lu [59] found that the activation energies for CH_4 and CO_2 consumption steps were relatively lower than that of CO production, and therefore deduced that the step of CO formation, in which the C species undergoes oxidation is the RDS. Their postulated rate expression based on this RDS showed good agreement with their obtained kinetic results and is described below [59]:

$$r_{ref} = \frac{k_{ref}P_{CH_4}P_{CO_2}}{\left(1+K_{CH_4}P_{CH_4}\right)\left(1+K_{CO_2}P_{CO_2}\right)} \tag{14}$$

In another study performed by Wang and Lu [60] over Ni/γ-Al_2O_3 catalyst , they postulated the same kinetic expression as given in Eq. (12) above, where they used the same principle of CO formation being a part of the RDS as described earlier [59], however this time they attributed the CO being formed via the reverse Boudouard reaction, in which C species combines with CO_2 on the catalyst surface [60].

The RDS does not necessarily have to be a single reaction step and can encompass multiple steps to incorporate the reaction behavior. This laid the foundation to the model that was initially proposed by Tsipouriari and Verykios [61] through their work on Ni/La_2O_3 and further refined by Verykios [62]. Tsipouriari and Verykios [61] proposed that the cracking of CH_4 as CH_4 adsorbs in equilibrium is one of the RDS. Meanwhile, due to the strong interaction between CO_2 and the La_2O_3 support, an oxycarbonate species is formed. This oxycarbonate species reacts with deposited carbon on the Ni-oxycarbonate interface to regenerate La_2CO_3 in the second RDS. Based on this mechanism, the proposed mechanism was follows [61]:

$$r_{CH_4} = \frac{K_1 k_2 K_3 k_4 P_{CH_4} P_{CO_2}}{K_1 k_2 K_3 P_{CH_4} P_{CO_2} + K_1 k_2 P_{CH_4} + K_3 k_4 P_{CO_2}} \quad (15)$$

The model proposed above was experimentally further verified by Verykios [62] by comparing to other Ni-based catalysts and therefore finalized this proposed model in his further study, reporting good agreement between the results obtained from the experiments and the mechanism proposed to fit the results. The Verykios [62] model for DRM has been used in various catalyst characterization and modeling studies [17, 63, 64]. Given that steam is one of the side products of DRM, a lumped kinetic model based on combining

DRM and SRM should be considered to accurately model the main as well as side reactions in a DRM setup.

2.2.2. Kinetics of SRM

The kinetics for SRM, in a similar manner to DRM, have mostly found two types of rate expression models: power-law and LHHW, the usages of which have been discusses in the section earlier. Moreover, as seen previously in the case for DRM [51], dissociation of CH_4 also serves as the RDS in most SRM experimental studies [65]. Ross and Steel [66] had studied the SRM reaction over a coprecipitated Ni/Al_2O_3 catalyst and observed that their results fit the power-law model as shown below, with the dissociation of CH_4 while adsorbing on catalytic surface to be the RDS:

$$r = k[P_{CH_4}][P_{CO_2}]^{-0.5} \tag{16}$$

Al-Ubaid and Wolf [67] had studied extensively reduced Ni aluminate catalysts, and found that in their limited operational domain, dissociation of H_2O species plays an important role in progressing the reaction and proposed a simplistic power-law model :

$$r_{CH_4} = 7.3 \times 10^4 e^{-16.5/RT} \frac{[CH_4]^{0.24}[H_2O]^{0.28}}{1+K[H_2]^{1.86}} \tag{17}$$

Due to the simplistic nature of the power-law models [51] as described previously, LHHW based models are developed for SRM. De Deken et al. [68] studied SRM over Ni catalyst supported on alumina and found that the oxidation of C to CO, as well as CO_2 on the catalytic surface, both formed the RDS for their results and therefore had two rate expressions, as listed below to describe the conversions:

$$r_{CO} = \frac{k_{CO}\left(\frac{P_{CH_4}P_{CO_2}}{P_{H_2}^3} - \frac{P_{CO}}{K_{P1}}\right)}{(1+K_{CO}P_{CO})^2} \tag{18}$$

$$r_{CO_2} = \frac{k_{CO_2}\left(\frac{P_{CH_4}P_{H_2O}^2}{P_{H_2}^4} - \frac{P_{CO_2}}{K_{P2}}\right)}{(1+K_{CO}P_{CO})^3} \quad (19)$$

Hou and Hughes [69] had carried out an extensive assessment for studying SRM kinetics over Ni/α-Al_2O_3 catalyst and found that surface reactions producing CO as well as CO_2 form the RDS with the following rate expressions:

$$r_1 = \frac{k_1\left(\frac{P_{CH_4}P_{H_2O}^{\alpha_{11}}}{P_{H_2}^{\alpha_{12}}}\right)\left(1-\frac{P_{CO}P_{H_2}^3}{K_{P1}P_{CH_4}P_{H_2O}}\right)}{(den)^2} \quad (20)$$

$$r_2 = \frac{k_2\left(\frac{P_{CO}P_{H_2O}^{\alpha_{21}}}{P_{H_2}^{\alpha_{22}}}\right)\left(1-\frac{P_{CO}P_{H_2}}{K_{P2}P_{CO}P_{H_2O}}\right)}{(den)^2} \quad (21)$$

$$r_3 = \frac{k_3\left(\frac{P_{CH_4}P_{H_2O}^{\alpha_{31}}}{P_{H_2}^{\alpha_{32}}}\right)\left(1-\frac{P_{CO_2}P_{H_2}^4}{K_{P3}P_{CH_4}P_{H_2O}^2}\right)}{(den)^2} \quad (22)$$

The model used by Hou and Hughes [69] brings us to the most theorized model for SRM, which was developed by Xu and Froment [70] on a Ni catalyst supported on $MgAl_2O_4$ for the SRM process. They had used an extensive reaction scheme in which three steps that contributed towards the production of CO and CO_2 species were considered to be the RDS, with the rest of the steps being considered at equilibrium [70]. The rate expressions that they derived are summarized below:

$$r_1 = \frac{k_1}{p_{H_2}^{2.5}}\left(p_{CH_4}p_{H_2O} - \frac{p_{H_2}^3 p_{CO}}{K_1}\right)/(DEN)^2 \quad (23)$$

$$r_2 = \frac{k_2}{p_{H_2}}\left(p_{CO}p_{H_2O} - \frac{p_{H_2}p_{CO_2}}{K_2}\right)/(DEN)^2 \quad (24)$$

$$r_3 = \frac{k_3}{p_{H_2}^{3.5}}\left(p_{CH_4}p_{H_2O}^2 - \frac{p_{H_2}^4 p_{CO_2}}{K_3}\right)/(DEN)^2 \quad (25)$$

$$DEN = 1 + K_{CO}p_{CO} + K_{H_2}p_{H_2} + K_{CH_4}p_{CH_4} + K_{H_2O}p_{H_2O}/p_{H_2} \quad (26)$$

The model for Xu and Froment is considered one of the most ideal models used to describe the SRM reaction and has been used in various experimental and modeling studies [17, 71-73] over the years. To develop an appropriate kinetic model, experimental data is usually obtained which is then later fit according to a specified rate law expression to obtain the kinetics. Although kinetic models are available for a pure Ni catalyst, there is still a great deal of research to determine the Ni-Cu bimetallic catalyst kinetics fully. Given the availability of DFT, there have been insights developed to understand the behavior of Ni-Cu catalyst to describe its mechanistic pathway for DRM, however there is a lack of kinetic models available to understand the Ni-Cu behavior in a reactor model setup. Therefore, while using lumped kinetics to assess the feasibility of DRM in an appropriate reactor setup, conventional tools need to be utilized to account for the Ni-Cu kinetics, which shall be described in later in Section 4.

2.2.3. Reactor bed modeling

There have been numerous studies done previously to describe various reforming technologies and mimic the behavior of experimental reactor setups to develop algorithms that allow the prediction of reaction parameters such as conversion or amount of catalyst required to model the behavior of the reforming reaction. Abbas et al. [71] had studied the SRM reaction over a NiO/Al_2O_3 catalyst in an adiabatic packed bed reactor, using the kinetics of Xu and Froment [70] and observed the effect of operating parameters such as temperature, pressure etc. on the feed conversions and H_2 yield. Their model was a one-dimensional heterogeneous model developed for the SRM process and they carried out an experimental campaign to validate this model and found that high temperature, lower

pressure and higher H_2O:C ratio yielded a very good performance in terms of conversion and product purity [71]. They also found that their developed model agreed extremely well with the experimental results [71].

Maqbool et al. [74] further continued the work on the developed one-dimensional model by Abbas et. al [71] including Ni/Al_2O_3, sulfide nickel and $Pt/Ni/Al_2O_3$ among other catalysts. The model accounted for heat and mass transfers and did not consider the effect of carbon deposition. Maqbool et al. [74] found that the developed model matched well with the chemical equilibrium calculations based on Gibbs free energy minimization, and concluded that among all catalysts, a Ni/Al_2O_3 catalyst was able to generate the maximum conversion and product selectivity owing to its fast kinetics.

Saidina Amin et al. [75] investigated the Rh/Al_2O_3 for DRM reaction by developing a one-dimensional heterogeneous fixed bed reactor model, employing all the transport equations necessary. Their model was able to predict CH_4 and CO_2 conversions and observe the syngas ratio and found that axial variations were negligible at higher temperatures [75]. Karimipourfard et al. [76] studied a tri-reformer setup by developing a homogeneous one-dimensional model and optimized for the feed conditions and inlet mole fractions to maximize the conversions and syngas ratio.

In two separate studies, Benguerba et al. [77, 78] studied both Ni and Ni-Co catalysts over Al_2O_3 support by developing one-dimensional homogeneous fixed bed reactor models using various kinetics to model the DRM behavior. In both studies, they were able to validate their experimental results with their developed models and found

that some of the carbon formation reactions could be ignored in their utilized kinetics, as well as finding dependency of temperature profile on the wall temperature [77, 78].

A precursor to the thesis, earlier in our group, Challiwala et al. had performed an extensive thermodynamic and kinetic assessment of a lumped DRM+SRM kinetic model using the kinetics of Verykios [62] and Xu and Froment [70]. They were able to evaluate the effects of changing the operating parameters on the equilibrium product distribution. While this study formed a validation between thermodynamic and kinetic assessment, it did not possess a means to predict the composition profiles inside a reactor setup and therefore to extend this work, and assess the scalability of this setup, by incorporating our novel Ni-Cu catalyst, an appropriate reactor bed model needed to be developed.

2.2.4. Strategies for scale-up

The primary method in which reactor scale-up is generally achieved is via the use of dimensional analysis. Two main forms of dimensional analysis exist: the Buckingham Pi theorem [79] and an inspectional analysis [80] technique. The Buckingham Pi theorem relies on establishing the dependence of one parameter in terms of the necessary independent parameters in the simplest dimensionless form possible. On the contrary, in inspectional analysis, if the governing differential equations and boundary conditions are known, they are converted to a dimensionless form to obtain a set of dimensionless numbers. The ratio of the solid-gas density was found to be a crucial property used for scaling up in terms of hydrodynamic similarity by Broadhurst and Becker [81] and using the Buckingham Pi theorem, they laid the foundations towards a ‘full set of scaling laws,’ that were coined by Glicksman [82].

By converting the equations of motion and mass conservations of both the fluid (gas) and particles inside the reactor into a dimensionless form, Glicksman [82] obtained a comprehensive set of dimensionless numbers that could be used for scale-up purposes. Since not all the parameters could be fulfilled during scale-up, the full set was modified by Glicksman [82] to reduce the number of parameters leading to the following set of parameters:

$$\frac{u_0}{u_{mf}}, \frac{u_0^2}{gd_p}, \frac{\rho_g}{\rho_p}, \frac{D}{H}, \phi, \text{particle size distribution} \quad (27)$$

u_0: Superficial gas velocity

u_{mf}: Minimum fluidization velocity

g: Acceleration due to gravity

d_p: Particle diameter

ρ_g: Gas density

ρ_p: Particle density

D: Bed diameter

H: Bed height

ϕ: Particle sphericity

In the simplified set above, the quantity for Reynolds number ($\frac{u_0}{u_{mf}}$) does not match at the two scales thereby causing an error in dimensionless scale-up [82].

In literature, other scaling laws have been reported. Horio et al. [83] for example had proposed the following criteria for scaling up fluidized beds:

$$\frac{u_0 - u_{mf}}{gD}, \frac{u_{mf}}{gD} \quad (28)$$

These criteria hold well for moderate Reynolds numbers (Re < 64) however they do not consider the chemical similarity inside the chemical reactors that needs to be considered during scale-up [83]. Mass transfer, reaction kinetics and the hydrodynamics of the fluid are three parameters that dictate the feed conversions and product selectivity inside a reactor and a scale-up will cause an influence in the role of these parameters. Hence this requires the rate determining step to be known in a fluidized bed reactor during a scale-up process. This step can be based on the reaction kinetics or influenced by limitations such as convection or diffusion. Therefore, Horio et al. [83] had developed a specific methodology to determine the influence of convection and diffusion during scale-up processes by devising a parameter, β, as follows:

$$\beta = \frac{\sqrt{D^*}g^{0.25}}{u_{mf}D_b^{0.25}} \tag{29}$$

D^*: Molecular diffusivity

D_b: Bubble diameter

The diffusion is said to be dominating if the value of $\beta > 10$, where the hydrodynamics do not cause a significant influence on the mass transfer. If $\beta < 0.1$, the mass transfer is dictated by convection and hence by hydrodynamics [83]. A rule of similarity in terms of the hydrodynamic properties was proposed by Horio et al. [83] at both small and larger reactor scales in which the properties such as diameter, height, etc. are varied according to the same proportions by a scale factor, m, which is linked to the ratios of bed diameter (D), bed height (h), bubble diameter (D_b) etc. according to the relation below:

$$m = \frac{D^l}{D^s} = \frac{h^l}{h^s} = \frac{D_b^l}{D_b^s} \tag{30}$$

In the above equation, ‘s’ and ‘l’ refer to the small and large reactor scales respectively.

Kelkar and Ng [84] added to the above methodology by studying scaling in which a chemical reaction was involved and therefore proposed a dimensionless mass transfer number (N_m) and a dimensionless reaction number (N_r). They linked their work to the work of Horio et al. [83] by means of the following relations:

$$N_r^l = \sqrt{m} N_r^s \tag{31}$$

For $\beta < 0.1$: $N_m^l = N_m^s$ (32)

For $\beta > 10$: $N_m^l = \frac{N_m^s}{m^{3/4}}$ (33)

Given that feed conversions and product distribution are affected in a scale-up process, Kelkar and Ng [84] also proposed a method of controlling the bubble size in the scale-up by maintaining hydrodynamic similarity where the bubble diameter is affected by the ratio, r_d, and is obtained as follows:

For $\beta < 0.1$: $r_d = m^{2/3}\left(\sqrt{m} + \left(\frac{N_m}{N_r}\right)^s \left(\sqrt{m} - 1\right)\right)^{2/3}$ (34)

For $\beta > 10$: $r_d = m^{2/7}\left(\sqrt{m} + \left(\frac{N_m}{N_r}\right)^s \left(\sqrt{m} - 1\right)\right)^{4/7}$ (35)

Hence, for most fluidized bed reactors, the bubble size needs to be maintained such that either $\beta > 10$ or $\beta < 0.1$ to keep the hydrodynamic similarity intact while performing scale-up.

2.2.5. Understanding carbon deposition

One of the biggest hurdles of DRM technology, as discussed earlier, is to minimize the deposition of carbon on the DRM catalyst. Solving this problem is not precisely

straightforward due to the tradeoffs involved in various aspects such as catalytic activity [20]. A variety of competing reactions occur concurrently in the DRM regime. Table 1 shows a comprehensive list of these competing reactions in DRM.

Table 1: List of competing reactions in DRM [85]

Reaction	ΔH_{298K} (kJ/mol)
$CH_4 + CO_2 \leftrightarrow 2CO + 2H_2$	+247
$CO_2 + H_2 \leftrightarrow CO + H_2O$	+41
$2CH_4 + CO_2 \leftrightarrow C_2H_6 + CO + H_2O$	+106
$2CH_4 + 2CO_2 \leftrightarrow C_2H_4 + 2CO + 2H_2O$	+284
$C_2H_6 \leftrightarrow C_2H_4 + H_2$	+136
$CO + 2H_2 \leftrightarrow CH_3OH$	−90.6
$CO_2 + 3H_2 \leftrightarrow CH_3OH + H_2O$	−49.1
$CH_4 \leftrightarrow C + 2H_2$	+74.9
$2CO \leftrightarrow C + CO_2$	−172.4
$CO_2 + 2H_2 \leftrightarrow C + 2H_2O$	−90
$H_2 + CO \leftrightarrow H_2O + C$	−131.3
$CH_3OCH_3 + CO_2 \leftrightarrow 3CO + 3H_2$	+258.4
$3H_2O + CH_3OCH_3 \leftrightarrow 2CO_2 + 6H_2$	+136
$CH_3OCH_3 + H_2O \leftrightarrow 2CO + 4H_2$	+204.8
$2CH_3OH \leftrightarrow CH_3OCH_3 + H_2O$	−37
$CO_2 + 4H_2 \leftrightarrow CH_4 + 2H_2O$	−165
$CO + 3H_2 \leftrightarrow CH_4 + H_2O$	−206.2

Four of these competing reactions in DRM, namely methane decomposition, carbon monoxide disproportionation (also known as Boudouard reaction), hydrogenation of carbon dioxide, and hydrogenation of carbon monoxide, contribute directly to carbon formation [85]. The reactions are listed below [85]:

Methane decomposition:

$$CH_4 \leftrightarrow C + 2H_2 \qquad \Delta H° = +74.9\ kJ.mol^{-1} \qquad (36)$$

Boudouard reaction:

$$2CO \leftrightarrow C + CO_2 \qquad \Delta H° = -172.4\ kJ.mol^{-1} \qquad (37)$$

Hydrogenation of carbon dioxide:

$$CO_2 + 2H_2 \leftrightarrow C + 2H_2O \qquad \Delta H° = -90.0\ kJ.mol^{-1} \qquad (38)$$

Hydrogenation of carbon monoxide:

$$CO + H_2 \leftrightarrow C + H_2O \qquad \Delta H° = -131.3\ kJ.mol^{-1} \qquad (39)$$

Given the thermodynamic nature of these reactions, temperature holds a crucial role in carbon deposition and limiting the impact of these undesirable reactions. Nikoo and Amin [85] found that only methane decomposition is favored at very high temperatures, whereas the other reactions occur at around 520 °C.

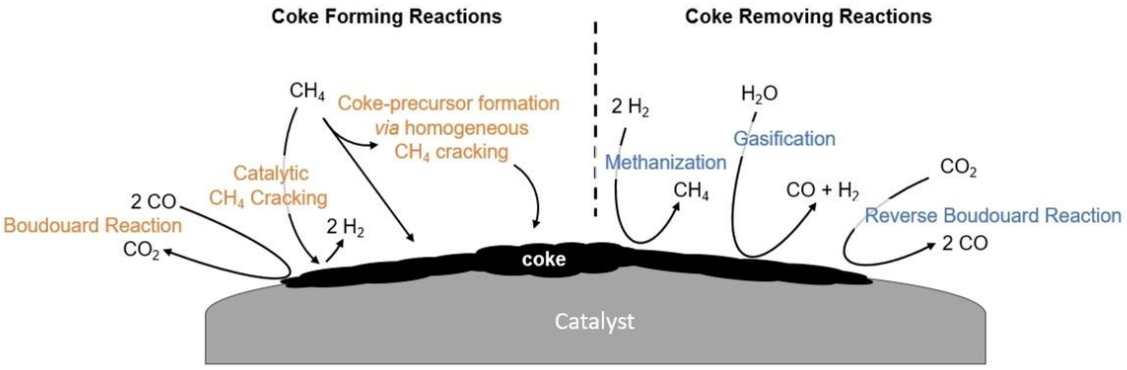

Figure 8: Summary of main reactions in coke deposition and removal from DRM catalysts [86]

Some major carbon forming and removing reactions can be found in Figure 8 above. In addition to the reactions mentioned above, the reverse-water gas shift (RWGS) reaction is also a critical side reaction as it diminishes the H_2:CO ratio to less than unity, and is given by [85]:

$$CO_2 + H_2 \leftrightarrow CO + H_2O \qquad \Delta H° = +41.0\ kJ.mol^{-1} \qquad (40)$$

Other studies such as that of Wang, Lu, and Millar [87] found that in the moderate temperature ranges of 550-700 °C, carbon deposition is mainly attributed to methane decomposition and the Boudouard reaction. Moreover, they also found that at temperatures above 820°C, Boudouard reaction and RWGS cease to exist as due to methane decomposition, the carbon species formed is highly reactive and readily oxidized by CO_2 [87]. Therefore, the crux lies in the fact that if carbon removal by CO_2 is equal to or faster than the formation of the said carbon, carbon deposition will be minimized, making higher temperatures as desirable for DRM [87]. However, attaining these temperatures is a highly energy-intensive process that is both economically and thermodynamically challenging to make DRM attractive as a practical industrial process.

These insights on carbon formation will be necessary while developing the appropriate reactor model to fully encapsulate the effect of DRM reaction and model the behavior for scaling the Ni-Cu catalyst more accurately.

3. RESEARCH PROBLEM AND OBJECTIVES

DRM presents a viable solution to monetize CH_4 and mitigate CO_2 emissions from the environment. The syngas produced from the DRM process can be used in FT synthesis or various other reactions. DRM yields a syngas ratio approximately around unity when compared to SRM. DRM is highly endothermic, and to make DRM industrially feasible, different catalysts have been explored. Ni-based catalysts are seen as economical, readily available and having an activity comparable to noble metal catalysts. However, due to side reactions, carbon formation is a major concern on these Ni-based catalysts, as discussed previously, thereby limiting their industrial viability. To address this challenge, previous studies in our research group were dedicated to developing novel catalytic systems that not only demonstrate better resistance to carbon formation but maintain activity due to the catalyst's redox properties on an atomistic level.

The problem addressed in this thesis is to study the scalability and carbon formation of the novel, medium loading Ni-Cu catalyst developed previously in our group. Moreover, to accomplish this goal, a novel approach of linking atomistic DFT insights with the macro-scale kinetics model was developed. The developed model's performance is shown to corroborate with experimental data, thereby proving its applicability for conducting scale-up studies. From this study, it is expected that the developed model will predict a lesser carbon formation for the novel Ni-Cu catalyst at different reactor scales.

Provided below are specific areas that form part of the problem statement of this work.

Problem 1: Is it possible to develop a 1-D model capable of predicting the performance of the medium loading Ni-Cu catalyst?

This problem will be addressed by developing a one-dimensional (1-D) pseudo-homogeneous reactor bed model using pure Ni catalyst that will incorporate the intrinsic lumped kinetics of DRM & SRM. The model will solve for the various transport, i.e., momentum, heat, and mass balances. The model will be able to generate conversion profiles for CH_4 and CO_2 and will be programmed to determine the carbon formation occurring in the reactor tube.

Problem 2: Would the results of the DFT kinetics improve the credibility of the macro reactor bed model?

As previously mentioned, the kinetic models are available for the pure Ni catalyst, but there are still not enough insights to determine the DRM kinetics for the Ni-Cu catalyst. Insights from DFT will be considered in a novel approach to utilize the rates of some elementary DRM reactions on the atomistic level and scale the kinetics for Ni catalyst to a bimetallic Ni-Cu catalytic system. The performance of Ni-Cu catalyst will be compared with the Ni catalyst using the 1-D model to determine if the novel approach is reasonable.

Problem 3: Does the novel medium Ni-Cu catalyst scale-up performance match the match the experimental results measured in our labs?

The 1-D model with Ni-Cu kinetics and Ni kinetics will first be validated against experimental results obtained by our research group on a laboratory scale to see the effect of changing various reaction parameters and obtain the conversion profiles. The model

will finally be scaled up from a laboratory scale to a bench scale to observe the performance of the 1-D model, especially with Ni-Cu catalyst in terms of carbon resistance and other parameter profiles to address this problem.

Addressing these questions is the base for the objectives of this study that can be described as follows:

- Generate transport equations to develop a 1-D pseudo-homogeneous model to solve reactor profiles at a suitable range of DRM operating conditions: pressure, temperature, and conversions.
- Implement insights available from DFT to investigate the micro-kinetic mechanism over an active site of mono-Ni catalyst and scale the kinetics for the Ni-Cu catalyst.
- Validate the developed 1-D model with experimental data for both the monometallic Ni catalyst and the bimetallic Ni-Cu catalyst using experimental data generated in our labs for different reactor setups.
- Perform scalability study using the 1-D model and process intensification methods to measure the performance of a Ni-Cu catalyst in terms of carbon resistance.

4. RESEARCH METHODOLOGY

As discussed in Section 3, the primary objective of this thesis involves combining theoretical and experimental work to develop a 1-D pseudo-homogeneous fixed bed reactor model for the scale-up of the novel carbon resistant, medium loading Ni-Cu catalyst. This section provides details on the approach undertaken to develop the mathematical model in MATLAB®. The discussion here concerns with providing details the development of the 1-D model initially for the pure Ni catalyst by incorporating the various transport equations for pressure (momentum), temperature (energy), and the flow rates (mass), as well as the lumped kinetics models available in the literature that were described previously. It also sheds light on how insights from DFT are used in a novel approach to scaling the kinetics from Ni catalyst to Ni-Cu for the 1-D model using reaction rates of elementary DRM reactions. A validation study will then be conducted to establish the accuracy of the developed model under various operational conditions against an extensive experimental campaign conducted to compare the performance of the medium loading Ni-Cu catalyst and the conventional Ni catalyst. Finally, the model will be scaled up to a larger diameter to test the carbon-resistance characteristic of the medium loading Ni-Cu catalyst and compare it with the conventional Ni catalyst.

4.1. Initial setup

Previously in our group, an existing reactor bed model had been developed by Challiwala et al. [17] using MATLAB® in a one-dimensional space. In the model, the conversions are only described for a unit reactor tube in the reactor. The reactor tube is

cylindrical in shape with the radius and length defined according to the reactor geometry in the experimental reactor setup, and is shown in Figure 9:

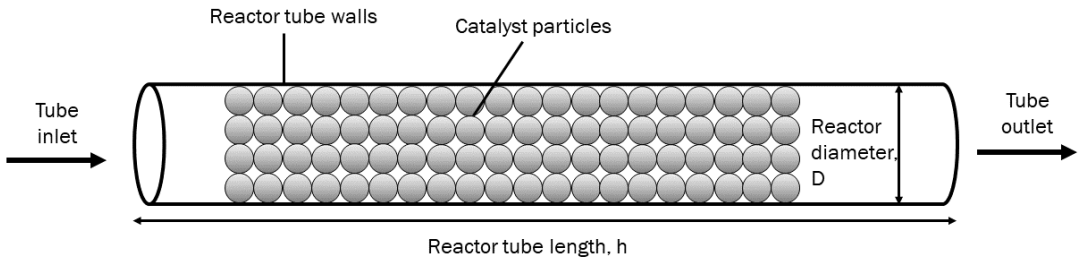

Figure 9: Reactor tube schematic used to develop the 1-D model

It is assumed that the conditions on the catalyst are the same as those on the passing fluid inside the reactor tube and hence, a pseudo-homogeneous model is considered. The weight of the catalyst inside the reactor tube is taken as the representative of the reactor length. All transport balances were done using one-dimensional correlations by only accounting for variations along the length of the reactor tube (axial directions). Radial and tangential variations were ignored due to the miniature scale of the setup at the laboratory level. Moreover, the primary concern of this model is to understand the overall conversions in the reforming process.

The 1-D pseudo-homogeneous model assumed negligible interfacial resistances to heat and mass transport between the solid (catalyst) and fluid (gas) boundaries. Due to this assumption, the effectiveness factor of the catalyst pellets inside the reactor tube is equal to one. Apart from the formation of carbon (which is a solid formed in this case), a single-phase gas flow is considered for the entering and exiting mixture of components.

In the existing developed model by Challiwala et al. [17], while the kinetics of SRM and DRM were implemented, the model lacked the use of necessary transport equations such as momentum, heat and mass balances. In addition to that, carbon formation was not accounted for in the existing model. Therefore, this study was concerned by implementing an existing reactor bed model with the accountability of carbon formation, which is described later in Section 4.5 as well the necessary transport equations. Moreover, the existing reactor bed model was optimized for the Ni catalyst, hence the Ni-Cu kinetics were also added by the approach of using DFT insights.

4.2. Implementing momentum and mass balances

A MATLAB® code was developed that solves for the various ordinary differential equations pertaining to the flow rates (F_j) of the various component species involved in the model. The 1-D model was first optimized for an isothermal, isobaric system with the following operating conditions and input parameters tabulated below in Table 2:

Table 2: List of operating conditions and input parameters for initializing the 1-D model

Initial pressure	$\mathbf{P_{tot0}}$	1 bar
Initial temperature	T_0	650°C = 923.15 K
Initial total mass flow rate (STP)	Q_{tot0}	30 ml/min
Initial mass flow rate of CH_4 (STP)	$Q_{CH_4,0}$	3 ml/min
Initial mass flow rate of CO_2 (STP)	$Q_{CO_2,0}$	3 ml/min
Initial mass flow rate of H_2O (STP)	$Q_{H_2O,0}$	0.00001 ml/min

Initial mass flow rate of He (STP)	$Q_{He,0}$	24 ml/min
Diameter of tube	D	1 cm = 0.01 m
Porosity of bed	Ø	0.60 [88]
Bulk density of catalyst	ρ_b	1422 kg/m^3 [89]
Diameter of catalyst particle	D_p	160 microns = 0.00016 m

CH_4, CO_2, H_2O, and helium (He) as inert were chosen as the inputs into the 1-D model. This initial flow consisted of 10% CH_4, 10% CO_2, and the remainder being He in all cases, as seen in the table above. The cross-sectional area of the reactor tube (A_t) was measured in m^2 by the relation $A_t = \frac{\pi D^2}{4}$.

Weight (W) of the catalyst was varied inside the catalyst between 1, 5 and 10 mg, and hence all transport equations were solved with catalyst weight (measured in grams, g, as independent parameter). The various conversion profiles were obtained, ranging from from 400 °C to 800 °C by changing the initial temperature in the code. The profiles could be converted to model along the reactor bed length (h) via the following equation to interchange between weight and length:

$$W = \rho_b \times A_t \times h \tag{41}$$

Since we are assuming the catalyst to fully occupy the reactor tube, the weight of the catalyst relates to the volume of the reactor (V) as well as the initial total volumetric flow (Q_{tot0}) at STP by means of gas hourly space velocity (GHSV) [90]:

$$GHSV = \frac{Q_{tot0}}{V} = \frac{Q_{tot0}}{W/\rho_b} \tag{42}$$

Moreover, the weight of the catalyst also helps to determine weight hourly space velocity (WHSV) by relating it to the initial total mass flow rate (MF_{tot0}) [91]:

$$\text{WHSV} = \frac{MF_{tot0}}{W} \tag{43}$$

The GHSV as well as WHSV will be helpful later to compare the results from an experimental point of view, especially, during assessing the scale-up of this model. Both quantities could be used as a tool to adjust the code accordingly to predict the conversions for a particular flow condition.

Ideal gas law was assumed to be valid to model the gases inside the reactor model. However, the model will have some form of non-ideality since DRM generally deals with high pressure and temperature. The non-ideality shall be accounted for in a future model with an appropriate equation of state such as Peng-Robinson Equation of State (PR EOS) or the Soave-Redlich-Kwong Equation of State (SRK EOS).

The initial component (I_i) and initial total (F_{tot0}) molar flow rates (measured in mol/hr), and initial mole fractions ($y_{init,i}$) were calculated as:

$$I_i = Q_{i,0} \times 60 \times \frac{\rho_i}{M_{m,i}}; \quad i = CH_4, CO_2, H_2O, He \tag{44}$$

$$F_{tot0} = I_{CH_4} + I_{CO_2} + I_{H_2O} + I_{He} \tag{45}$$

$$y_{init,i} = \frac{I_i}{F_{tot0}} \tag{46}$$

In the equations above, component density (ρ_i) is measured in g/L while the component molecular mass ($M_{m,i}$) is measured in g/mol.

4.3. Implementing pressure drop calculation

Pressure drop (measured in bar/g) accounts for the change in pressure along the reactor bed and is calculated via Ergun's equation [92], as shown below:

$$\frac{dP}{dW} = -\frac{\beta_0}{10A_t\rho_b}\left(\frac{P_{tot0}}{P}\right)\frac{T}{T_0}\frac{F_{tot}}{F_{tot0}} \quad (47)$$

β_0: Constant

A_t: Cross-sectional area of reactor tube

ρ_b: bulk density of catalyst

P_{tot0}: Initial total pressure inside reactor tube

P: Total pressure inside reactor tube

T: Temperature inside reactor tube

T_0: Initial temperature at reactor inlet

F_{tot}: Total molar flow rate inside reactor tube

F_{tot0}: Initial total molar flow rate at reactor inlet

Pressure drop first requires the gas densities (initial and instantaneous) to be calculated. To calculate the gas density at entrance conditions, the initial component molar fractions are converted to initial mass fractions ($x_{init,i}$) by first calculating initial total mass flow rate (MF_{tot0}) in g/hr:

$$MF_{tot0} = \sum_i\left(I_i M_{m,i}\right) \quad (48)$$

$$x_{init,i} = \frac{I_i M_{m,i}}{MF_{tot0}} \quad (49)$$

Hence the initial gas density (ρ_0) was calculated in kg/m^3 by the ideal gas equation, with temperature (T) measured in kelvin (K):

$$\rho_0 = 100 \times \frac{P_{tot0} \sum_i x_{init,i} M_{m,i}}{RT} \quad (50)$$

The universal gas constant, R, is taken to be 8.314 J/mol.K

The code in MATLAB® updates the component flow rates (F_j) upon each successful iteration by incorporating the products CO, H_2 as well as the elemental carbon, C. Therefore, to get the instantaneous gas density (ρ), the total molar flow rate (F_{tot}), component molar fractions (y_j), total mass flow rate (MF_{tot}) and component mass fractions (x_j) are calculated as follows:

$$F_{tot} = F_{CH_4} + F_{CO_2} + F_{H_2O} + F_{He} + F_{CO} + F_{H_2} + F_C \quad (51)$$

$$y_j = \frac{F_j}{F_{tot}}; \; j = CH_4, CO_2, H_2O, He, CO, H_2, C \quad (52)$$

$$MF_{tot} = \sum_j \left(F_j M_{m,j}\right) \quad (53)$$

$$x_j = \frac{F_j M_{m,j}}{MF_{tot}} \quad (54)$$

$$\rho = 100 \times \frac{P \sum_i x_{init,i} M_{m,i}}{RT} \quad (55)$$

The next step is to calculate the component volumetric flow rates (Q_j) in m^3/s by utilizing the component molar flow rates:

$$Q_j = \frac{F_j M_{m,j}}{3600 \rho_j} \quad (56)$$

By using the volumetric flow rates, the superficial velocity (u) in m/s and the superficial mass velocity (G) in $kg/m^2.s$ can be generated as follows [92]:

$$u = \frac{\sum_j Q_j}{A_t} \quad (57)$$

$$G = \rho u \quad (58)$$

Moreover, the partial pressures of each species, p_j (measured in bar, excluding carbon) were calculated as:

$$p_j = P\frac{F_j}{F_{tot}-F_C} \tag{59}$$

Before calculating the pressure drop, the viscosity of the gas mixture (μ) still needs to be evaluated. Since the system is dealing with low viscosities, the pure component viscosities (μ_i) of each gas can be calculated as per Chapman-Enskog theory at the specified reaction temperature. With an initial ambient temperature of 650 °C, data from [93] which is tabulated in Table 3 could be used, therefore:

Table 3: Pure component viscosities used for each component for viscosity calculations [93]

Species	Pure component viscosity, μ_i (kg/m.s)
CH_4	2.53×10^{-5}
CO_2	3.74×10^{-5}
H_2O	3.26×10^{-5}
He	4.18×10^{-5}
CO	3.86×10^{-5}
H_2	1.84×10^{-5}

After obtaining the pure component viscosities, the viscosity of the gas mixture (measured in kg/m.s) can be found by using Wilke's correlation [94]:

$$\mu = \sum_{i=1}^{n} \frac{\mu_i}{1+\frac{1}{y_i}\sum_{j=1}^{j=n} y_j \phi_{ij}}; \quad j \neq i \tag{60}$$

$$\phi_{ij} = \frac{\left[1+\left(\mu_i/\mu_j\right)^{\frac{1}{2}}\left(M_{m,j}/M_{m,i}\right)^{\frac{1}{4}}\right]^2}{\left(\frac{4}{\sqrt{2}}\right)\left[1+\left(M_{m,i}/M_{m,j}\right)\right]^{\frac{1}{2}}} \tag{61}$$

μ_i, μ_j: Viscosities of pure components in gas mixture

y_i, y_j: Mole fractions of pure components in the gas mixture

ϕ_{ij}: Dimensionless constant

$M_{m,i}, M_{m,j}$: Molecular weight of pure components in the gas mixture

Once the gas mixture's viscosity is obtained, the last step to calculate the pressure drop is by modeling the parameter, β_0 [92]:

$$\beta_0 = \frac{G(1-\emptyset)}{\rho_0 g_c D_p \emptyset^3}\left[\frac{150(1-\emptyset)\mu}{D_p} + 1.75G\right] \quad (62)$$

G: Superficial mass velocity

$\emptyset$: Porosity/void fraction

ρ_0: Initial gas density

g_c: Conversion factor (taken as 1.0 for metric units)

D_p: Diameter of catalyst particle

μ: Viscosity of gas mixture

Implementing β_0 in the Ergun's equation listed previously in Eq. 47 obtains the pressure profile inside the reactor tube.

4.4. Implementing energy balance

Due to reactions can be exothermic or endothermic, the temperature is an important parameter that affects the reactants' conversion profiles. Since the temperature change will subsequently bring about changes in pressure, an energy balance needs to be taken into account while modeling the reactor tube [92]:

$$\frac{dT}{dW} = \frac{\frac{Ua}{\rho_b}(T_a - T) + \sum_{i=1}^{q}(-r_{ij})[\Delta H_{Rxij}(T)]}{\sum_{j=1}^{m} F_j C_{P_j}} \quad (63)$$

where, U is the heat transfer coefficient for the reactor tube (measured in J/m^2.h.K) and is taken to be 1000 [95]. a is the heat exchange area per unit volume of the reactor (measured in m^{-1}) and is measured by the relation $a = \frac{4}{D}$ where *D* refers to the diameter of the reactor tube (measured in m).

r_{ij} refers to the rate of reaction for each of the seven reactions involved (measured in mol/g.h) while $\Delta H_{Rxij}(T)$ is the heat of each reaction (measured in J/mol). T_a is the initial ambient temperature at the start of the reactor (measured in K). These reactions are described in Section 4.5.

F_j and C_{P_j} refer to the flow rates (measured in mol/h) and heat capacities (measured in J/mol.K) of each component present in the reaction mixture, respectively. The heat capacities are a function of temperature (measured in K), and were calculated using the formulas obtained in literature for a gaseous mixture via the relations listed in Table 4 [96]:

Table 4: Heat capacity relations used for each component for energy balance calculation [96]

Species	Heat capacity relation, C_{P_j} (J/mol.K)
CH_4	$4.182 \times (5.34 + 0.0115T)$
CO_2	$4.182 \times (10.34 + 0.00274T - 195500T^{-2})$
H_2O	$4.182 \times (8.22 + 0.00015T - 0.00000134T^2)$
He	$4.182 \times (4.97)$
CO	$4.182 \times (6.60 + 0.00120T)$
H_2	$4.182 \times (6.62 + 0.00081T)$
C	$4.182 \times (2.673 + 0.002617T - 116900T^{-2})$

The above relations were incorporated into the equations above to develop an iterative procedure in the 1-D model where an entire temperature profile along the reactor can be obtained by specifying an initial temperature.

4.5. Implementing reaction kinetics

After an extensive literature review, and based on the wide applicability, the kinetic model of Xu and Froment [70] was used to model the SRM kinetics. To construct the 1-D model and implement the lumped kinetics, the SRM reactions were taken [70], namely:

Reaction-1 $CH_4 + H_2O \leftrightarrow CO + 3H_2$ (64)

Reaction-2 $CO + H_2O \leftrightarrow CO_2 + H_2$ (65)

Reaction-3 $CH_4 + 2H_2O \leftrightarrow CO_2 + 4H_2$ (66)

The above three reactions have the following reaction rates (all modeled in mol/g.h) [70]:

Reaction-1 $$r_1 = \frac{k_1}{p_{H_2}^{2.5}}\left(p_{CH_4}p_{H_2O} - \frac{p_{H_2}^3 p_{CO}}{K_1}\right)/(DEN)^2 \quad (23)$$

Reaction-2 $$r_2 = \frac{k_2}{p_{H_2}}\left(p_{CO}p_{H_2O} - \frac{p_{H_2}p_{CO_2}}{K_2}\right)/(DEN)^2 \quad (24)$$

Reaction-3 $$r_3 = \frac{k_3}{p_{H_2}^{3.5}}\left(p_{CH_4}p_{H_2O}^2 - \frac{p_{H_2}^4 p_{CO_2}}{K_3}\right)/(DEN)^2 \quad (25)$$

The denominator, DEN above, is defined as [70]:

$$DEN = 1 + K_{CO}p_{CO} + K_{H_2}p_{H_2} + K_{CH_4}p_{CH_4} + K_{H_2O}p_{H_2O}/p_{H_2} \quad (26)$$

It is already known that in the temperature range in which the 1-D model will operate, carbon formation will occur [85]. Therefore, apart from the kinetics of SRM, methane cracking (Reaction-C1), hydrogenation of carbon monoxide (Reaction-C2) and

Boudouard reaction (Reaction-C3) account for the formation of carbon and its subsequent gasification [73, 97], namely:

Reaction-C1 $CH_4 \leftrightarrow C + H_2$ (67)

Reaction-C2 $CO + H_2 \leftrightarrow C + H_2O$ (68)

Reaction-C3 $2CO \leftrightarrow C + CO_2$ (69)

The above three carbon formation reactions have the following reaction rates (all modeled in mol/g.h) [73, 97]:

Reaction-C1 $$r_{C1} = k_M^+ \widetilde{K}_{CH_4} \left(p_{CH_4} - \frac{p_{H_2}}{K_M^{\neq}}\right) / (DEN2)^2 \quad (70)$$

Reaction-C2 $$r_{C2} = \left(k_O^- K_{CO} p_{CO} - \frac{k_O^{+\prime}}{K_{O,H_2O}} \frac{p_{H_2O}}{p_{H_2}}\right) / (DEN2)^2 \quad (71)$$

Reaction-C3 $$r_{C3} = k_B^+ K_{CO-B} \left(p_{CO} - \frac{1}{K_B^*} \frac{p_{CO_2}}{p_{CO}}\right) / (DEN3)^2 \quad (72)$$

The denominators, DEN2 and DEN3 above, are defined as [73, 97]:

$$DEN2 = 1 + K_{CO} p_{CO} + \widetilde{K}_{CH_4} p_{CH_4} + \frac{1}{K_r''} p_{H_2}^{1.5} + \frac{1}{K_{O,H_2O}} \frac{p_{H_2O}}{p_{H_2}} \quad (73)$$

$$DEN3 = 1 + K_{CO-B} p_{CO} + \frac{1}{K_{O,CO_2} K_{CO-B}} \frac{p_{CO_2}}{p_{CO}} \quad (74)$$

The DRM reaction was considered as below by implementing the kinetics provided by Verykios [62]:

Reaction-4 $CH_4 + CO_2 \leftrightarrow 2CO + 2H_2$ (75)

The DRM reaction has the following reaction rate (all modeled in mol/g.h) [62]:

Reaction-4 $$r_4 = \frac{K_1' k_2' K_3' k_4 p_{CH_4} p_{CO_2}}{K_1' k_2' K_3' p_{CH_4} p_{CO_2} + K_1' k_2' p_{CH_4} + K_3' k_4 p_{CO_2}} \quad (76)$$

All the various constants used in Equations 23-26, 70-74 and 76, in addition to the heat of all seven modeled reactions, $\Delta H_{Rxij}(T)$, in Equations 64-66, 67-69 and 75, are all summarized in Table 5 [62, 70, 73, 97]:

Table 5: List of constants used in the equations used to model the lumped reaction kinetics [62, 70, 73, 97]

Parameter	Expression	Unit
$\mathbf{k_1}$	$4.225 \times 10^{15} \cdot e^{\left(\frac{-240100}{RT}\right)}$	$\frac{mol \cdot bar^{0.5}}{g \cdot h}$
$\mathbf{k_2}$	$1.955 \times 10^{6} \cdot e^{\left(\frac{-67130}{RT}\right)}$	$\frac{mol}{g \cdot h \cdot bar}$
$\mathbf{k_3}$	$1.020 \times 10^{15} \cdot e^{\left(\frac{-243900}{RT}\right)}$	$\frac{mol \cdot bar^{0.5}}{g \cdot h}$
$\mathbf{K_1}$	$e^{\left(\frac{-11650}{T}+13.076\right)}$	bar^2
$\mathbf{K_2}$	$e^{\left(\frac{1910}{T}-1.764\right)}$	-
$\mathbf{K_3}$	$e^{\left(\frac{-9740}{T}+11.312\right)}$	bar^2
$\mathbf{K_{CO}}$	$8.23 \times 10^{-5} \cdot e^{\left(\frac{70650}{RT}\right)}$	bar^{-1}
$\mathbf{K_{H_2}}$	$6.12 \times 10^{-9} \cdot e^{\left(\frac{82900}{RT}\right)}$	bar^{-1}
$\mathbf{K_{CH_4}}$	$6.65 \times 10^{-4} \cdot e^{\left(\frac{38280}{RT}\right)}$	bar^{-1}
$\mathbf{K_{H_2O}}$	$1.77 \times 10^{5} \cdot e^{\left(\frac{-88680}{RT}\right)}$	-
$\mathbf{k_M^+}$	$5.5619 \times 10^{4} \cdot e^{\left(\frac{-65053}{RT}\right)}$	$\frac{mol}{g \cdot h}$
$\mathbf{k_O^-}$	$1.33 \times 10^{-6} \cdot e^{\left(\frac{75955}{RT}\right)}$	$\frac{mol}{g \cdot h}$
$\mathbf{k_O^{+\prime}}$	$1.67 \times 10^{9} \cdot e^{\left(\frac{-148916}{RT}\right)}$	$\frac{mol}{g \cdot h}$
$\mathbf{k_B^+}$	$2.673 \times 10^{7} \cdot e^{\left(\frac{-108379}{RT}\right)}$	$\frac{mol}{g \cdot h}$

$\mathbf{K_{CO-B}}$	$e^{\left(\frac{-115}{R}\right)} \times e^{\left(\frac{92543}{RT}\right)}$	bar^{-1}
$\mathbf{K_B^*}$	$e^{\left(\frac{-170.44}{R}\right)} \times e^{\left(\frac{162483}{RT}\right)}$	bar^{-1}
$\mathbf{\widetilde{K}_{CH_4}}$	0.1099	bar^{-1}
$\mathbf{K_M^{\neq}}$	$e^{\left(\frac{142.5}{R}\right)} \times e^{\left(\frac{-123226}{RT}\right)}$	-
$\mathbf{K_{O,H_2O}}$	$1.7372 \times 10^4 \cdot e^{\left(\frac{-60615}{RT}\right)}$	-
$\mathbf{K_r''}$	$2.51893 \times 10^5 \cdot e^{\left(\frac{-95489}{RT}\right)}$	$bar^{1.5}$
$\mathbf{K_{O,CO_2}}$	$3.0190322 \times 10^7 \cdot e^{\left(\frac{-89805}{RT}\right)}$	bar
$\mathbf{K_1'k_2'}$	$2.61 \times 10^{-3} \cdot e^{\left(\frac{-4300}{T}\right)}$	$\frac{mol}{g \cdot s \cdot kPa}$
$\mathbf{K_3'}$	$5.17 \times 10^{-5} \cdot e^{\left(\frac{8700}{T}\right)}$	bar^{-1}
$\mathbf{k_4}$	$5.35 \times 10^{-1} \cdot e^{\left(\frac{-7500}{T}\right)}$	$\frac{mol}{g \cdot h}$
$\mathbf{\Delta H_1}$	224000	J/mol
$\mathbf{\Delta H_2}$	-37300	J/mol
$\mathbf{\Delta H_3}$	187500	J/mol
$\mathbf{\Delta H_{C1}}$	74870	J/mol
$\mathbf{\Delta H_{C2}}$	-131325	J/mol
$\mathbf{\Delta H_{C3}}$	173300	J/mol
$\mathbf{\Delta H_4}$	247000	J/mol

Upon doing an extensive literature review as described earlier, to find and model the reaction kinetics for the 1-D model, it was determined that the kinetics from Xu and Froment [70] model the kinetics of SRM accurately, while the kinetics of Verykios [62]

model achieve the same for DRM. Based on these kinetics, the various differential equations for the change in flow rate of species with respect to the weight of catalyst were set up in the MATLAB® code and were solved via the *ode15s* solver. Hence the mass conservation equation set was obtained as follows:

$$\frac{dF_{CH_4}}{dW} = -r_1 - r_3 - r_4 - r_{C1} \quad (77)$$

$$\frac{dF_{CO_2}}{dW} = r_2 + r_3 - r_4 + r_{C3} \quad (78)$$

$$\frac{dF_{H_2O}}{dW} = -r_1 - r_2 - 2r_3 + r_{C2} \quad (79)$$

$$\frac{dF_{He}}{dW} = 0 \quad (80)$$

$$\frac{dF_{CO}}{dW} = r_1 - r_2 + 2r_4 - r_{C2} - 2r_{C3} \quad (81)$$

$$\frac{dF_{H_2}}{dW} = 3r_1 + r_2 + 4r_3 + 2r_4 + 2r_{C1} - r_{C2} \quad (82)$$

$$\frac{dF_C}{dW} = r_{C1} + r_{C2} + r_{C3} \quad (83)$$

4.6. Implementing kinetics for medium loading Ni-Cu catalyst

The objective of developing 1-D model is to test the reaction profiles for the pure Ni catalyst and extend this model to incorporate other catalysts. As stated earlier, one such catalyst that we previously determined to possess reasonable carbon resistance in DRM environment is the bimetallic Ni-Cu catalyst [47]. In the code developed, the lumped kinetics of both DRM and SRM were implemented as described in the previous section. However, these kinetics are only available for pure Ni catalyst. As it stands, there is a knowledge gap to determine the precise kinetics for the bimetallic Ni-Cu catalyst.

Therefore, to get a more nuanced picture of carbon formation and how this formation affects the kinetics of the reforming system, especially for the synthesized bimetallic Ni-Cu catalyst, insights from DFT calculations were considered on the elementary carbon formation reaction. DFT is used to determine the energy barriers for various elementary reactions of DRM from a computational standpoint. Hence, to scale the intrinsic lumped kinetics from pure Ni to the synthesized Ni-Cu bimetallic catalyst, a novel approach has been implemented by creating an arbitrary factor that takes the carbon formation rates from the DRM elementary reactions into account. Hence, the elementary reactions by which carbon forms in the Ni-Cu catalyst need to be determined.

It has been illustrated by Omran et al. [46] that one of the significant sources by which carbon is formed on the surface of the bimetallic Ni-Cu catalyst is with the dissociation of the CH_4 molecule as it adsorbs on to the catalyst surface. The dissociation occurs as one H atom desorbs from the molecule, and the process continues until elemental carbon remains, in essence:

$$CH_4 \rightarrow CH_4* \tag{84}$$

$$CH_4* \rightarrow CH_3* + H* \tag{85}$$

$$CH_3* \rightarrow CH_2* + H* \tag{86}$$

$$CH_2* \rightarrow CH* + H* \tag{87}$$

$$CH* \rightarrow C* + H* \tag{88}$$

Another source of carbon formation on the DRM catalyst has been via the CO2 molecule as its eventual disintegration gives:

$$CO* \rightarrow C* + O* \tag{89}$$

The rate of the elementary reaction CO* → C* + O* was incorporated into r_{C3} (Eq. 65) while the rate for CH* → C* + H* was incorporated into r_{C1} (Eq. 63). This incorporation was done using rate constants, as an empirical factor was obtained to account for the change in carbon formation into these reactions during the simulation of the code for the bimetallic Ni-Cu catalyst. This approach is unique that has not been done previously in the literature. The rate constants for the kinetics of pure Ni catalyst were obtained via the work achieved by Fan et al. [98], which were available at a temperature of 700 °C. The rate constants for the two carbon formation reactions from the work of Omran et al. [46] were interpolated at the same temperature of 700 °C to develop the empirical factor. The results are provided in the Table 6:

Table 6: Rate constants calculated for the coking reactions on both pure Ni and Ni-Cu bimetallic catalysts [46, 98]

Reaction	Catalyst	Rate constant, k (s^{-1})
CO* → C* + O*	Pure Ni	3.69×10^{-3}
CO* → C* + O*	Bimetallic Ni-Cu	1.04×10^{-3}
CH* → C* + H*	Pure Ni	3.18×10^{7}
CH* → C* + H*	Bimetallic Ni-Cu	4.75×10^{6}

Therefore, the empirical factor, EF, obtained for both coking reactions can be obtained as follows:

$$EF_{CO^*} = \frac{k_{CO^*}(Ni - Cu)}{k_{CO^*}(Ni)} = 2.83 \times 10^{-1}$$

$$EF_{CH^*} = \frac{k_{CH^*}(Ni - Cu)}{k_{CH^*}(Ni)} = 1.49 \times 10^{-1}$$

When calculating the conversion profiles for the Ni-Cu catalyst, the rate of reaction of r_{C1} (Eq. 70) is multiplied by EF_{CH^*} while the rate of r_{C3} (Eq. 72) is multiplied by EF_{CO^*} to capture the effect of incorporating Cu in a Ni catalyst via the developed 1-D model.

4.7. Scaling up DRM reactor

The main aspect of this work is to utilize the 1-D pseudo-homogeneous model to perform scalability assessment for the DRM process. The objective is to assess the feasibility of such a model from an industrial perspective and to be use as a guide to predict the carbon formation using the novel medium loading Ni-Cu catalyst developed previously in our group. Earlier in Section 2.2.4, a comprehensive strategy for achieving scale-up was described using dimensional analysis correlations. One correlation was the usage of a scale factor, m, as described by Kelkar and Ng [84] using ratio of the bed diameters (D) at both small and larger reactor scales. Assuming that the bed diameter is equivalent to the tube diameter, the scale factor for the scale-up from lab scale ($D = 1$ cm) to bench scale ($D = 2.2$ cm) is given as:

$$m = \frac{D^l}{D^s} = \frac{2.2\ \text{cm}}{1\ \text{cm}} \cong 2$$

The methodology proposed by Kelkar and Ng [84] is provided and intended for scaling-up to commercial scales ($m \geq 16$). Since the scale factor obtained for our intended scale-up is far behind the commercial scale, therefore such strategies of dimensional analysis are not applicable for the developed 1-D model. However, should this 1-D model be further modified by advanced multiscale modeling which includes radial and tangential variations, then a proper dimensional analysis could be performed to achieved scale-up.

Since our objective is more concerned with comparing with the pilot scale results available, a scale-up has only been achieved in a more physical sense by scaling-up the tube diameter. In the scale-up, it is assumed that the catalyst particles are unchanged in size from the lab scale and all other assumptions mentioned previously in Section 4.1 are maintained for scale-up. Hence, as previously described, GHSV and WHSV will be important tools while assessing the scalability of the 1-D model. Figure 10 below summarizes the scale-up schematic.

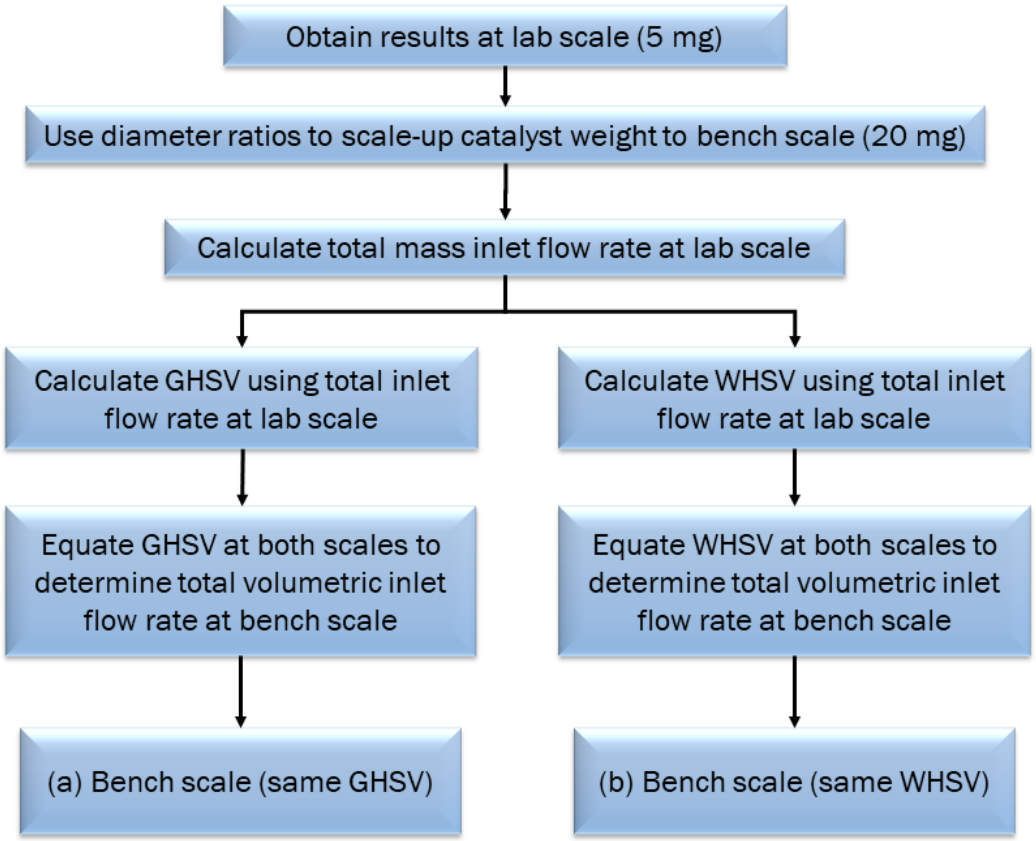

Figure 10: Step-by-step procedure describing how scale-up will be achieved by creating two different data sets (a) and (b) with different conditions.

All results achieved up until this point are obtained by considering the tube diameter (D) as 1 cm for the laboratory scale. For the bench scale, a tube diameter of 2.2 cm will be considered. Therefore, the next step is to scale the catalyst weight and adjust the reactor inlet parameters accordingly. By determining the amount of catalyst at the bench scale, the factor between the diameters at both the scales needs to be assessed. To ensure consistency, the scale-up is achieved based on the results obtained at catalyst weight of 5 mg used during laboratory experiments performed by Chatla et al. [47] in our research team. The mass of catalyst was scaled up by following a step-by-step procedure:

$$\frac{D_{\text{bench scale}}}{D_{\text{lab scale}}} = \frac{2.2\ \text{cm}}{1\ \text{cm}} \cong 2$$

Hence,

$$\frac{A_{t-\text{bench scale}}}{A_{t-\text{lab scale}}} = \frac{\frac{\pi}{4} \times (D_{\text{bench scale}})^2}{\frac{\pi}{4} \times (D_{\text{lab scale}})^2} = 4$$

Since the catalyst weight is scaled up at the same characteristic reactor length (h), the mass of catalyst is scaled-up accordingly:

$$\frac{W_{\text{bench scale}}}{W_{\text{lab scale}}} = \frac{\rho_b \times V_{\text{bench scale}}}{\rho_b \times V_{\text{lab scale}}} = \frac{h \times A_{t-\text{bench scale}}}{h \times A_{t-\text{lab scale}}} = 4$$

Therefore, the mass of catalyst at the bench scale is taken to be as 5×4=20 mg. Following the procedure outlined in our previous publication by Challiwala et al. [21], two sets of results at the bench scale will be generated using the 1-D model for both pure Ni and Ni-Cu catalysts: (a) for 20 mg at the same GHSV as lab scale, by adjusting total inlet flow rate, and (b) for 20 mg at the same WHSV as lab scale, by adjusting total inlet flow rate.

(a) Bench scale – maintaining same GHSV

All inlet conditions and parameters will remain constant as mentioned in Table 2 except for changes in total inlet mass flow rate (STP) for (a) and (b), which determines the changes in component inlet flows. To determine these for (a) and (b), both GHSV and WHSV needs to be calculated from the results obtained at laboratory scale.

Firstly, the GHSV is calculated as follows:

$$\mathrm{GHSV} = \frac{Q_{tot0}}{W/\rho_b} = \frac{30\,\frac{\mathrm{ml}}{\mathrm{min}} \times \frac{60\ \mathrm{min}}{1\ \mathrm{hr}} \times \frac{1\ \mathrm{m^3}}{1 \times 10^6\ \mathrm{ml}}}{\frac{5\ \mathrm{mg} \times \frac{1\ \mathrm{kg}}{1 \times 10^6\ \mathrm{mg}}}{1422\ \frac{\mathrm{kg}}{\mathrm{m^3}}}} = 511920\ \mathrm{hr^{-1}}$$

Moreover, for the results at 5 mg on laboratory scale, the characteristic length, h was found to be 4.48×10^{-5} m.

Therefore, the total mass inlet flow rate (STP) for (a) can be calculated as shown below:

$$\mathrm{GHSV}_{\text{lab scale}} = \mathrm{GHSV}_{\text{bench scale}}$$

$$\frac{30\ \frac{\mathrm{ml}}{\mathrm{min}}}{\frac{\pi}{4} \times (1\ \mathrm{cm})^2 \times \mathrm{h}} = \frac{\mathrm{x}}{\frac{\pi}{4} \times (2.2\ \mathrm{cm})^2 \times \mathrm{h}}$$

The total inlet flow rate was found to be 145.2 ml/min and based on this, the component inlet flow rates were adjusted, mentioned later in Table 8, by keeping the component ratio similar as the one in lab scale.

(b) Bench scale – maintaining same WHSV

To obtain the total inlet flow rate for (b), firstly the total mass inlet flow rate needs to be determined. This can be achieved using the standard gas densities for each of the inlet components at the laboratory scale (the inlet flow rate of H_2O was unchanged since

it is very small in comparison to other components in the feed) and hence the following is obtained, tabulated in Table 7:

Table 7: Mass inlet flow rates for various components during WHSV scale-up

Species	Mass inlet flow rate (STP), ml/min	Mass inlet flow rate, g/hr
CH_4	3	0.1289
CO_2	3	0.3559
He	24	0.2572
TOTAL	**30**	**0.7419**

Therefore, the WHSV is calculated as follows:

$$\text{WHSV} = \frac{\text{MF}_{\text{tot0}}}{\text{W}} = \frac{0.7419\ \frac{\text{g}}{\text{hr}}}{5\ \text{mg} \times \frac{1\ \text{g}}{1000\ \text{mg}}} = 148.4\ \text{hr}^{-1}$$

Therefore, the total mass inlet flow rate for (c) can be calculated as shown below, which is found to be 2.968 g/hr:

$$\text{WHSV}_{\text{lab scale}} = \text{WHSV}_{\text{bench scale}}$$

$$148.4\ \text{hr}^{-1} = \frac{\text{x}}{20\ \text{mg} \times \frac{1\ \text{mg}}{1000\ \text{g}}}$$

Based on the total mass inlet flow rate, and using the standard gas densities, the total inlet flow rate for (c) was found to be 120 ml/min.

The change in inlet flows for the various scale-up sets are summarized below in Table 8:

Table 8: Summary of total inlet flow rates used for the various scale-up assessments

		Lab scale – 5 mg	Bench scale – same GHSV (a) (STP)	Bench scale – same WHSV (a) (STP)
Initial total mass flow rate (STP)	Q_{tot0}	30 ml/min	145.2 ml/min	120 ml/min
Initial mass flow rate of CH_4 (STP)	$Q_{CH_4,0}$	3 ml/min	14.52 ml/min	12 ml/min
Initial mass flow rate of CO_2 (STP)	$Q_{CO_2,0}$	3 ml/min	14.52 ml/min	12 ml/min
Initial mass flow rate of He (STP)	$Q_{He,0}$	24 ml/min	116.16 ml/min	96 ml/min

5. RESULTS AND DISCUSSION

This section will describe the results based on the calculations conducted on MATLAB® to develop a 1-D pseudo-homogeneous model. Conversion profiles for CH_4 and CO_2 obtained from the 1-D model for both pure Ni and medium loading Ni-Cu systems were first compared against thermodynamic data. These conversions were then compared against experimental results for synthesized pure Ni and medium loading Ni-Cu catalysts in addition to the industrial 20 wt% Ni/γ-Al_2O_3 (Riogen) catalyst at various diluent loadings as shown in Table 9. Comparison with experimental results shows reasonable agreement of the model with the experimental data, especially for CH_4 conversions. Two factors, the weight of catalyst and the total volumetric inlet flow rate, are then compared with the obtained results, and the results show that the 1-D model follows the effect of altering these factors on the CH_4 conversion reasonably well in line with theoretical expectation. Next, scaling the reactor is achieved at a bench scale (2.2 cm ID) from the lab scale (1 cm ID) results. In addition to obtaining conversions, some light is shed on the predictability of carbon formation at the bench scale. The results show agreement in line with theoretical expectations and the conversions show reasonable predictability of the 1-D model at bench scale.

5.1. Validation with thermodynamic data

The written code in MATLAB® was run to obtain the conversion rates for CH_4 and CO_2 from the 1-D model. Conversions were obtained over a range of temperatures from 400 °C to 800 °C. Profiles were generated along the bed length calculated as a function of

the weight of the catalyst from 1 mg to 10 mg for both pure Ni and the medium loading Ni-Cu bimetallic catalysts. In order to assess the validity of the model, the profiles were obtained on isothermal conditions, which assumes that the entirety of the reactor tube is maintained at a particular specified temperature, as in the case of experimental setup at TAMUQ [99]. Apart from the conversions obtained from the kinetic 1-D model prepared in MATLAB®, conversions obtained from thermodynamic data were also obtained at the same inlet conditions. These conversions from thermodynamic equilibriums were calculated via the methodology using Gibbs free energy minimization that was described previously in the group by Challiwala et al. [17] for each temperature and were plotted against the conversions obtained from the 1-D model. The conversion profiles for CH_4 and CO_2 can be found below in Figure 11 and Figure 12, respectively.

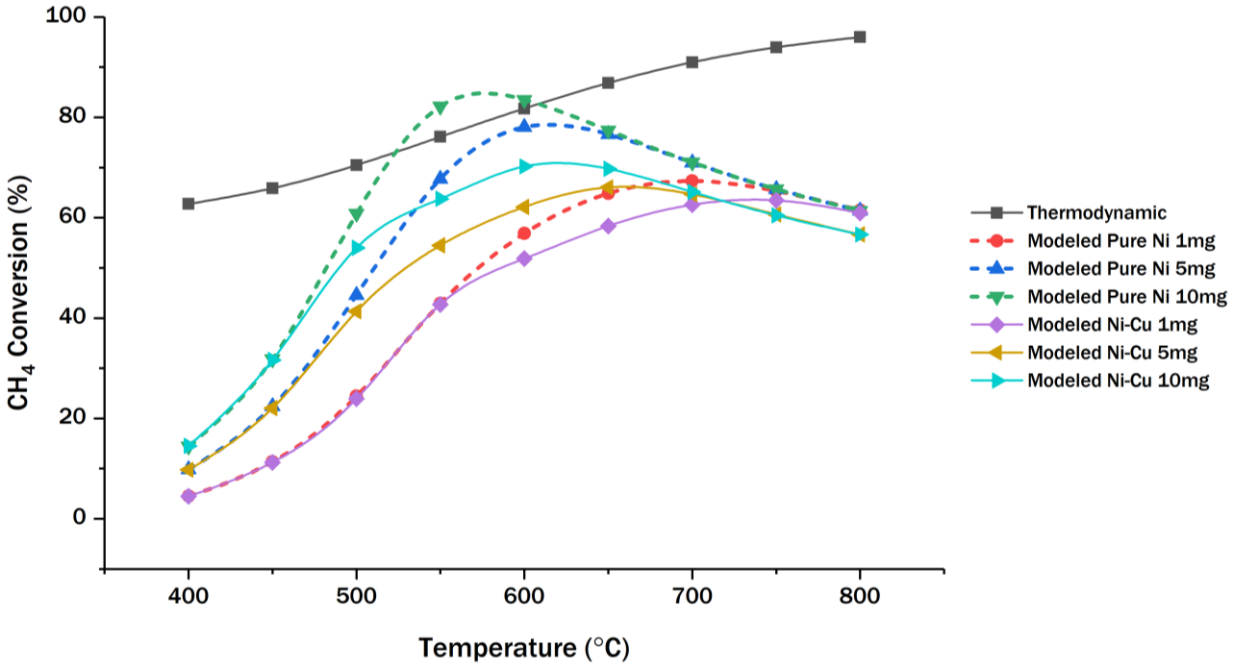

Figure 11: CH_4 conversions obtained from 1-D model for various catalysts at different weights

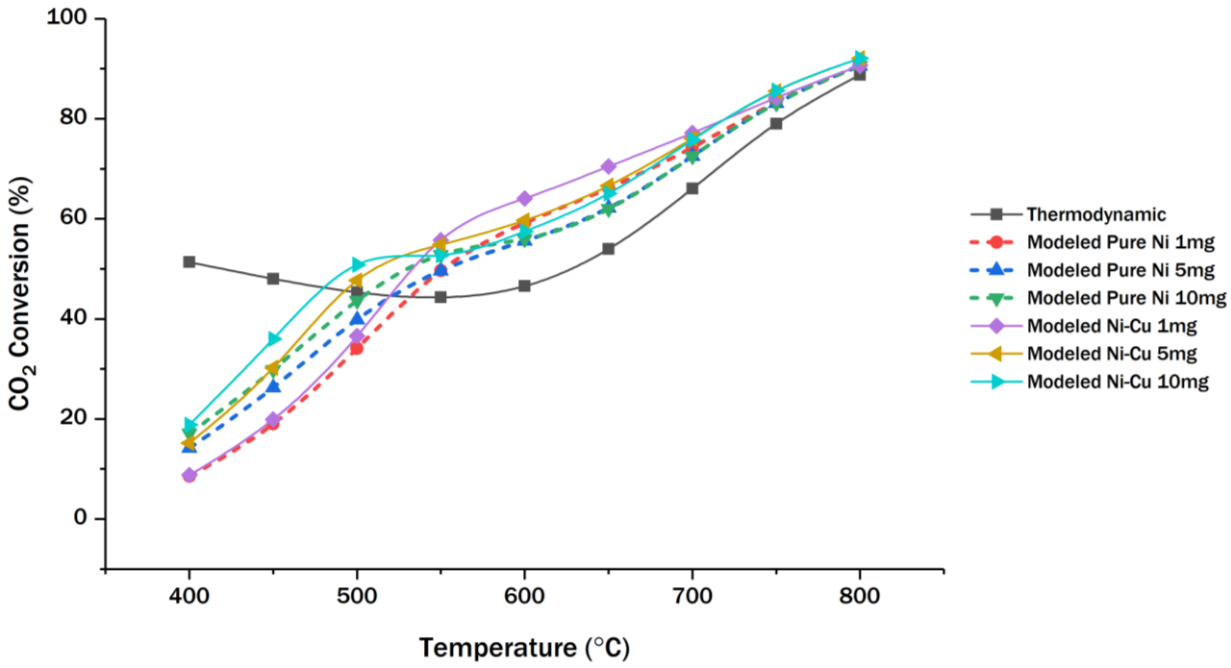

Figure 12: CO_2 conversions obtained from 1-D model for various catalysts at different weights

For CH_4, as seen in Figure 11, the conversions obtained from the 1-D model follow a peak where the highest peaks are obtained near approximately 575 °C for 10 mg of pure Ni and 610 °C for 10 mg of Ni-Cu catalyst. The differences in the peaks for both catalysts can be explained by the nature of the equilibrium reactions taking place on the catalytic surface which in turn is affected by the different kinetics of both the catalysts. The conversions for pure Ni are higher towards the peak, reaching almost 84% for 10 mg whereas in the Ni-Cu catalyst, the highest peak reaches approximately 70% for 10 mg. Interestingly, at a temperature of 600 °C, the predicted conversion at 10 mg of pure Ni is approximately 83.5%, which is the closest to the thermodynamic conversion of 82% at the same temperature: bearing a 1.8% difference. Therefore, pure Ni at 10 mg data is only relatively close to the thermodynamic data around the catalytic DRM regime of 550-650

°C whereas in other temperatures, the thermodynamic conversions differ vastly from the ones predicted by the model. It should be noted that for CH_4, the thermodynamic conversions keep increasing in almost, a linear manner, as the temperature increases. From Figure 11 above, the conversions for CH_4 obtained from the 1-D model are lower than those obtained from thermodynamic data, all except the case of pure Ni at 10 mg, in which the modeled conversion slightly exceeds the one predicted from thermodynamic equilibrium.

Conversions for CO_2 show a different trend than CH_4. As seen in **Error! R eference source not found.**, for CO_2, from the model, as the temperature increases, the conversion of CO_2 increases in all cases. For CO_2, however, the conversions from the 1-D model are lesser than thermodynamic data below 470 °C, after which the predicted conversions are higher than those obtained via thermodynamic data as seen in Figure 12 above. The conversions obtained from the 1-D model have slight differences between 400-500 °C, with highest conversion being predicted for Ni-Cu catalyst at 10 mg. After 550 °C, conversions from the 1-D model increase slightly more for the Ni-Cu catalyst at 1 mg than other catalytic data. The conversion of CO_2 is slightly more for the medium loading Ni-Cu catalyst than pure Ni catalyst for all temperatures. Conversions from thermodynamic data keep decreasing until they reach a minimum of around 44% at approximately 575 °C, after which they increase again. At 575 °C, Ni-Cu catalyst at 1 mg exhibits the highest conversion of about 60% from the kinetic data, whereas pure Ni catalyst at 5 mg exhibits a conversion of approximately 52%. This conversion of 52% is the closest the kinetic data gets to the thermodynamic data gets at the same temperature of

575 °C, bearing a difference of about 18.1%. Between 475-575 °C, the data from the 1-D model comes in close agreement with the conversions obtained from thermodynamic data at a range of about 44-47%. Around the catalytic DRM regime of 550-650 °C, the Ni-Cu catalyst at 1 mg exhibits the highest conversions.

The differences in the conversions for both CH_4 and CO_2 between the ones obtained from thermodynamic data and the ones predicted by the 1-D model can be explained by the nature of the model. At the moment, the model does not account for all the side reactions that occur in DRM and only utilizes the major reactions, especially for carbon formation, i.e. methane cracking, the hydrogenation of CO and the Boudouard reaction. These other side reactions, which are described in Table 1, are accounted for in the thermodynamic equilibrium. Due to the lack of kinetic models available for those side reactions, they were not accounted for in the developed 1-D model. However, if those side reactions are implemented in the developed 1-D model, then the conversions predicted by the model, will probably come in close agreement with the thermodynamic equilibrium. The exact effect of all reactions on DRM with the variation in temperature or catalyst weight however is not yet determined and more work is required to determine the precise effect of varying those parameters on the influence of each side reaction.

Another important factor that affects the conversions obtained from the model is the accountability of non-ideality. Since the model assumes negligible interfacial resistances between the catalyst and the reactant gas that flows inside the reactor, it assumes that the model is in ideal gas conditions. However, in the thermodynamic equilibrium, the effect of non-ideality was included by using the Peng-Robinson equation

of state. Therefore, if the effect of non-ideality is included in the model by means of an appropriate equation of state such as Peng-Robinson (PR) etc., the discrepancies between the modeled conversions and the ones obtained from thermodynamic data might be reduced.

It should be noted that at temperatures beyond 650 °C, the thermodynamic equilibrium is expected to dominate the DRM reaction [17]. Since commercial processes can end up at temperatures of beyond 1000 °C, therefore the idea of using DRM is to lower the temperature requirement so that no CO_2 is produced from using higher temperatures.

Before moving towards assessing validation of the 1-D model with experimental data, it was considered to compare the results from the developed 1-D model with existing DRM models. Various reactor bed modeling studies such as those by Yang and Twaiq [100] or by Benguerba et al. [77] had been conducted where Ni/Al_2O_3 was used as a catalyst and both studies had used the kinetic model of Richardson and Paripatyadar [48] for the DRM reaction. Both modeling studies [77, 100] were carried out at larger scales, where a higher inlet flow rate was used than the developed 1-D model and the catalyst loading varied between 200 mg to 200 g of catalyst. At these higher catalyst loadings, the results of these studies were closer to thermodynamic equilibrium results that were mentioned previously. Since our developed 1-D model had used a very less catalyst weight (5 mg) in comparison to these studies, the developed 1-D model was in the kinetic regime and therefore was not able to get the results very close to the thermodynamic profile.

5.2. Validation with experimental data

After assessing the validation of the predicted conversions from the 1-D model with thermodynamic data, the next step was to validate the conversions obtained from the 1-D model with experimental data. An experimental campaign was conducted previously by our research group on both, synthesized pure Ni and medium loading Ni-Cu catalytic systems along with the industrial 20 wt% Ni/γ-Al_2O_3 (Riogen) catalyst inside a bench top reactor at the TAMUQ laboratory.

5.2.1. Experimental setup

The model itself was built initially on a lab scale to mirror the setup present in the TAMUQ laboratory. The experimental campaign for DRM was carried out in a Micromeritics benchtop reactor in which a vertical quartz reactor was kept at a pressure of 1 bar (with 0.9 cm ID). Approximately 5.5 mg of the catalyst was used with various amounts of sand (SiO_2) as the diluent. The reactant gas comprised of CH_4:CO_2:He = 1:1:8 in addition to hydrogen used as a reducing gas. The reaction was performed at 650 °C and the catalyst was reduced *in-situ* with pure hydrogen at the same temperature for approximately 1 h. The total inlet flow rate (STP) of the reactant gas was set to 30 ml/min [47]. Data was analyzed at every 3 seconds. For comparison, the conversions at a TOS of 10 h were considered in case of the in-house synthesized pure Ni and Ni-Cu catalysts. For the Riogen catalyst, since the catalyst underwent rapid deactivation, therefore only the starting maximum conversion was considered. The effluent gas from the reactor was analyzed by a Cirrus 2 Mass spectrometer [47]. A diagram schematic of the experimental reactor setup is shown in Figure 13.

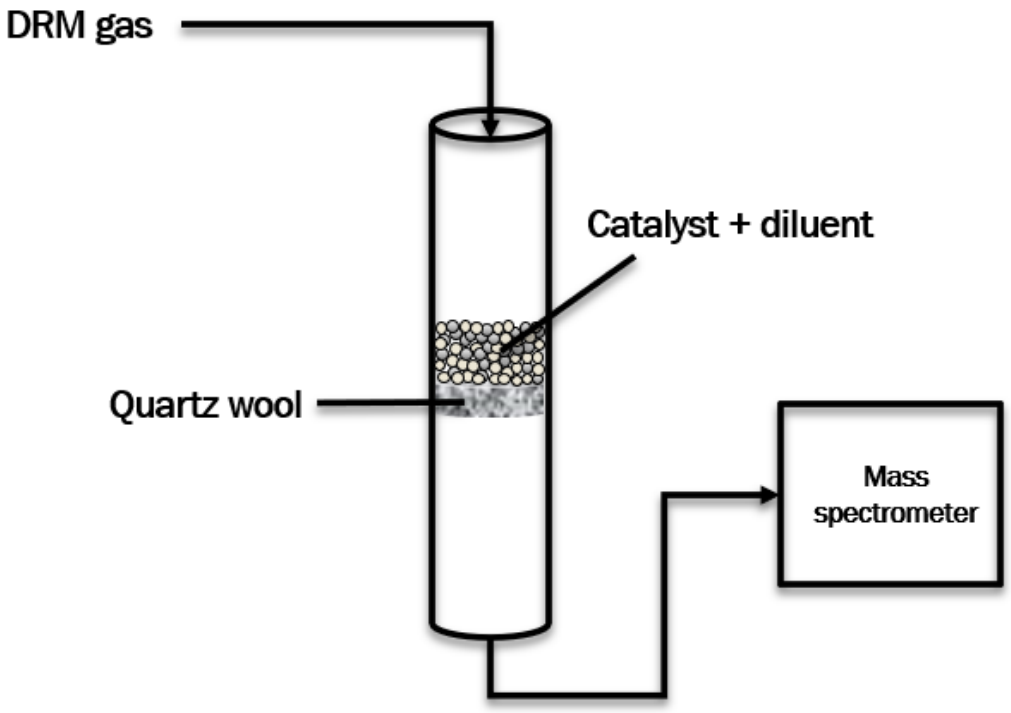

Figure 13: Schematic of the experimental setup to determine the DRM feed conversions

5.2.2. Comparing conversions

Data from the 1-D model was therefore also compared at the similar conditions with catalyst weight of 5 mg and the tube diameter being set to 1 cm. The experiments were carried out using industrial Riogen (pure Ni catalyst) at various diluent loadings, and both synthesized pure Ni and Ni-Cu catalysts at different loadings, which are summarized in Table 9 below.

Table 9: Summary of various catalysts studied in experimental campaign

Catalyst type	Diluent (sand) loading
20 wt% Ni/γ-Al_2O_3 (Riogen)	25 mg
20 wt% Ni/γ-Al_2O_3 (Riogen)	100 mg
20 wt% Ni/γ-Al_2O_3 (Riogen)	250 mg

Pure Ni, 20 wt%	100 mg
Medium loading Ni-Cu, 20 wt%	100 mg

The catalysts mentioned in Table 9 above are known catalysts used for DRM reaction and therefore to test the validity of the 1-D model, the conversions obtained from experimental data using these catalysts were plotted against the conversions obtained for both CH_4 and CO_2 from the 1-D model, as shown below in Figure 14 and Figure 15, respectively.

Results from the catalysts studied via the experimental campaign had an uncertainty of about ±5% from the reported conversion values. The conversion results from the experimental campaign slightly fluctuate as time progresses but the overall profile is relatively stable, therefore, to compare the data, the stable profile is taken as an average of the multiple data points obtained at 650 °C. This is because the model developed assumes the reactor has reached a steady-state and those conversions are then taken for comparison.

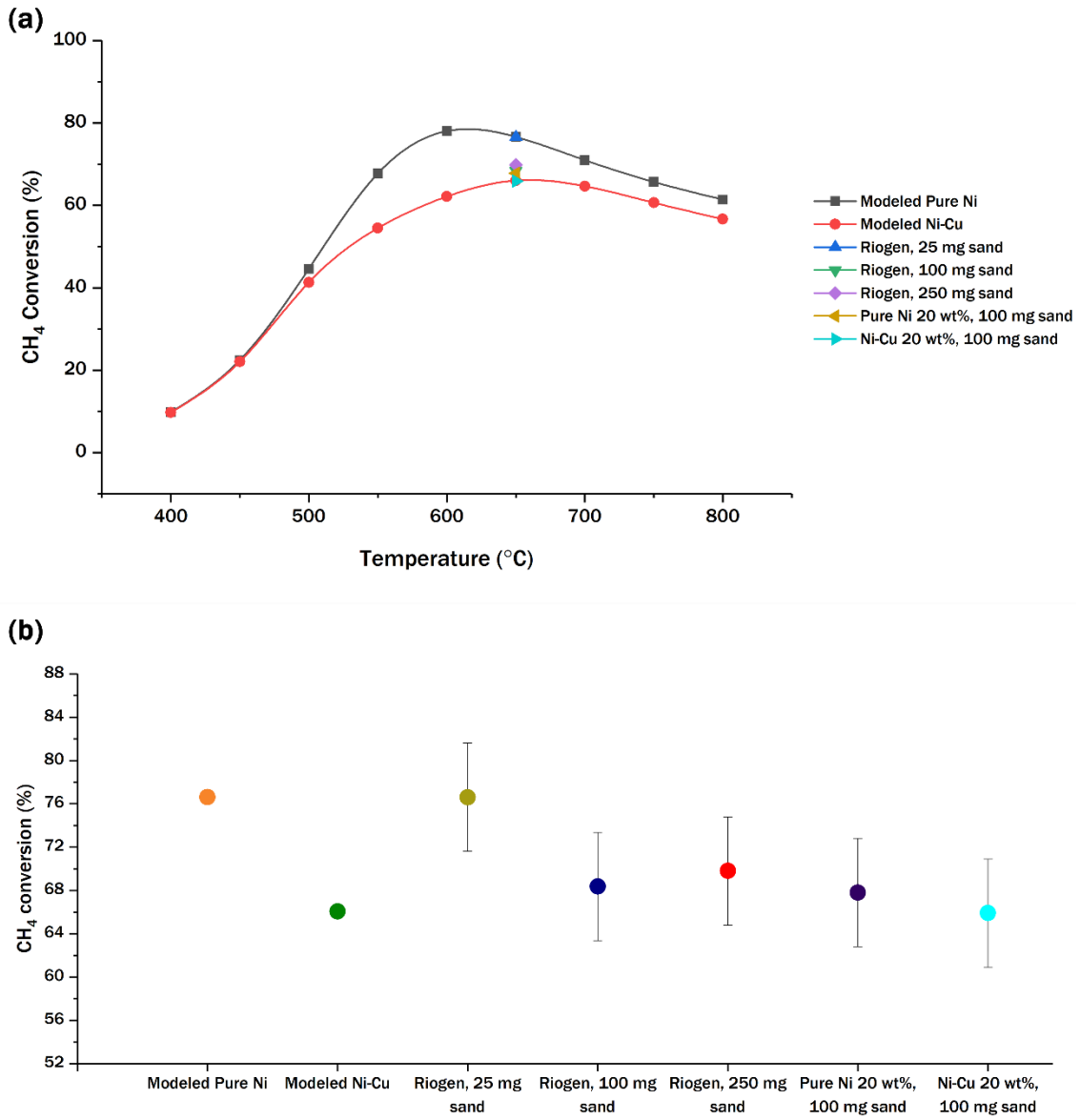

Figure 14: Comparison of CH4 conversions obtained from 1-D model (a) with experimental results for various catalysts (b) at a more focused view at 650 °C

At the conditions fixed as described before (30 ml/min total volumetric inlet flow at STP, 5 mg catalyst weight and 650 °C), for the CH_4 conversions, the 1-D model provides a conversion of about 77% for pure Ni catalyst which comes in reasonable agreement to the conversion obtained via 20 wt% Ni/γ-Al_2O_3 (Riogen) with 25 mg sand.

Simultaneously, the conversion reported by the 1-D model comes to about 66% for medium loading Ni-Cu catalyst also is in certain agreement of 66% obtained by the experimentally synthesized Ni-Cu catalyst at 20 wt%, considering that the experimental conversions have some uncertainties. It should be noted that all conversions obtained from experiments, just like the 1-D model, are lower from the thermodynamic conversions. All the other conversions obtained from experiments at 650 °C, apart from come in close agreement with the modeled conversions, lie within the conversions obtained from the 1-D model. These results highlight the fact that the CH_4 conversions are represented to a good degree by the 1-D model.

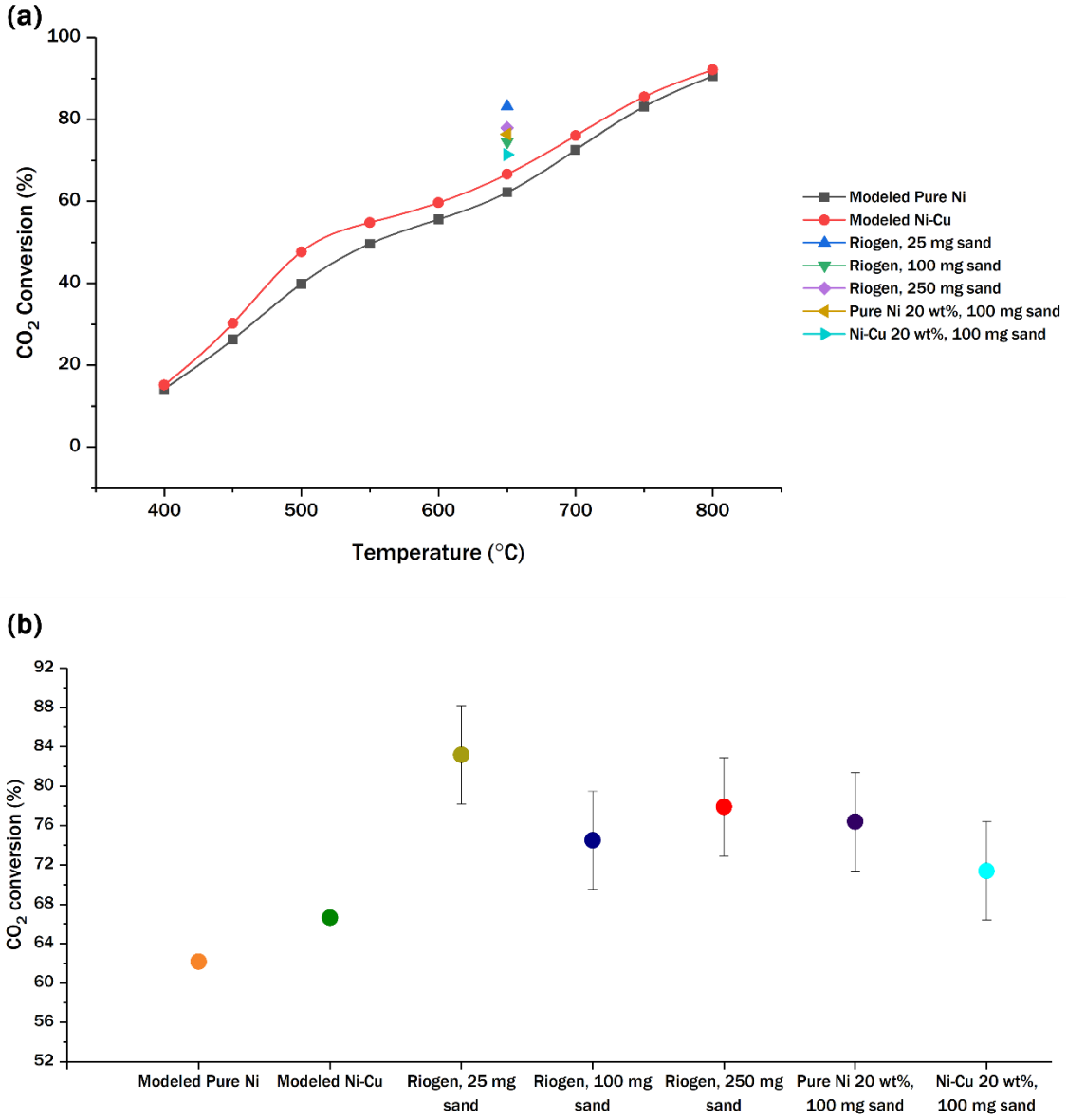

Figure 15: Comparison of CO_2 conversions obtained from 1-D model (a) with experimental results for various catalysts (b) at a more focused view at 650 °C

For CO_2, the 1-D model predicts a conversion of about 62% for pure Ni catalyst and comes closest to the conversion of about 75% obtained via the 20 wt% Ni/γ-Al_2O_3 (Riogen) with 100 mg sand; bearing a difference of 17.3%. Simultaneously, a conversion

of 67% is reported by the 1-D model for medium loading Ni-Cu catalyst. The experimentally synthesized Ni-Cu catalyst at 20 wt% is closest to the predicted conversion from the model, with a conversion of about 71%; bearing a difference of 5.63%. Hence it could be said that CO_2 conversions have some considerable difference between the experimentally obtained conversions and the ones predicted from the 1-D model.

The 1-D model generally reported less CO_2 conversions compared to the rest of the experimental results for various reasons. For one, the model does not take the effect of diluent into account, as the model assumes the reactor tube to be fully dispersed with the catalyst alone. While the model does come closer to experimental results to some degree, the model also does not consider the amount of loading (wt%) for both pure Ni and medium loading. The amount of loading could possibly cause some effect on the reported conversions and its exact effect on the conversions still needs to be determined.

5.2.3. Sensitivity analysis

Apart from validation with experimental results for various catalysts, a sensitivity analysis was conducted on the 1-D model to see the effect of various factors that could impact the conversions. Two of the factors studied were the weight of the catalyst and the total inlet volumetric flow rate, and whether they, in line with theory, impact conversion accordingly. Data was generated from the 1-D model and thermodynamic data for various inlet volumetric flow rates plotted against the experimental data for conversion of CH_4 for different catalyst weights. For consistency, all results were fixed at a temperature of 650 °C. Experimentally synthesized pure Ni at various catalyst weights (between 2.5 mg and 10 mg) and varying diluent loadings (between 25 mg and 250 mg of sand) and was

compared against the kinetic profiles of pure Ni and Ni-Cu bimetallic catalysts from the model. The results can be seen below in Figure 16**Error! Reference source not found.**.

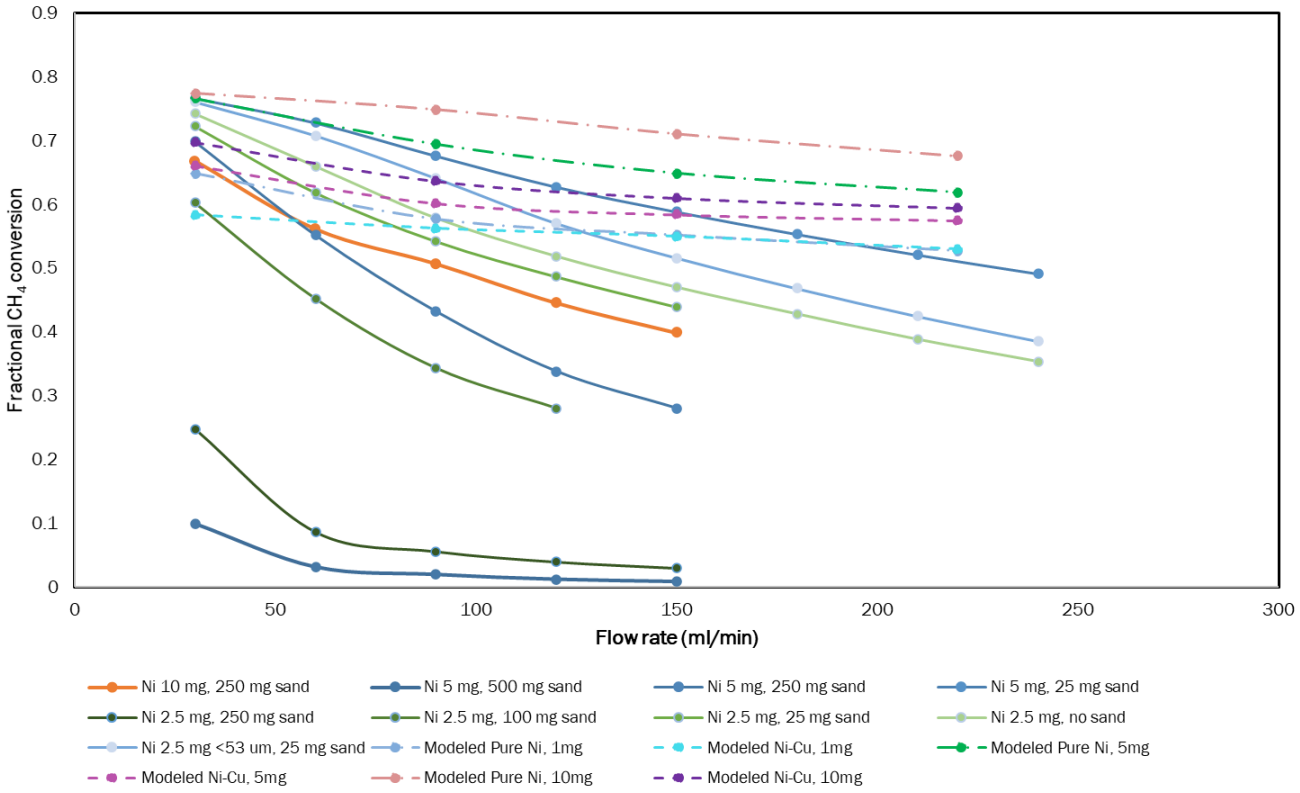

Figure 16: Comparison of CH_4 conversions obtained from 1-D model with experimental results at different inlet mass flow rates (STP)

For CH_4, it can be seen earlier in Figure 11**Error! Reference source not found.**, t hat as the weight of the catalyst increases, the conversion of CH_4 also increases. This phenomenon can be explained simply as when there is more catalyst available, the reactants from the inlet feed get to be in more contact during the reaction to yield the DRM end products. This trend can also be seen in Figure 16 above for a fixed inlet flow rate. As the inlet flow rate increases, the conversion should drop over the reactor bed, and similar results are present in the data above in Figure 16. This behavior is because as the inlet

flow rate is increased, more of the reactant mixture flows over the reactor bed, and given the amount of catalyst is fixed, less of the reactant mixture is in contact with the catalyst resulting in a decrease in conversion. While for the experimental results, one can observe a steeper decrease in conversions, the conversions drop less sharply for the results generated from the 1-D model.

Moreover, from the synthesized catalysts in the 1-D model, the decrease in conversion is more profound at higher catalyst weights than lower ones. This trend can be explained by the limitation of the 1-D model, which is the result of not considering all side reactions in the code. It should also be noted that any axial dispersions and effects of changes in heat in more than one dimension are not being accounted for in the 1-D model, which might cause the conversions to change at higher temperatures.

From the results presented above, the model validates to a good degree for CH_4 conversions, but for the CO_2, the model is not able to validate as well with similar accuracy.

5.3. Scale-up towards bench scale

Two data sets need to be considered for the assessment of the model at different reactor scales: the data at the lab scale (which is obtained from the TAMUQ laboratory in the experimental campaign) and the data at the bench scale (which shall be obtained in TOTAL's pilot scale reactor). Based on the parameters described for scaling-up the lab scale results (obtained at 5 mg of catalyst weight) to a bench scale (obtained at 20 mg of catalyst weight) in Section 4.7, conversion profiles were generated for both CH_4 and CO_2. These profiles are shown in Figure 17 and Figure 18. Most importantly, since the

prediction of carbon formation was an intended aim for developing a mathematical model, the code was programmed to calculate the amount of carbon formed (in g/hr) for both the lab scale (at 5 mg) and the scale-up (20 mg). The results for carbon formation are described in Figure 19.

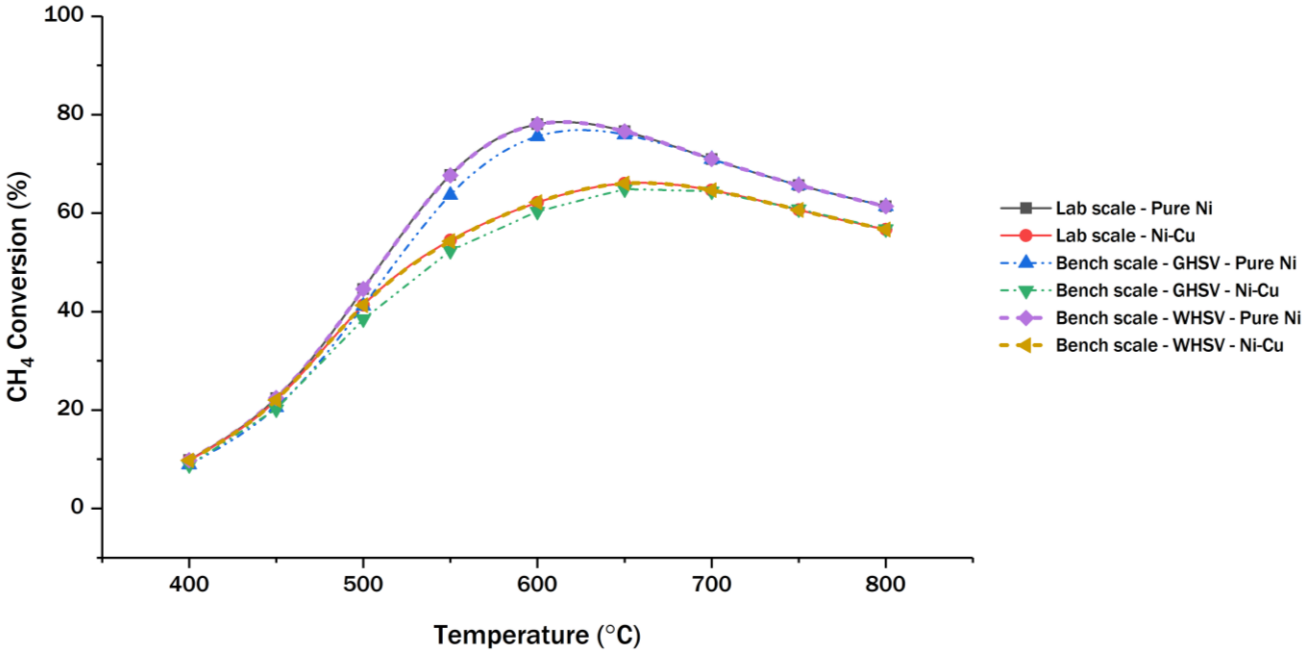

Figure 17: CH_4 conversions obtained from 1-D model at both lab and bench scales

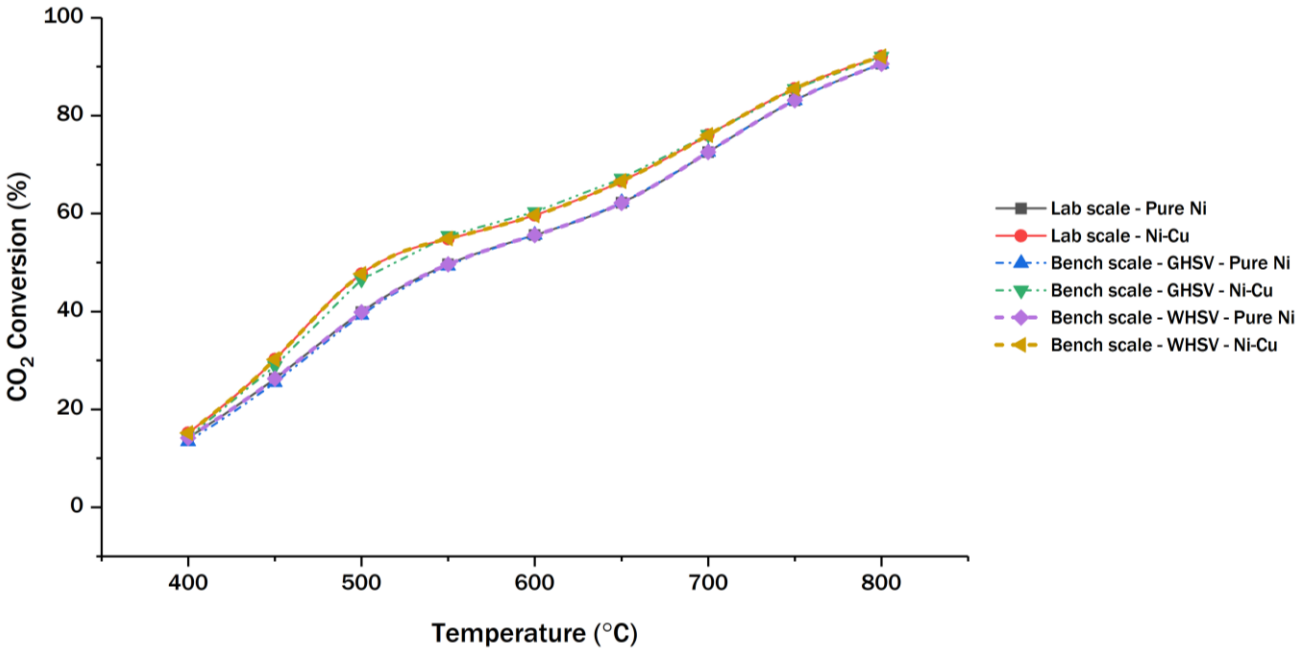

Figure 18: CO_2 conversions obtained from 1-D model at both lab and bench scales

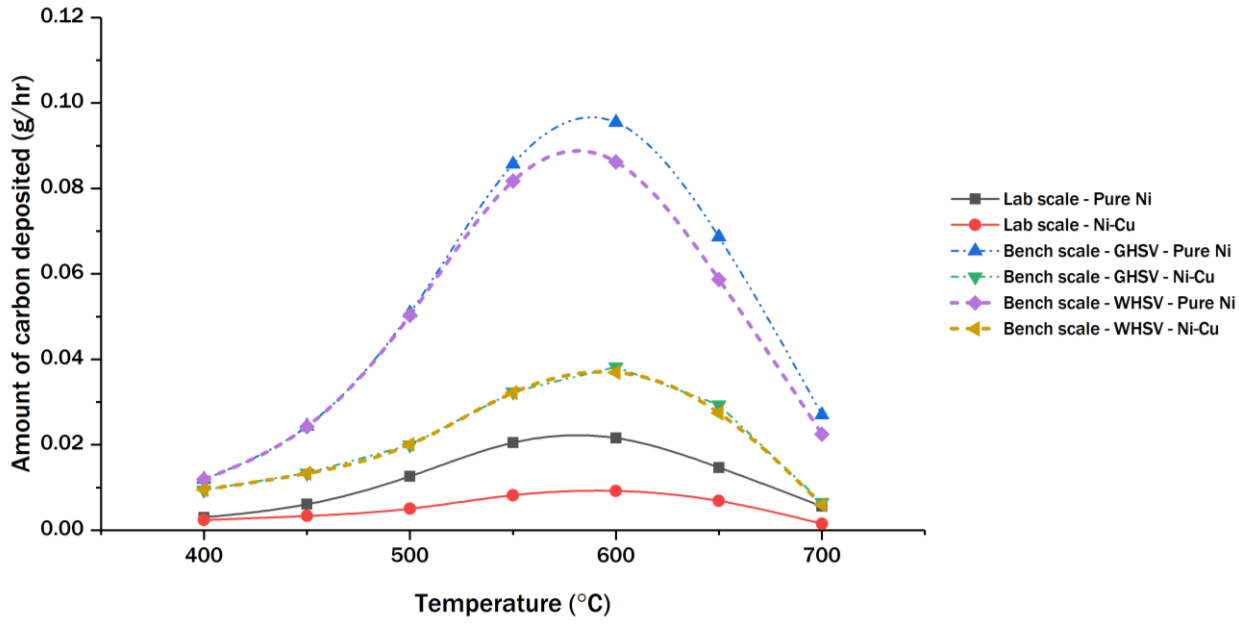

Figure 19: Amount of carbon formation obtained via 1-D model at both lab and bench scales

As mentioned earlier in Section 4.7, the scale-up was achieved by scaling the lab scale results obtained at 5 mg of catalyst weight into bench scale at 20 mg of catalyst weight in two different data sets: (a) bench scale at the same GHSV as lab scale and (b) bench scale at the same WHSV as lab scale, for both pure Ni and medium loading Ni-Cu catalysts. The results were obtained as follows:

(a) Bench scale – same GHSV

From Figure 17, it can be seen that CH_4 conversions for data set (a) follow the same trend as lab scale. As temperature increases, the conversions initially rise reaching a maximum and then starts to decline. increasing with temperature reaching a maximum, and then decreasing. The conversions obtained in data set (a) are closer to the values obtained in lab scale, bearing almost a 3-4% difference in the range of 550-650 °C. The peak CH_4 conversions for data set (a) are very slightly lower than lab scale results but follow a similar pattern where the peaks occur between 620-625 °C.

For the conversion of CO_2, as seen in Figure 18, the results from data set (a) follow a similar trend to the results obtained with lab scale generally where the conversion increases with rising temperature. However, the CO_2 conversions from data set (a), differ very slightly from lab scale, with a % difference of less than 1% throughout the entire range of 400-800 °C.

As expected during scale-up shown in Figure 19, the amount of carbon formation observed in data set (a) is higher than that obtained from the results in lab scale throughout the temperature range. Nonetheless, the overall trend shown by the results in data set (a) is similar in essence with lab results, with peak carbon formation occurring around 600

°C in both cases. In data set (b), at 600 °C, pure Ni is predicted to form about 0.095 g/hr of carbon.

(b) Bench scale – same WHSV

CH_4 conversions, as seen already in data set (a), form a similar trend in data set (b) when compared to lab results, and in fact are in reasonably close agreement with lab scale results with peak CH_4 conversion occurring at 625 °C, just as observed in lab scale from Figure 17.

As seen in Figure 18, the results from data set (b), also come close to the lab scale results with a reasonable degree in terms of CO_2 conversions and follow the same trend where CO_2 conversion once again increases with temperature.

Moreover, in terms of carbon formation the results from data set (b) resemble closely the trend observed in data set (a) where carbon formation reaches a peak around 600 °C, with pure Ni being predicted to form about 0.086 g/hr of carbon, as observed in Figure 19.

In both data sets (a) and (b), it can be observed that for CH_4, both sets of scale-up follow patterns similar to lab scale, in terms of conversions as the temperature increases, where conversions initially rise reaching a maximum and then starts to decline. For both CH_4 and CO_2 conversions, it is important to note that the laboratory scale results are in close agreement with the results obtained in data set (b). Once again, as seen before on the lab scale, the conversions for CH_4 on pure Ni catalyst are higher than that obtained at Ni-Cu catalyst in all three data sets of scale-up.

It is interesting to note in both lab and bench scales, the amount of carbon formed in the Ni-Cu catalyst is lesser than that formed in case of pure Ni catalyst. Such trend also coincides with the experimental results [47] achieved previously in our group that describe the minimization of carbon formation in case of Ni-Cu bimetallic catalyst and also agrees with findings from DFT done previously by Omran et al. [46], hence it can be deduced that the model is fairly reasonable in predicting the carbon formation.

Both GHSV and WHSV are usually the parameters used for scale-up purposes during reactor design. Based on the results for sets (b) and (c), in both conversions, scale-up results provided by the 1-D model are reasonable and hold some promise, however these results need to be validated with an experimental campaign carried out using the same conditions used in the scale-up via the model. Variations in the results can be attributed to the nature of kinetics involved in the model, which currently does not include every side reaction possible that affects the conversion outcome, as previously mentioned in Section 5.1. In addition to that, the model is also simplistic in nature as it only takes one-dimensional variations and ignores variations in other directions that might also contribute to changing temperature and pressure profiles, ultimately affecting the results. As previously stated, the model currently assumes ideal gas flow, and the effects of non-ideality can also bring about more realistic results by the implementation of an appropriate equation of state such as Peng-Robinson (PR), Soave-Redlich-Kwong (SRK) or Redlich-Kwong (RK) etc. that accounts for the polar and non-polar behavior of various compounds. Although the bench scale results are provided for a single tube at 2.2 cm ID,

it is important to consider that the actual bench scale reactor at TOTAL® might be multi-tubular.

The developed 1-D model had been based on several assumptions. While the results at the bench scale are acceptable in comparison, it is important to note that not all thermo-physical characteristics will be accounted for as the scale-up is moved towards bigger scales. One of the biggest assumptions is that the conditions on the catalyst are equal to the ones as the reactor fluid that passes through it inside the reactor, and therefore both the catalyst and fluid are considered as a single pseudo-homogeneous phase. Pseudo-homogeneous models are those where the density of all liquid, gas or solid phases is considered to be constant in addition to the viscosity and such models are isotropic in directions [101]. Since at larger scales, there will be some form of interaction between the catalyst and the passing fluid as the fluid diffuses inside the catalyst, the conditions at the catalyst boundary may not be the same during scale-up. Therefore, the pseudo-homogeneous model will require modifications to account for the changing conditions at the catalyst boundary via means of multiscale modeling. At larger scales, variations in radial and tangential directions will be present and hence more transport equations will be required to model the variations in those dimensions. Finally, while the fluid flow inside the reactor can be considered in a single phase even at larger scales, there will be considerable interfacial resistances to heat and mass transport between the fluid and the catalyst in the reactor tube, and therefore changes in effectiveness factor needs to be considered while moving towards scale-up.

6. CONCLUSION AND RECOMMENDATIONS

6.1. Conclusion

DRM provides an optimistic outlook to produce various chemicals and products by utilizing both CO_2 and CH_4 and converting into reliable chemical precursors, syngas among others. Using the novel medium loading Ni-Cu catalyst for the DRM process provides a solution to the problem of carbon formation in DRM at the laboratory (atomistic) scale. This study has considered an effective design approach for the catalytic process for the DRM. This approach concerns the potential scalability of the unique Ni-Cu system utilizing modeling tools. Hence, a 1-D, pseudo-homogeneous reactor bed model that was developed earlier in MATLAB® was used to assess the conversions of the DRM reactants as well provide insight on the carbon formation that occurs inside the reactor tube. This existing model was upgraded by accounting for carbon formation using three main reactions: (1) methane cracking (2) hydrogenation of CO and (3) Boudouard reaction and was advanced further to include the effect of transport properties such as momentum, heat and mass balances. In order to obtain the kinetics for the Ni-Cu catalyst, the kinetics were first obtained for the conventional Ni catalyst which were than scaled to the Ni-Cu domain via a novel approach that uses DFT insights.

The model was initially assessed on the laboratory scale (at tube diameter of 1 cm), using several catalyst weights (1 mg, 5 mg, and 10 mg) for both the pure Ni as well as the medium loading Ni-Cu catalyst. The model was not able to demonstrate the conversion trend as shown by the conversions obtained from thermodynamic data for both CH_4 and

CO_2, with the differences occurring due to the non-accountability of side reactions as well as non-ideality in the developed 1-D model.

Next, these results were validated using experimental data for both synthesized pure Ni and medium loading Ni-Cu catalysts as well as the industrial 20 wt% Ni/γ-Al_2O_3 catalyst for a fixed catalyst weight of 5 mg at 650 °C. It was found that the model was able to predict the conversions for both CH_4 within a 5% of an error margin, however this accuracy was not demonstrated reasonably for CO_2 conversions. Finally, the model was scaled-up from the laboratory scale at 5 mg catalytic weight to a bench scale (at tube diameter of 2.2 cm). The conversions were once again assessed by adjusting various parameters such as GHSV and WHSV. The model demonstrated almost similar patterns in conversions for both CH_4 and CO_2 during the scale-up process. The results from the scale-up in which WHSV was maintained at the same level as lab scale, came to moderately good agreement with the lab scale results found using the model. In terms of the carbon formed, the carbon formation shows similar patterns to those achieved at the lab scale, with more carbon being formed at the bench scale; however, interestingly the model also predicts that in all cases, the amount of carbon formed in medium loading Ni-Cu catalyst is always lesser than that formed from the pure Ni catalyst, thereby meeting expectations from previous studies [46, 47], both from DFT and experimental approaches.

The pseudo-homogeneous, 1-D model is the most basic model that can help assess scalability and an attempt was made to scale-up from a lab scale to a bench scale in this work, which showed some promise. The next logical step would be to move towards a pilot scale and then towards a commercial scale. In order to do that, more robust models

will be required, and the developed 1-D model will need to be upgraded. First step would be to upgrade the 1-D model to a two-dimensional (2-D) pseudo-homogeneous model which shall account for more variations in the reactor profile, especially in the radial direction. From there, the 2-D model will be upgraded towards a multiscale model that will require advance techniques including those suggested by Kelkar and Ng [84] that involve dimensional analysis to achieve an accurate scale-up, especially at the commercial level.

One of the aspects of this work is to implement the lumped kinetics of DRM process for the medium loading Ni-Cu catalyst. A novel approach used in this study with the help of rate constants achieved via DFT, helps in addressing the kinetics of the medium loading Ni-Cu catalyst. As demonstrated by the validation scale-up studies, for the DRM reactor bed model opens a pathway to further develop such a model. DFT also helps in providing a tool to understand the geometrical variations and understand catalysis at a microscopic level. It is certain that DFT serves as potential solution to explore insights at an atomistic level especially for DRM.

6.2. Recommendations and future work

Given that the developed 1-D model serves as a tool to predict carbon formation and understanding the process parameters to achieve a certain desired conversion, the developed model is a vital tool to assess new catalysts as well. However, there is still further work that could be done in this regard.

I. Validation of scale-up results

While the scale-up results are in line with theoretical expectations especially with regards to carbon formation, a validation with data achieved experimentally still needs to be done for the bench scale results. Therefore, further tests are required to develop a bench reactor experimental setup with the specified diameters and synthesized catalysts as used in laboratory scale. The conversions as well as carbon formation needs to be assessed by carrying out trials using this bench reactor setup and validated against the data obtained from the model, to assess fully the validity of the 1-D model.

II. Updating the model

Since the pseudo-homogeneous model is overly simplified in terms of the assumptions used, the model may not hold validity while moving towards larger reactor scales. The model currently studies the reactor flow profile using only length as a dimension. However, the effects of axial and radial dispersions inside the reactor tube cannot be ignored, especially at the bench reactor scale. The model can be updated by using computational fluid dynamics (CFD) to understand the reactor profiles from a two-dimensional (2-D) setup and understand the variations in pressure and flow to further provide accuracy to the developed model. Moreover, advanced multiscale modeling techniques need to be used to develop robust reactor models that can fully capture the precise effects during the DRM reaction. Developing such multiscale advanced models will also allow us to have a better picture to perform a more accurate scale-up using dimensional analysis as highlighted in Section 2.2.4.

As previously mentioned, a thermodynamic assessment needs to be done, and changes in fugacity coefficients need to be accounted for by using an appropriate equation

of state, which is determined by assessing the various reaction conditions. In addition, the impact of each reaction currently included in the model is affected by changing temperatures due to existence of equilibrium and this effect is not fully captured by the model. This may require an optimization study by assessing which reactions are more dominant over others at a particular temperature and pressure to fully maximize the state of equilibrium reached by the model. Furthermore, the model currently only includes the main reactions leading towards carbon formation and many side reactions were ignored. However, these reactions could possibly affect the state of equilibrium in the reaction and appropriate kinetic models need to be implemented to fully capture their effect on the DRM process in the model.

III. Using DFT for further work

It was observed that the medium loading Ni-Cu catalyst helps to minimize the formation of DRM from work done in previous studies [46, 47]. Given DFT has been essential to understand the mechanistic pathways of this catalyst, DFT can be therefore further used to study effects of modified Ni-Cu catalytic systems. There is slight promise on the addition of an alkali atom such as Na or K to conventional Ni catalyst [102-104], as it helps to minimize carbon formation and improve selectivity. However, there is lack of literature on DFT studies of adding such a promoter to the medium loading Ni-Cu catalyst. Therefore, further studies in DFT are required to elucidate the effect upon adding such additional alkali promoters to the medium-loading Ni-Cu catalyst and observe whether if such an addition causes any changes to the mechanism of carbon formation and affect energy barriers for the elementary DRM steps.

REFERENCES

[1] S. Sengupta, "U.N. Climate Talks End With Few Commitments and a 'Lost' Opportunity," ed: The New York Times, 2019.

[2] P. Friedlingstein *et al.*, "Global Carbon Budget 2020," *Earth Syst. Sci. Data,* vol. 12, no. 4, pp. 3269-3340, 2020, doi: 10.5194/essd-12-3269-2020.

[3] H. Ritchie. "Energy mix." Our World In Data. https://ourworldindata.org/energy-mix (accessed 2020).

[4] C. Hepburn *et al.*, "The technological and economic prospects for CO2 utilization and removal," *Nature,* vol. 575, no. 7781, pp. 87-97, Nov 2019, doi: 10.1038/s41586-019-1681-6.

[5] NASA. "Global Temperature | Vital Signs - Climate Change: Vital Signs of the Planet." NASA. https://climate.nasa.gov/vital-signs/global-temperature/ (accessed 2020).

[6] UNECE, "How natural gas can support the uptake of renewable energy," United Nations Ecconomic Commission for Europe, Geneva, Switzerland, 2019, vol. 66. [Online]. Available: https://www.unece.org/fileadmin/DAM/energy/se/pdfs/CSE/PATHWAYS/publ/NG_RE.pdf

[7] H. E. Alfadala and M. M. El-Halwagi. (2017) Qatar's Chemical Industry: Monetizing Natural Gas. *Chemical Engineering Practice (CEP)*. 38-41. Available:

https://www.aiche.org/resources/publications/cep/2017/february/qatars-chemical-industry-monetizing-natural-gas

[8] N. O. Elbashir, "Introduction to Natural Gas Monetization," in *Natural Gas Processing from Midstream to Downstream*, 2018, pp. 1-14.

[9] N. Woodroof, "The main challenges of fully monetising natural gas resources," Oilfield Technology, 2019. [Online]. Available: https://www.oilfieldtechnology.com/special-reports/13052019/the-main-challenges-of-fully-monetising-natural-gas-resources/

[10] C. Karakaya and R. J. Kee, "Progress in the direct catalytic conversion of methane to fuels and chemicals," *Progress in Energy and Combustion Science*, vol. 55, pp. 60-97, 2016, doi: 10.1016/j.pecs.2016.04.003.

[11] M. D. Burkart, N. Hazari, C. L. Tway, and E. L. Zeitler, "Opportunities and Challenges for Catalysis in Carbon Dioxide Utilization," *ACS Catalysis*, vol. 9, no. 9, pp. 7937-7956, 2019, doi: 10.1021/acscatal.9b02113.

[12] N. E. T. Laboratory. "Syngas Composition " U.S. Department of Energy. http://www.netl.doe.gov/research/coal/energy-systems/gasification/gasifipedia/syngas-composition (accessed 2021).

[13] A. York, T. Xiao, and M. Green, "Brief Overview of the Partial Oxidation of Methane to Synthesis Gas," *Topics in Catalysis*, vol. 22, no. 3/4, pp. 345-358, 2003, doi: 10.1023/a:1023552709642.

[14] L. Chen, Z. Qi, S. Zhang, J. Su, and G. A. Somorjai, "Catalytic Hydrogen Production from Methane: A Review on Recent Progress and Prospect," *Catalysts*, vol. 10, no. 8, 2020, doi: 10.3390/catal10080858.

[15] A. H. Elbadawi, L. Ge, Z. Li, S. Liu, S. Wang, and Z. Zhu, "Catalytic partial oxidation of methane to syngas: review of perovskite catalysts and membrane reactors," *Catalysis Reviews*, vol. 63, no. 1, pp. 1-67, 2020, doi: 10.1080/01614940.2020.1743420.

[16] S. A. Ghoneim, R. A. El-Salamony, and S. A. El-Temtamy, "Review on Innovative Catalytic Reforming of Natural Gas to Syngas," *World Journal of Engineering and Technology*, vol. 4, pp. 116-139, 25 February 2016 2016, doi: 10.4236/wjet.2016.4101.

[17] M. S. Challiwala, M. M. Ghouri, P. Linke, M. M. El-Halwagi, and N. O. Elbashir, "A combined thermo-kinetic analysis of various methane reforming technologies: Comparison with dry reforming," *Journal of CO2 Utilization*, vol. 17, pp. 99-111, 2017, doi: 10.1016/j.jcou.2016.11.008.

[18] M. Usman, W. M. A. Wan Daud, and H. F. Abbas, "Dry reforming of methane: Influence of process parameters—A review," *Renewable and Sustainable Energy Reviews*, vol. 45, pp. 710-744, 2015, doi: 10.1016/j.rser.2015.02.026.

[19] B. Fidalgo, A. Dominguez, J. Pis, and J. Menendez, "Microwave-assisted dry reforming of methane," *International Journal of Hydrogen Energy*, vol. 33, no. 16, pp. 4337-4344, 2008, doi: 10.1016/j.ijhydene.2008.05.056.

[20] W.-J. Jang, J.-O. Shim, H.-M. Kim, S.-Y. Yoo, and H.-S. Roh, "A review on dry reforming of methane in aspect of catalytic properties," *Catalysis Today*, vol. 324, pp. 15-26, 2019, doi: 10.1016/j.cattod.2018.07.032.

[21] M. S. Challiwala, B. A. Wilhite, M. M. Ghouri, and N. O. Elbashir, "Multidimensional modeling of a microfibrous entrapped cobalt catalyst Fischer-Tropsch reactor bed," *AIChE Journal*, vol. 64, no. 5, pp. 1723-1731, 2018, doi: 10.1002/aic.16053.

[22] D. Uykun Mangaloğlu, M. Baranak, Ö. Ataç, and H. Atakül, "Effect of the promoter presence in catalysts on the compositions of Fischer–Tropsch synthesis products," *Journal of Industrial and Engineering Chemistry*, vol. 66, pp. 298-310, 2018, doi: 10.1016/j.jiec.2018.05.044.

[23] L. Zhong *et al.*, "Cobalt carbide nanoprisms for direct production of lower olefins from syngas," *Nature*, vol. 538, no. 7623, pp. 84-87, Oct 6 2016, doi: 10.1038/nature19786.

[24] J. M. Lavoie, "Review on dry reforming of methane, a potentially more environmentally-friendly approach to the increasing natural gas exploitation," *Front Chem*, vol. 2, p. 81, 2014, doi: 10.3389/fchem.2014.00081.

[25] D. Pakhare and J. Spivey, "A review of dry (CO2) reforming of methane over noble metal catalysts," *Chem Soc Rev*, vol. 43, no. 22, pp. 7813-37, Nov 21 2014, doi: 10.1039/c3cs60395d.

[26] S. Afzal, D. Sengupta, A. Sarkar, M. El-Halwagi, and, and N. Elbashir, "Optimization Approach to the Reduction of CO2 Emissions for Syngas

Production Involving Dry Reforming," *ACS Sustainable Chemistry & Engineering*, vol. 6, no. 6, pp. 7532-7544, 2018, doi: 10.1021/acssuschemeng.8b00235.

[27] S. Arora and R. Prasad, "An overview on dry reforming of methane: strategies to reduce carbonaceous deactivation of catalysts," *RSC Advances*, vol. 6, no. 110, pp. 108668-108688, 2016, doi: 10.1039/c6ra20450c.

[28] N. A. K. Aramouni, J. G. Touma, B. A. Tarboush, J. Zeaiter, and M. N. Ahmad, "Catalyst design for dry reforming of methane: Analysis review," *Renewable and Sustainable Energy Reviews*, vol. 82, pp. 2570-2585, 2018, doi: 10.1016/j.rser.2017.09.076.

[29] B. Abdullah, N. A. Abd Ghani, and D.-V. N. Vo, "Recent advances in dry reforming of methane over Ni-based catalysts," *Journal of Cleaner Production*, vol. 162, pp. 170-185, 2017, doi: 10.1016/j.jclepro.2017.05.176.

[30] Y. Wang, L. Yao, S. H. Wang, D. H. Mao, and C. W. Hu, "Low-temperature catalytic CO2 dry reforming of methane on Ni-based catalysts: A review," (in English), *Fuel Process Technol*, vol. 169, pp. 199-206, Jan 2018, doi: 10.1016/j.fuproc.2017.10.007.

[31] H. Toulhoat, "Heterogeneous Catalysis: Use of Density Functional Theory," *Encyclopedia of Materials: Science and Technology*, K. H. J. Buschow *et al.*, Eds.: Elsevier, 2010, pp. 1-7.

[32] Y.-A. Zhu, D. Chen, X.-G. Zhou, and W.-K. Yuan, "DFT studies of dry reforming of methane on Ni catalyst," *Catalysis Today*, vol. 148, no. 3-4, pp. 260-267, 2009, doi: 10.1016/j.cattod.2009.08.022.

[33] V. C. H. Kroll, H. M. Swaan, and C. Mirodatos, "Methane Reforming Reaction with Carbon Dioxide Over Ni/SiO2Catalyst," *Journal of Catalysis*, vol. 161, no. 1, pp. 409-422, 1996, doi: 10.1006/jcat.1996.0199.

[34] Z. Wang, X. M. Cao, J. Zhu, and P. Hu, "Activity and coke formation of nickel and nickel carbide in dry reforming: A deactivation scheme from density functional theory," *Journal of Catalysis*, vol. 311, pp. 469-480, 2014, doi: 10.1016/j.jcat.2013.12.015.

[35] W.-J. Jang *et al.*, "Key properties of Ni–MgO–CeO2, Ni–MgO–ZrO2, and Ni–MgO–Ce(1−x)Zr(x)O2catalysts for the reforming of methane with carbon dioxide," *Green Chemistry*, vol. 20, no. 7, pp. 1621-1633, 2018, doi: 10.1039/c7gc03605a.

[36] A. G. Bhavani, W. Y. Kim, J. W. Lee, and J. S. Lee, "Influence of Metal Particle Size on Oxidative CO2Reforming of Methane over Supported Nickel Catalysts: Effects of Second-Metal Addition," *ChemCatChem*, vol. 7, no. 9, pp. 1445-1452, 2015, doi: 10.1002/cctc.201500003.

[37] J. Zhang, H. Wang, and A. Dalai, "Development of stable bimetallic catalysts for carbon dioxide reforming of methane," *Journal of Catalysis*, vol. 249, no. 2, pp. 300-310, 2007, doi: 10.1016/j.jcat.2007.05.004.

[38] Z. Bian, S. Das, M. H. Wai, P. Hongmanorom, and S. Kawi, "A Review on Bimetallic Nickel-Based Catalysts for CO2 Reforming of Methane," *ChemPhysChem*, vol. 18, no. 22, pp. 3117-3134, Nov 17 2017, doi: 10.1002/cphc.201700529.

[39] J.-H. Lee, E.-G. Lee, O.-S. Joo, and K.-D. Jung, "Stabilization of Ni/Al2O3 catalyst by Cu addition for CO2 reforming of methane," *Applied Catalysis A: General*, vol. 269, no. 1-2, pp. 1-6, 2004, doi: 10.1016/j.apcata.2004.01.035.

[40] M. M. Ghouri, "Density functional theory study of dry reforming of methane on nickel and nickel based bimetallic catalysts," in *Qatar Foundation Annual Research Conference*, Doha, Qatar, 2018: HBKU Press, doi: 10.5339/qfarc.2018.EEPD778.

[41] F. Wang, Y. Li, W. Cai, E. Zhan, X. Mu, and W. Shen, "Ethanol steam reforming over Ni and Ni–Cu catalysts," *Catalysis Today*, vol. 146, no. 1-2, pp. 31-36, 2009, doi: 10.1016/j.cattod.2009.01.027.

[42] T. Wu, W. Cai, P. Zhang, X. Song, and L. Gao, "Cu–Ni@SiO2 alloy nanocomposites for methane dry reforming catalysis," *RSC Advances*, vol. 3, no. 46, 2013, doi: 10.1039/c3ra43203c.

[43] H. Liu, R. Zhang, R. Yan, J. Li, B. Wang, and K. Xie, "Insight into CH4 dissociation on NiCu catalyst: A first-principles study," *Applied Surface Science*, vol. 258, no. 20, pp. 8177-8184, 2012, doi: 10.1016/j.apsusc.2012.05.017.

[44] H. Liu *et al.*, "Study on carbon deposition associated with catalytic CH4 reforming by using density functional theory," *Fuel*, vol. 113, pp. 712-718, 2013, doi: 10.1016/j.fuel.2013.06.022.

[45] R. Zhang, X. Guo, B. Wang, and L. Ling, "Insight Into the Effect of CuNi(111) and FeNi(111) Surface Structure and Second Metal Composition on Surface Carbon Elimination by O or OH: A Comparison Study with Ni(111) Surface," *The Journal of Physical Chemistry C*, 2015, doi: 10.1021/acs.jpcc.5b03868.

[46] A. Omran, S. H. Yoon, M. Khan, M. Ghouri, A. Chatla, and N. Elbashir, "Mechanistic Insights for Dry Reforming of Methane on Cu/Ni Bimetallic Catalysts: DFT-Assisted Microkinetic Analysis for Coke Resistance," *Catalysts*, vol. 10, no. 9, 2020, doi: 10.3390/catal10091043.

[47] A. Chatla, M. M. Ghouri, O. W. El Hassan, N. Mohamed, A. V. Prakash, and N. O. Elbashir, "An experimental and first principles DFT investigation on the effect of Cu addition to Ni/Al2O3 catalyst for the dry reforming of methane," *Applied Catalysis A: General*, vol. 602, 2020, doi: 10.1016/j.apcata.2020.117699.

[48] J. T. Richardson and S. A. Paripatyadar, "Carbon dioxide reforming of methane with supported rhodium," *Applied Catalysis*, vol. 61, no. 1, pp. 293-309, 1990/05/07/ 1990, doi: https://doi.org/10.1016/S0166-9834(00)82152-1.

[49] A. Nandini, K. K. Pant, and S. C. Dhingra, "Kinetic study of the catalytic carbon dioxide reforming of methane to synthesis gas over Ni-K/CeO2-Al2O3 catalyst," *Applied Catalysis A: General*, vol. 308, pp. 119-127, 2006/07/10/ 2006, doi: https://doi.org/10.1016/j.apcata.2006.04.014.

[50] U. Oemar, Y. Kathiraser, L. Mo, X. K. Ho, and S. Kawi, "CO2 reforming of methane over highly active La-promoted Ni supported on SBA-15 catalysts: mechanism and kinetic modelling," *Catalysis Science & Technology*, 10.1039/C5CY00906E vol. 6, no. 4, pp. 1173-1186, 2016, doi: 10.1039/C5CY00906E.

[51] Y. Kathiraser, U. Oemar, E. T. Saw, Z. Li, and S. Kawi, "Kinetic and mechanistic aspects for CO2 reforming of methane over Ni based catalysts," *Chemical Engineering Journal*, vol. 278, pp. 62-78, 2015, doi: 10.1016/j.cej.2014.11.143.

[52] M. C. J. Bradford and M. A. Vannice, "Catalytic reforming of methane with carbon dioxide over nickel catalysts II. Reaction kinetics," *Applied Catalysis A: General*, vol. 142, no. 1, pp. 97-122, 1996, doi: 10.1016/0926-860x(96)00066-x.

[53] J. W. Kim, J. A. Ha, H. Jung, B. I. Ahn, S. H. Lee, and J. G. Choi, "Kinetic analysis of supported Ni-catalyzed CO2/CH4 reactions using photoacoustic spectroscopy," *Phys Chem Chem Phys*, vol. 9, no. 43, pp. 5828-33, Nov 21 2007, doi: 10.1039/b709102h.

[54] M. F. Mark, W. F. Maier, and F. Mark, "Reaction kinetics of the CO2 reforming of methane," *Chemical Engineering & Technology*, vol. 20, no. 6, pp. 361-370, 1997, doi: 10.1002/ceat.270200602.

[55] E. Akpan, Y. Sun, P. Kumar, H. Ibrahim, A. Aboudheir, and R. Idem, "Kinetics, experimental and reactor modeling studies of the carbon dioxide reforming of methane (CDRM) over a new Ni/CeO2–ZrO2 catalyst in a packed bed tubular

reactor," *Chemical Engineering Science,* vol. 62, no. 15, pp. 4012-4024, 2007, doi: 10.1016/j.ces.2007.04.044.

[56] A. M. Becerra, M. E. Iriarte, and A. E. Castro Luna, "Catalytic activity of a nickel on alumina catalyst in the CO2 reforming of methane," *Reaction Kinetics and Catalysis Letters,* vol. 79, no. 1, pp. 119-125, 2003, doi: 10.1023/a:1024167919727.

[57] Z. L. Zhang and X. E. Verykios, "Carbon dioxide reforming of methane to synthesis gas over supported Ni catalysts," *Catalysis Today,* vol. 21, no. 2-3, pp. 589-595, 1994, doi: 10.1016/0920-5861(94)80183-5.

[58] T. Osaki, T. Horiuchi, K. Suzuki, and T. Mori, "Catalyst performance of MoS2 and WS2 for the CO2-reforming of CH4 Suppression of carbon deposition," *Applied Catalysis A: General,* vol. 155, no. 2, pp. 229-238, 1997, doi: 10.1016/s0926-860x(96)00391-2.

[59] S. Wang and G. Q. Lu, "Chapter 8 - Reaction kinetics and deactivation of Ni-based catalysts in CO2 reforming of methane," in *Reaction Engineering for Pollution Prevention*, M. A. Abraham and R. P. Hesketh Eds. Amsterdam: Elsevier Science, 2000, pp. 75-84.

[60] S. Wang and G. Q. Lu, "A Comprehensive Study on Carbon Dioxide Reforming of Methane over Ni/γ-Al2O3 Catalysts," *Industrial & Engineering Chemistry Research,* vol. 38, no. 7, pp. 2615-2625, 1999, doi: 10.1021/ie980489t.

[61] V. A. Tsipouriari and X. E. Verykios, "Kinetic study of the catalytic reforming of methane with carbon dioxide to synthesis gas over Ni/La2O3 catalyst," *Catalysis Today*, vol. 64, no. 1-2, pp. 83-90, 2001, doi: 10.1016/s0920-5861(00)00511-3.

[62] X. Verykios, "Catalytic dry reforming of natural gas for the production of chemicals and hydrogen," *International Journal of Hydrogen Energy*, vol. 28, no. 10, pp. 1045-1063, 2003, doi: 10.1016/S036031990200215X.

[63] X. Li, D. Li, H. Tian, L. Zeng, Z.-J. Zhao, and J. Gong, "Dry reforming of methane over Ni/La2O3 nanorod catalysts with stabilized Ni nanoparticles," *Applied Catalysis B: Environmental*, vol. 202, pp. 683-694, 2017, doi: 10.1016/j.apcatb.2016.09.071.

[64] J. Munera, S. Irusta, L. Cornaglia, E. Lombardo, D. Vargascesar, and M. Schmal, "Kinetics and reaction pathway of the CO2 reforming of methane on Rh supported on lanthanum-based solid," *Journal of Catalysis*, vol. 245, no. 1, pp. 25-34, 2007, doi: 10.1016/j.jcat.2006.09.008.

[65] C. Sprung, B. Arstad, and U. Olsbye, "Methane Steam Reforming over a Ni/NiAl2O4 Model Catalyst-Kinetics," *ChemCatChem*, vol. 6, no. 7, pp. 1969-1982, 2014, doi: 10.1002/cctc.201402017.

[66] J. R. H. Ross and M. C. F. Steel, "Mechanism of the steam reforming of methane over a coprecipitated nickel-alumina catalyst," *Journal of the Chemical Society, Faraday Transactions 1: Physical Chemistry in Condensed Phases*, vol. 69, no. 0, 1973, doi: 10.1039/f19736900010.

[67] A. Al-Ubaid and E. E. Wolf, "Steam reforming of methane on reduced non-stoichiometric nickel aluminate catalysts," *Applied Catalysis*, vol. 40, pp. 73-85, 1988, doi: 10.1016/s0166-9834(00)80427-3.

[68] J. C. De Deken, E. F. Devos, and G. F. Froment, "Steam Reforming of Natural Gas: Intrinsic Kinetics, Diffusional Influences, and Reactor Design," in *Chemical Reaction Engineering—Boston*, vol. 196, (ACS Symposium Series, no. 196): AMERICAN CHEMICAL SOCIETY, 1982, ch. 16, pp. 181-197.

[69] K. Hou and R. Hughes, "The kinetics of methane steam reforming over a Ni/α-Al2O catalyst," *Chemical Engineering Journal*, vol. 82, no. 1-3, pp. 311-328, 2001, doi: 10.1016/s1385-8947(00)00367-3.

[70] J. Xu and G. F. Froment, "Methane steam reforming, methanation and water-gas shift: I. Intrinsic kinetics," *AIChE Journal*, vol. 35, no. 1, pp. 88-96, 1989, doi: 10.1002/aic.690350109.

[71] S. Z. Abbas, V. Dupont, and T. Mahmud, "Kinetics study and modelling of steam methane reforming process over a NiO/Al2O3 catalyst in an adiabatic packed bed reactor," *International Journal of Hydrogen Energy*, vol. 42, no. 5, pp. 2889-2903, 2017, doi: 10.1016/j.ijhydene.2016.11.093.

[72] H. J. Jun, M.-J. Park, S.-C. Baek, J. W. Bae, K.-S. Ha, and K.-W. Jun, "Kinetics modeling for the mixed reforming of methane over Ni-CeO2/MgAl2O4 catalyst," *Journal of Natural Gas Chemistry*, vol. 20, no. 1, pp. 9-17, 2011, doi: 10.1016/s1003-9953(10)60148-x.

[73] J. De Wilde and G. F. Froment, "Computational Fluid Dynamics in chemical reactor analysis and design: Application to the ZoneFlow™ reactor for methane steam reforming," *Fuel,* vol. 100, pp. 48-56, 2012, doi: 10.1016/j.fuel.2011.08.068.

[74] F. Maqbool, S. Z. Abbas, S. Ramirez-Solis, V. Dupont, and T. Mahmud, "Modelling of one-dimensional heterogeneous catalytic steam methane reforming over various catalysts in an adiabatic packed bed reactor," *International Journal of Hydrogen Energy,* vol. 46, no. 7, pp. 5112-5130, 2021, doi: 10.1016/j.ijhydene.2020.11.071.

[75] N. A. Saidina Amin, I. Istadi, and N. P. Yee, "Mathematical Modelling of Catalytic Fixed-Bed Reactor for Carbon Dioxide Reforming of Methane over Rh/Al2O3 Catalyst," *Bulletin of Chemical Reaction Engineering & Catalysis,* vol. 3, no. 1-3, 2008, doi: 10.9767/bcrec.3.1-3.7120.21-29.

[76] D. Karimipourfard, N. Nemati, M. Bayat, F. Samimi, and M. R. Rahimpour, "Mathematical Modeling and Optimization of Syngas Production Process: A Novel Axial Flow Spherical Packed Bed Tri-Reformer," *Chemical Product and Process Modeling,* vol. 13, no. 2, 2018, doi: 10.1515/cppm-2017-0031.

[77] Y. Benguerba, L. Dehimi, M. Virginie, C. Dumas, and B. Ernst, "Modelling of methane dry reforming over Ni/Al2O3 catalyst in a fixed-bed catalytic reactor," *Reaction Kinetics, Mechanisms and Catalysis,* vol. 114, no. 1, pp. 109-119, 2014, doi: 10.1007/s11144-014-0772-5.

[78] Y. Benguerba, M. Virginie, C. Dumas, and B. Ernst, "Methane Dry Reforming over Ni-Co/Al2O3: Kinetic Modelling in a Catalytic Fixed-bed Reactor," *International Journal of Chemical Reactor Engineering,* vol. 15, no. 6, 2017, doi: 10.1515/ijcre-2016-0170.

[79] E. Buckingham, "On Physically Similar Systems; Illustrations of the Use of Dimensional Equations," *Physical Review,* vol. 4, no. 4, pp. 345-376, 1914, doi: 10.1103/PhysRev.4.345.

[80] L. R. Glicksman, M. R. Hyre, and P. A. Farrell, "Dynamic similarity in fluidization," *International Journal of Multiphase Flow,* vol. 20, pp. 331-386, 1994, doi: 10.1016/0301-9322(94)90077-9.

[81] T. E. Broadhurst and H. A. Becker, "Onset of fluidization and slugging in beds of uniform particles," *AIChE Journal,* vol. 21, no. 2, pp. 238-247, 1975, doi: 10.1002/aic.690210204.

[82] L. R. Glicksman, "Scaling relationships for fluidized beds," *Chemical Engineering Science,* vol. 39, no. 9, pp. 1373-1379, 1984, doi: 10.1016/0009-2509(84)80070-6.

[83] M. Horio, A. Nonaka, Y. Sawa, and I. Muchi, "A new similarity rule for fluidized bed scale-up," *AIChE Journal,* vol. 32, no. 9, pp. 1466-1482, 1986, doi: 10.1002/aic.690320908.

[84] V. V. Kelkar and K. M. Ng, "Development of fluidized catalytic reactors: Screening and scale-up," *AIChE Journal,* vol. 48, no. 7, pp. 1498-1518, 2002, doi: 10.1002/aic.690480714.

[85] M. K. Nikoo and N. A. S. Amin, "Thermodynamic analysis of carbon dioxide reforming of methane in view of solid carbon formation," *Fuel Process Technol,* vol. 92, no. 3, pp. 678-691, 2011, doi: 10.1016/j.fuproc.2010.11.027.

[86] K. Wittich, M. Krämer, N. Bottke, and S. A. Schunk, "Catalytic Dry Reforming of Methane: Insights from Model Systems," *ChemCatChem,* vol. 12, no. 8, pp. 2130-2147, 2020, doi: 10.1002/cctc.201902142.

[87] S. Wang, G. Q. Lu, and G. J. Millar, "Carbon Dioxide Reforming of Methane To Produce Synthesis Gas over Metal-Supported Catalysts: State of the Art," *Energy & Fuels,* vol. 10, no. 4, pp. 896-904, 1996, doi: 10.1021/ef950227t.

[88] B. Lal, A. Qasim, A. M. Shariff, and H. Mukhtar, "Effect of Bed Porosity on CO2 and CH4 Adsorption inside Packed Bed Column for CO2-CH4 Gas Mixture," *Recent Advances in Petrochemical Science,* vol. 4, no. 1, 2017, doi: 10.19080/rapsci.2017.04.555629.

[89] B. Kneale, "Alumina-based catalysts, their production and use," United Kingdom Patent EP0308140 Patent Appl. 88308312, 1989. [Online]. Available: https://data.epo.org/publication-server/document?iDocId=518877&iFormat=0

[90] Y. I. Yoon, I. H. Baek, and S. D. Park, "Enhancement of H2 Production by Combination with CO2 Absorption in Steam Methane Reforming in Bench Scale," (in English), *Journal of Industrial and Engineering Chemistry,* vol. 13, no. 5, pp. 842-849, 2007. [Online]. Available: https://www.cheric.org/research/tech/periodicals/view.php?seq=583938.

[91] L. Buchori, I. Istadi, and P. Purwanto, "Effects of Weight Hourly Space Velocity and Catalyst Diameter on Performance of Hybrid Catalytic-Plasma Reactor for Biodiesel Synthesis over Sulphated Zinc Oxide Acid Catalyst," *Bulletin of Chemical Reaction Engineering & Catalysis*, vol. 12, no. 2, 2017, doi: 10.9767/bcrec.12.2.775.227-234.

[92] H. S. Fogler, *Elements of Chemical Reaction Engineering* 5th ed. Pearson, 2016.

[93] EngineeringToolbox. "Gases - Dynamic Viscosity." Engineering Toolbox. https://www.engineeringtoolbox.com/gases-absolute-dynamic-viscosity-d_1888.html (accessed 12 December, 2020).

[94] C. R. Wilke, "A Viscosity Equation for Gas Mixtures," *The Journal of Chemical Physics*, vol. 18, no. 4, pp. 517-519, 1950, doi: 10.1063/1.1747673.

[95] R. K. Sinnott, *Chemical Engineering Design*, 4th ed. (Coulson & Richardson's Chemical Engineering). Corporate Drive, MA: Elsevier, 2005.

[96] B. E. Poling, G. H. Thomson, D. G. Friend, R. L. Rowley, and W. V. Wilding, "Section 2: Physical and Chemical Data," in *Perry's Chemical Engineers' Handbook*, D. W. Green and R. H. Perry Eds., 8th ed.: McGraw-Hill, 2008.

[97] J. W. Snoeck, G. F. Froment, and M. Fowles, "Steam/CO2Reforming of Methane. Carbon Filament Formation by the Boudouard Reaction and Gasification by CO2, by H2, and by Steam: Kinetic Study," *Industrial & Engineering Chemistry Research*, vol. 41, no. 17, pp. 4252-4265, 2002, doi: 10.1021/ie010666h.

[98] C. Fan, Y.-A. Zhu, M.-L. Yang, Z.-J. Sui, X.-G. Zhou, and D. Chen, "Density Functional Theory-Assisted Microkinetic Analysis of Methane Dry Reforming on

Ni Catalyst," *Industrial & Engineering Chemistry Research,* vol. 54, no. 22, pp. 5901-5913, 2015, doi: 10.1021/acs.iecr.5b00563.

[99] S. Afzal *et al.*, "Controlling the rate of change of Ni dispersion in commercial catalyst by ALD overcoat during dry reforming of methane," *International Journal of Hydrogen Energy,* vol. 45, no. 23, pp. 12835-12848, 2020, doi: 10.1016/j.ijhydene.2020.03.008.

[100] K. Z. Yang and F. Twaiq, "Modelling of the dry reforming of methane in different reactors: a comparative study," *Reaction Kinetics, Mechanisms and Catalysis,* vol. 122, no. 2, pp. 853-868, 2017, doi: 10.1007/s11144-017-1277-9.

[101] G. F. B. Froment, K. B.

De Wilde, J., *Chemical Reactor Analysis and Design*, 5th ed. Hudson, NY: John Wiley and Sons, 2010.

[102] M. Németh *et al.*, "Na-promoted Ni/ZrO2 dry reforming catalyst with high efficiency: details of Na2O–ZrO2–Ni interaction controlling activity and coke formation," *Catalysis Science & Technology*, vol. 7, no. 22, pp. 5386-5401, 2017, doi: 10.1039/c7cy01011g.

[103] J. Juan-Juan, M. C. Román-Martínez, and M. J. Illán-Gómez, "Effect of potassium content in the activity of K-promoted Ni/Al2O3 catalysts for the dry reforming of methane," *Applied Catalysis A: General,* vol. 301, no. 1, pp. 9-15, 2006, doi: 10.1016/j.apcata.2005.11.006.

[104] A. E. Castro Luna and M. E. Iriarte, "Carbon dioxide reforming of methane over a metal modified Ni-Al2O3 catalyst," *Applied Catalysis A: General*, vol. 343, no. 1-2, pp. 10-15, 2008, doi: 10.1016/j.apcata.2007.11.041.

APPENDIX A

MATLAB MODEL

The 1-D model was designed in MATLAB® with the help of two files:

1.) The 'ODE' file which housed the various reactions of the lumped kinetics model along with the parameters defining the catalyst as well as pressure drop and temperatures.

2.) The caller function file in which the input parameters are put for the inlet and can be varied to obtain the desired conversion and carbon formation amounts.

The code written for each file is shown below:

ODE file:

```
function dfdw=Combined9_reforming_Kinetics_basic_ode(l,F)
% feed conditions
% a = CO
% b = H2O
% c = CO2
% d = H2
% e = He
% f = CH4
% partial pressures in bar
%global Ptot0 Dp phi At Rhob Ftot Rhoinit G beta0 mumix

global Ptot0 Dp phi At Rhob Rhoinit stattemp tubedia
global r_SRM_1 r_SRM_2 r_SRM_3 r_DRM rc1 rc2 rcB

% temperatures in K
%global T0 Ftot0 H_SRM_1 H_SRM_2 H_SRM_3 H_DRM H_c1 H_c2 H_b

global Ftot0 H_SRM_1 H_SRM_2 H_SRM_3 H_DRM H_c1 H_c2 H_b

%T0 = 1100;
R=8.314;
Ftot=F(1)+F(2)+F(3)+F(4)+F(5)+F(6)+F(7); %total molar flow rate mol/hr

P(1) = F(8)*F(1)/(Ftot-F(7)); %bar
P(2) = F(8)*F(2)/(Ftot-F(7));
P(3) = F(8)*F(3)/(Ftot-F(7));
P(4) = F(8)*F(4)/(Ftot-F(7));
P(5) = F(8)*F(5)/(Ftot-F(7));
P(6) = F(8)*F(6)/(Ftot-F(7));
```

```
P(7)=0;

T0=F(9);

global initialCH4 initialCO2 initialH2O initialCO initialH2 initialHe ICH4 ICO2 IH2O IHe ICO IH2

XCH4= (initialCH4-F(6))/initialCH4; %conversion
XCO2= (initialCO2-F(3))/initialCO2;
XH2O= (initialH2O-F(2))/initialH2O;
XHe= (initialHe-F(5))/initialHe;
XCO= (initialCO-F(1))/initialCO;
XH2 = (initialH2-F(4))/initialH2;

xiCH4=ICH4/Ftot0; % initial molar fraction
xiCO2=ICO2/Ftot0;
xiH2O=IH2O/Ftot0;
xiHe=IHe/Ftot0;
xiCO=ICO/Ftot0;
xiH2=IH2/Ftot0;

ITMF=(initialCH4*16.04)+(initialCO2*44.01)+(initialH2O*18.016)+(initialHe*4.003)+(initialCO*28.01)+(initialH2*2); %initial total

xmiCH4=(initialCH4*16.04)/ITMF; %initial mass fraction
xmiCO2=(initialCO2*44.01)/ITMF;
xmiH2O=(initialH2O*18.016)/ITMF;
xmiHe=(initialHe*4.003)/ITMF;
xmiCO=(initialCO*28.01)/ITMF;
```

```
tialCO initialH2 initialHe ICH4 ICO2 IH2O IHe ICO IH2

sion

(initialH2O*18.016)+(initialHe*4.003)+(initialCO*28.01)+(initialH2*2); %initial total mass flow rate, g/hr

ss fraction
```

```
xmiH2=(initialH2*2)/ITMF;
sigma0=(xmiCH4*16.04)+(xmiCO2*44.01)+(xmiH2O*18.016)+(xmiHe*4.003)+(xmiCO*28.01)+(xmiH2*2); %g/mol
Rhoinit=100*(Ptot0*sigma0)/(R*stattemp);  %kg/m3

Rhob=1422;                                % Catalyst bulk density kg/m3
At=3.14/4*tubedia^2;                           % Crossectional area of the bed m2

xCH4=F(6)/Ftot; %molar fraction
xCO2=F(3)/Ftot;
xH2O=F(2)/Ftot;
xHe=F(5)/Ftot;
xCO=F(1)/Ftot;
xH2=F(4)/Ftot;

TMF=(F(6)*16.04)+(F(3)*44.01)+(F(2)*18.016)+(F(5)*4.003)+(F(1)*28.01)+(F(4)*2); %total mass flow rate, g/hr

xmCH4=(F(6)*16.04)/TMF; %mass fraction
xmCO2=(F(3)*44.01)/TMF;
xmH2O=(F(2)*18.016)/TMF;
xmHe=(F(5)*4.003)/TMF;
xmCO=(F(1)*28.01)/TMF;
xmH2=(F(4)*2)/TMF;

sigma1=(xmCH4*16.04)+(xmCO2*44.01)+(xmH2O*18.016)+(xmHe*4.003)+(xmCO*28.01)+(xmH2*2); %g/mol
Rhogas=100*(F(8)*sigma1)/(R*T0); %kg/m3

QCH4=F(6)*16.04*(1/(0.716*3600*1000));  %m3/s, wherein 0.716 g/L, 0.716, 0.59, 0.1785, 1.250, 0.0899 are the densities of methane
QCO2=F(3)*44.01*(1/(0.716*3600*1000));  %m3/s, wherein 0.716, 0.716, 0.59, 0.1785, 1.250, 0.0899 are the densities of methane, co
```

```
O*18.016)+(xmiHe*4.003)+(xmiCO*28.01)+(xmiH2*2); %g/mol
kg/m3

 % Catalyst bulk density kg/m3
       % Crossectional area of the bed m2

+(F(5)*4.003)+(F(1)*28.01)+(F(4)*2); %total mass flow rate, g/hr

8.016)+(xmHe*4.003)+(xmCO*28.01)+(xmH2*2); %g/mol

/s, wherein 0.716 g/L, 0.716, 0.59, 0.1785, 1.250, 0.0899 are the densities of methane, co2, h2o, he, co, h2 gases respectively.
/s, wherein 0.716, 0.716, 0.59, 0.1785, 1.250, 0.0899 are the densities of methane, co2, h2o, he, co, h2 gases respectively.
```

```
QH2O=F(2)*18.016*(1/(0.590*3600*1000)); %m3/s, wherein 0.716, 0.716, 0.59, 0.1785, 1.250, 0.0899 are the densities of methane, co
QHe=F(5)*4.003*(1/(0.1785*3600*1000));  %m3/s, wherein 0.716, 0.716, 0.59, 0.1785, 1.250, 0.0899 are the densities of methane, co
QCO=F(1)*28.01*(1/(1.250*3600*1000));   %m3/s, wherein 0.716, 0.716, 0.59, 0.1785, 1.250, 0.0899 are the densities of methane, co
QH2=F(4)*2*(1/(0.0899*3600*1000));      %m3/s, wherein 0.716, 0.716, 0.59, 0.1785, 1.250, 0.0899 are the densities of methane, co
vel=(QCH4+QCO2+QH2O+QHe+QCO+QH2)/At ;   %m/s

G=Rhogas*vel; %kg/m2.s

PCO=P(1);
PH2O=P(2);
PCO2=P(3);
PH2=P(4);
PHe=P(5);
PCH4=P(6);

%Viscosity calculation combining Chapman-Enskog pure viscosities and
%extending via Wilke's correlation
muCO=3.86E-05; %kg/m.s
muH2O=3.26E-05;
muCO2=3.74E-05;
muH2=1.84E-05;
muHe=4.18E-05;
muCH4=2.53E-05;

frCO=muCO/(1+(xH2O*0.431177728/xCO)+(xCO2*0.63132096/xCO)+(xH2*0.13955419/xCO)+(xHe*0.158201429/xCO)+(xCH4*0.459072093/xCO));
frH2O=muH2O/(1+(xCO*0.566162827/xH2O)+(xCO2*0.699379399/xH2O)+(xH2*0.174732484/xH2O)+(xHe*0.194483864/xH2O)+(xCH4*0.536366414/xH2
frCO2=muCO2/(1+(xCO*0.389310616/xCO2)+(xH2O*0.328453461/xCO2)+(xH2*0.101348754/xCO2)+(xHe*0.117847326/xCO2)+(xCH4*0.345518205/xCO
```

```
/s, wherein 0.716, 0.716, 0.59, 0.1785, 1.250, 0.0899 are the densities of methane, co2, h2o, he, co, h2 gases respectively.
/s, wherein 0.716, 0.716, 0.59, 0.1785, 1.250, 0.0899 are the densities of methane, co2, h2o, he, co, h2 gases respectively.
/s, wherein 0.716, 0.716, 0.59, 0.1785, 1.250, 0.0899 are the densities of methane, co2, h2o, he, co, h2 gases respectively.
/s, wherein 0.716, 0.716, 0.59, 0.1785, 1.250, 0.0899 are the densities of methane, co2, h2o, he, co, h2 gases respectively.
s

skog pure viscosities and

.63132096/xCO)+(xH2*0.13955419/xCO)+(xHe*0.158201429/xCO)+(xCH4*0.459072093/xCO));
*0.699379399/xH2O)+(xH2*0.174732484/xH2O)+(xHe*0.194483864/xH2O)+(xCH4*0.536366414/xH2O));
)*0.328453461/xCO2)+(xH2*0.101348754/xCO2)+(xHe*0.117847326/xCO2)+(xCH4*0.345518205/xCO2));
```

```
frH2=muH2/(1+(xCO*0.931657986/xH2)+(xH2O*0.888387114/xH2)+(xCO2*1.097200523/xH2)+(xHe*0.462090708/xH2)+(xCH4*0.98844932/xH2));
frHe=muHe/(1+(xCO*1.198745249/xHe)+(xH2O*1.1223157/xHe)+(xCO2*1.448072121/xHe)+(xH2*0.52448141/xHe)+(xCH4*1.256338799/xHe));
frCH4=muCH4/(1+(xCO*0.525439665/xCH4)+(xH2O*0.467539713/xCH4)+(xCO2*0.641308297/xCH4)+(xH2*0.169466062/xCH4)+(xHe*0.189772045/xCH

mumix=frCO+frH2O+frCO2+frH2+frHe+frCH4; %kg/m.s

% Steam reforming LHHW parameters using Xu and Froment (1989) expressions
K1=exp(-11650/T0+13.076);   %bar^2
K2=exp(1910/T0-1.764);  %unitless
K3=exp(-9740/T0+11.312);    %bar^2
%
KCH4=6.65e-4*exp(38280/8.314/T0);   %bar^-1
KCO=8.23e-5*exp(70650/8.314/T0);     %bar^-1
KH2=6.12e-9*exp(82900/8.314/T0);    %bar^-1
KH2O=1.77e5*exp(-88680/8.314/T0);    %unitless
%
kin1=4.225e15*exp(-240100/8.314/T0);      %(mol.bar^0.5)/(g.h)
kin2=1.955e6*exp(-67130/8.314/T0);      %(mol)/(g.h.bar)
kin3=1.0202e15*exp(-243900/8.314/T0);       %(mol.bar^0.5)/(g.h)
%
DEN=1+KCH4*PCH4+KCO*PCO+KH2*PH2+KH2O*PH2O/PH2;      %unitless

km_c1=5.5619*10^4*exp(-65053/R/T0);     %mol/g.h
KCH4_c1=0.1099;                         %bar^-1
Km_c1=exp(142.5/R)*exp(-123226/R/T0);   %unitless
ko_c2=1.33*10^-6*exp(75955/R/T0);       %mol/g.h
ko_c2_1=1.67*10^9*exp(-148916/R/T0);    %mol/g.h
```

```
ko_c2_1=1.67*10^9*exp(-148916/R/T0);    %mol/g.h
KO_H2O_c2=1.7372*10^4*exp(-60615/R/T0); %unitless
kr_den2=2.51893*10^5*exp(-95489/R/T0);  %bar^1.5
DEN2=1+KCO*PCO+KCH4_c1*PCH4+1/kr_den2*PH2^1.5+1/KO_H2O_c2*PH2O/PH2; %unitless

r_SRM_1=kin1/PH2^2.5/DEN^2*(PCH4*PH2O-PH2^3*PCO/K1);   %mol/g.h      %CH4 + H2O <-> 3 H2 + CO
r_SRM_2=kin2/PH2/DEN^2*(PCO*PH2O-PH2*PCO2/K2);     %mol/g.h          %CO + H2O <->H2 + CO2
r_SRM_3=kin3/PH2^3.5/DEN^2*(PCH4*PH2O^2-PH2^4*PCO2/K3);    %mol/g.h  %CH4 + 2 H2O <-> 4 H2 + CO2

rc1=km_c1*KCH4_c1*(PCH4-PH2/Km_c1)/DEN2^2;  %mol/g.h               % Methane cracking CH4 <-> C+ 2H2

beta0=(G*(1-phi)/(Rhoinit*1.0*Dp*(phi^3)))*((150*(1-phi)*mumix/Dp)+(1.75*G));

rc2=(ko_c2*KCO*PCO-ko_c2_1*PH2O/KO_H2O_c2/PH2)/DEN2^2;   %mol/g.h   % Carbon gasification CO + H2 <-> C + H2O

%if T0<973
%if PCH4<PH2/Km_c1
%rc1=0;
%end

%if (ko_c2*KCO*PCO<ko_c2_1*PH2O/KO_H2O_c2/PH2)
%rc2=0;
%end
%end

% ----------------- DRM model of Verykios (2002)

```

```
% ----------------- DRM model of Verykios (2002)

Klk2_d=(3600/0.01)*(2.61*10^-3)*exp(-4300/T0);       %mol/(g.h.bar)
K3_d=(1/0.01)*(5.17*10^-5)*exp(8700/T0);             %bar^-1
k4_d=(3600)*(5.35*10^-1)*exp(-7500/T0);              %mol/g.h

r_DRM=Klk2_d*K3_d*k4_d*PCH4*PCO2/((Klk2_d*K3_d*PCH4*PCO2)+(Klk2_d*PCH4)+(K3_d*k4_d*PCO2));      % mol/g.h

%---------------------- DRM model of Richardson & Paripatyadar (1990)

%k1=1.29*10^6*exp(-102065/R/T0);
%KCO2_1=2.61*10^-2*exp(37641/R/T0);
%KCH4_1=2.60*10^-2*exp(40684/R/T0);
%KP1=6.78*10^14*exp(-259660/R/T0);

%r_DRM=k1*KCO2_1*KCH4_1*PCH4*PCO2/(1+KCO2_1*PCO2+KCH4_1*PCH4)^2*(1-(PCO*PH2)^2/(KP1*PCH4*PCO2));

%-------------------------------------------------

Kco_B=exp(-115/R)*exp(92543/R/T0);      %bar^-1
Ko_B=3.0190322*10^7*exp(-89805/R/T0);       %bar
k_B=2.673282*10^7*exp(-108379/R/T0);        %mol/g.h
K_B=exp(-170.44/R)*exp(162483/R/T0);        %bar^-1
DENB=1+(Kco_B*PCO)+(1*PCO2/Ko_B/Kco_B/PCO);    %unitless

rcB=(k_B*Kco_B*(PCO-(PCO2/K_B/PCO)))/(DENB^2);  % mol/g.h        %Boudouard reaction 2CO <-> C + CO2

r_SRM_1=1*r_SRM_1;
r_SRM_2=1*r_SRM_2;
```

```
r_SRM_2=1*r_SRM_2;
r_SRM_3=1*r_SRM_3;
r_DRM=1*r_DRM;
% rc1=1.49E-1*rc1;
% rc2=1*rc2;
% rcB=2.83E-1*rcB;

rc1=1*rc1;
rc2=1*rc2;
rcB=1*rcB;

a=4/tubedia;     %heat exchange area per unit volume of reactor, m^-1
U=1000;          % heat transfer coefficient, J.m^-2.h.K
Ta=stattemp;          % ambient temperature, K

% All heat capacities are in J/mol.K, taken from Perry's Handbook Table 2-151
Cp1=4.182*(6.60+(0.00120*T0)); %CO
Cp2=4.182*(8.22+(0.00015*T0)+(0.00000134*T0^2));  %H2O
Cp3=4.182*(10.34+(0.00274*T0)-(195500/T0^2)); %CO2
Cp4=4.182*(6.62+(0.00081*T0)); %H2
Cp5=4.182*4.97; %He
Cp6=4.182*(5.34+(0.0115*T0)) ; %CH4
Cp7=4.182*(2.673+(0.002617*T0)-(116900/T0^2)); %C

SUM1=U*a*(Ta-T0)/(Rhob*1000); %J/g/h
SUM2=(r_SRM_1*-H_SRM_1)+(r_SRM_2*-H_SRM_2)+(r_SRM_3*-H_SRM_3)+(r_DRM*-H_DRM)+(rc1*-H_c1)+(rc2*-H_c2)+(rcB*-H_b); %J/g/h
DOWN=(F(1)*Cp1)+(F(2)*Cp2)+(F(3)*Cp3)+(F(4)*Cp4)+(F(5)*Cp5)+(F(6)*Cp6)+(F(7)*Cp7); %J/K/h
```

```

H_SRM_1=224000; %J/mol @948 K taken from J. De Wilde GF Froment/Fuel 100 (2012) 48-56
H_SRM_2=-37300; %J/mol @948 K taken from J. De Wilde GF Froment/Fuel 100 (2012) 48-56
H_SRM_3=187500; %J/mol @948 K taken from J. De Wilde GF Froment/Fuel 100 (2012) 48-56
H_DRM=247000;   %J/mol @298 K
H_c1=74870;     %J/mol @298 K taken from J. De Wilde GF Froment/Fuel 100 (2012) 48-56
H_c2=-131325;   %J/mol @298 K taken from J. De Wilde GF Froment/Fuel 100 (2012) 48-56
H_b=173300;     %J/mol @298 K taken from J. Xu GF Froment/AIChE 35 (1989) 88-96



dfdw(1,1)=r_SRM_1-r_SRM_2-rc2+2*r_DRM-2*rcB;                    %CO unit: mol/g/h
dfdw(2,1)=-(r_SRM_1+r_SRM_2+2*r_SRM_3)+rc2;                %H2O
dfdw(3,1)=r_SRM_2+r_SRM_3-r_DRM+rcB;                        %CO2
dfdw(4,1)=3*r_SRM_1+r_SRM_2+4*r_SRM_3+2*rc1-rc2+2*r_DRM;   %H2
dfdw(5,1)=0;                                               %He
dfdw(6,1)=-(r_SRM_1+r_SRM_3)-rc1-r_DRM;                    %CH4
dfdw(7,1)=rc1+rc2+rcB;                                      %C
dfdw(8,1)=1*-(beta0/(At*Rhob))*(F(9)/stattemp)*(Ptot0/F(8))*(Ftot/Ftot0)/100/1000;       % ERGUN equation from Fogler  bar/g
dfdw(9,1)=0*(SUM1+SUM2)/DOWN;  %Eqn from Fogler 8-76     K/g

%rate=[r_SRM_1,r_SRM_2,r_SRM_3,r_DRM,rc1,rc2,rcB];

end
```

Caller function file:

```
% feed conditions
% a = CO
% b = H2O
% c = CO2
% d = H2
% e = He
% f = CH4
% g= C
%guess=[0.0001,1,0.0001,0.0001,0,1];
global initialCH4 initialCO2 initialH2O initialCO initialH2 initialHe ICH4 ICO2 IH2O IHe ICO IH2 tubedia

tubedia=0.01;       % tube diameter in meters, obtained from MA Effi reactor dimension.
QCH4_STP=3;       %ml/min
QCO2_STP=3;       % ml/min
QHe_STP=24;             % ml/min
QH2O_STP=0.00001;   % ml/min
global stattemp             % static temperature value, or the intial temperature value.
ICH4=QCH4_STP*60*0.716*(1/(16.04*1000));       %mol/hr
ICO2=QCO2_STP*60*1.977*(1/(44.01*1000));
IHe=QHe_STP*60*0.1786*(1/(4.003*1000));
IH2O=QH2O_STP*60*0.590*(1/(18.016*1000));
ICO=1E-10;
IH2=1E-10;

global Ptot0 Dp phi At Rhob Rhoinit
global r_SRM_1 r_SRM_2 r_SRM_3 r_DRM rc1 rc2 rcB;

phi=0.60;                              %porosity of bed
Dp=0.00016;                              %Size of the Catalyst particle m
```

```
Dp=0.00016;                              %Size of the Catalyst particle m
catalystweight=0.001;                       %grams
stepsize=10;
counter1=1;
forwardweight=catalystweight/stepsize;

for counter1=1:(stepsize+1)

weight=[0:catalystweight/stepsize:forwardweight];

forwardweight=(counter1)*catalystweight/stepsize;

%m=guess';
% temperatures in K
%global T0 Ftot0 H_SRM_1 H_SRM_2 H_SRM_3 H_DRM H_c1 H_c2 H_b

global Ftot0 H_SRM_1 H_SRM_2 H_SRM_3 H_DRM H_c1 H_c2 H_b

%beta0=(G*(1-phi)/(Rhoinit*1.0*Dp*(phi^3)))*((150*(1-phi)*mumix/Dp)+(1.75*G));

% [t,para]=ode15s('Combined_reforming_Kinetics_basic_ode',weight,guess);

trange=[650,50,650]+273.15;
% disp(guess(3));
l=1;
for T0=trange(1):trange(2):trange(3)
    m=1;
    for Ptot0=1:1:1

```

```
    for Ptot0=1:1:1

    stattemp=T0;

    guess=[ICO,IH2O,ICO2,IH2,IHe,ICH4,1E-10, 1, stattemp];
    initialCH4=guess(6);
    initialCO2=guess(3);
    initialH2O=guess(2);
    initialCO=guess(1);
    initialH2=guess(4);
    initialHe=guess(5);
    Ptot0=guess(8);
    T0=guess(9);
    Ftot0=initialCH4+initialCO2+initialH2O+initialHe;
    guess(6)=QCH4_STP*guess(8)*10^-1/8.314/T0*60;  %mol/hr flow of methane
    guess(3)=QCO2_STP*guess(8)*10^-1/8.314/T0*60;  %mol/hr flow of carbon dioxide
    guess(2)=QH2O_STP*guess(8)*10^-1/8.314/T0*60;  %mol/hr flow of steam
    guess(1)=guess(6)/1000;
    guess(4)=guess(6)/1000;
    guess(5)=guess(6)/1000;
    guess(7)=guess(6)/1000;
    options = odeset('NonNegative',1);
    [t,para]=ode15s('Combined9_reforming_Kinetics_basic_ode',weight,guess,options);
    CO2_Pcent(1,m)=(guess(3)-para(end,3))*100/guess(3)
    CH4_Pcent(1,m)=(guess(6)-para(end,6))*100/guess(6)
    H2O_Pcent(1,m)=(1-guess(2))*100;
    m=m+1;
    end
    l=l+1;
```

```
    end
    l=l+1;
end
%plot(t, para);
Cl=guess( 1)*1+guess( 2)*0+guess( 3)*1+guess( 4)*0+guess( 5)*0+guess( 6)*1+guess( 7)*1;
Ol=guess( 1)*1+guess( 2)*1+guess( 3)*2+guess( 4)*0+guess( 5)*0+guess( 6)*0+guess( 7)*0;
Hl=guess( 1)*0+guess( 2)*2+guess( 3)*0+guess( 4)*2+guess( 5)*0+guess( 6)*4+guess( 7)*0;
C=para(end, 1)*1+para(end, 2)*0+para(end, 3)*1+para(end, 4)*0+para(end, 5)*0+para(end, 6)*1+para(end, 7)*1;
O=para(end, 1)*1+para(end, 2)*1+para(end, 3)*2+para(end, 4)*0+para(end, 5)*0+para(end, 6)*0+para(end, 7)*0;
H=para(end, 1)*0+para(end, 2)*2+para(end, 3)*0+para(end, 4)*2+para(end, 5)*0+para(end, 6)*4+para(end, 7)*0;
c=Cl-C
o=Ol-O
h=Hl-H
syngasratio=para(end,4)/para(end,1)
carbondeposited=para(end,7)*12   %g/hr
%carbonratio=para(end,7)/para(end,6)

rate_data_srm1(counter1)=r_SRM_1;
rate_data_srm2(counter1)=r_SRM_2;
rate_data_srm3(counter1)=r_SRM_3;
rate_data_drm(counter1)=r_DRM;
rate_data_c1(counter1)=rc1;
rate_data_c2(counter1)=rc2;
rate_data_cb(counter1)=rcB;
counter1=counter1+1;

end

figure;
```

```
H=para(end, 1)*0+para(end, 2)*2+para(end, 3)*0+para(end, 4)*2+para(end, 5)*0+para(end, 6)*4+para(end, 7)*0;
c=C1-C
o=O1-O
h=H1-H
syngasratio=para(end,4)/para(end,1)
carbondeposited=para(end,7)*12    %g/hr
%carbonratio=para(end,7)/para(end,6)

rate_data_srm1(counter1)=r_SRM_1;
rate_data_srm2(counter1)=r_SRM_2;
rate_data_srm3(counter1)=r_SRM_3;
rate_data_drm(counter1)=r_DRM;
rate_data_c1(counter1)=rc1;
rate_data_c2(counter1)=rc2;
rate_data_cb(counter1)=rcB;
counter1=counter1+1;

end

figure;
subplot(3,1,1);
plot(t, para(:,1), 'r+', t, para(:,2), 'go', t, para(:,3), 'b*', t, para(:,4), 'cx', t, para(:,5), 'ms', t, para(:,6), 'yd', t, p
legend('CO','H2O','CO2','H2','He','CH4','C');
subplot(3,1,2);
plot(t, para(:,8), 'r+');
legend('pressure drop profile');
subplot(3,1,3);
plot(t, para(:,9), 'go');
legend('temperature profile');
```

```
para(end, 2)*2+para(end, 3)*0+para(end, 4)*2+para(end, 5)*0+para(end, 6)*4+para(end, 7)*0;

end,4)/para(end,1)
ara(end,7)*12    %g/hr
(end,7)/para(end,6)

unter1)=r_SRM_1;
unter1)=r_SRM_2;
unter1)=r_SRM_3;
nter1)=r_DRM;
ter1)=rc1;
ter1)=rc2;
ter1)=rcB;
+1;

, 'r+', t, para(:,2), 'go', t, para(:,3), 'b*', t, para(:,4), 'cx', t, para(:,5), 'ms', t, para(:,6), 'yd', t, para(:,7), 'kv');
,'CO2','H2','He','CH4','C');

, 'r+');
drop profile');

, 'go');
re profile');
```